Max-Planck-Institut für Meteorologie
Max Planck Institute for Meteorology

Report No. 349

the atmospheric general circulation model ECHAM5

PART I

Model description

by

E. Roeckner • G. Bäuml • L. Bonaventura • R. Brokopf • M. Esch
M. Giorgetta • S. Hagemann • I. Kirchner • L. Kornblueh
E. Manzini • A. Rhodin • U. Schlese • U. Schulzweida • A. Tompkins

Hamburg, November 2003

Authors

E. Roeckner, G. Bäuml, L. Bonaventura, R. Brokopf, M. Esch, M. Giorgetta, S. Hagemann, L. Kornblueh, U. Schlese, U. Schulzweida	Max-Planck-Institut für Meteorologie Hamburg, Germany
I. Kirchner	Freie Universität Berlin, Berlin, Germany
E. Manzini	Istituto Nazionale di Geofisica e Vulcanologia, Bologna, Italy
A. Rhodin	Deutscher Wetterdienst, Offenbach, Germany
A. Tompkins	European Centre for Medium Range Weather Forecasts, Reading, UK

Max-Planck-Institut für Meteorologie
Bundesstrasse 55
D - 20146 Hamburg
Germany

Tel.: +49-(0)40-4 11 73-0
Fax: +49-(0)40-4 11 73-298
e-mail: <name>@dkrz.de
Web: www.mpimet.mpg.de

Max-Planck-Institut für Meteorologie
Max Planck Institute for Meteorology

Report No. 349

the atmospheric general circulation model ECHAM5

PART I

Model description

by

E. Roeckner · G. Bäuml · L. Bonaventura · R. Brokopf · M. Esch
M. Giorgetta · S. Hagemann · I. Kirchner[1] · L. Kornblueh
E. Manzini[2] · A. Rhodin[3] · U. Schlese · U. Schulzweida · A. Tompkins[4]

Hamburg, November 2003

ISSN 0937 - 1060

[1]Freie Universität Berlin, Berlin, Germany
[2]Istituto Nazionale di Geofisica e Vulcanologia, Bologna, Italy
[3]Deutscher Wetterdienst, Offenbach, Germany
[4]European Centre for Medium Range Weather Forecasts, Reading, UK

Abstract

A detailed description of the fifth-generation ECHAM model is presented. Compared to the previous version, ECHAM4, a number of substantial changes have been introduced in both the numerics and physics of the model. These include a flux-form semi-Lagrangian transport scheme for positive definite variables like water components and chemical tracers, a new longwave radiation scheme, separate prognostic equations for cloud liquid water and cloud ice, a new cloud microphysical scheme and a prognostic-statistical cloud cover parameterization. The number of spectral intervals is increased in both the longwave and shortwave part of the spectrum. Changes have also been made in the representation of land surface processes, including an implicit coupling between the surface and the atmosphere, and in the representation of orographic drag forces. Also, a new dataset of land surface parameters has been compiled for the new model. On the other hand, horizontal and vertical diffusion, cumulus convection and also the spectral dynamics remain essentially unchanged.

Acknowledgments

The authors are grateful to Jean-Jacques Morcrette, ECMWF, for providing the ECMWF version of the RRTM code and to Francois Lott, LMD, who made the SSO scheme available to us. We gratefully acknowledge the help of David Dent, ECMWF, in improving the Legendre Transformation code, and we thank Eckhard Tschirschnitz, NEC, for substantial support with respect to scalability and code optimization for vector and cache-based platforms.

Contents

1. Introduction

The fifth-generation atmospheric general circulation model (ECHAM5) developed at the Max Planck Institute for Meteorology (MPIM) is the most recent version in a series of ECHAM models evolving originally from the spectral weather prediction model of the European Centre for Medium Range Weather Forecasts (ECMWF; Simmons et al. (1989)). The changes compared to the previous version, ECHAM4 (Roeckner et al., 1996), can be classified as follows:

- New formulations

  Advection scheme for positive definite variables; longwave radiation code; cloud cover parameterization; separate treatment of cloud water and cloud ice; cloud microphysics; subgrid scale orographic effects

- Major changes

  Land surface processes and land surface dataset

- Minor changes

  Shortwave radiation; vertical diffusion; cumulus convection; orbit calculation

- Technical changes

  Fortran 95; portability; flexibility; parellel version

One should note that some of the 'minor changes', such as the doubling of spectral intervals in the shortwave radiation code, led to a significant change in simulated climate. From a technical point of view, ECHAM5 is more flexible compared to its predecessors. It has been tested on various platforms and it includes options like a single column version, a simple data assimilation (nudging), extension to the middle atmosphere, and coupling to a mixed layer ocean (Q-flux approach).

The changes in physical processes, compared to ECHAM4, are summarized as follows:

For positive definite variables (water vapour, cloud variables and chemical tracers) a mass- conserving and shape-preserving advection scheme is applied (Lin and Rood, 1996).

The new longwave radiation code (RRTM) has been developed by Mlawer et al. (1997) and has been adopted in the version used at ECMWF. It is based on the two-stream approximation instead of the emissivity method applied in ECHAM4. The scheme has a higher spectral resolution (16 bands instead of 6) and it is computationally more efficient at high vertical resolution because the CPU-time depends linearly on the number of layers (quadratic in ECHAM4). The solar radiation code is basically unchanged, except that the number of spectral bands is increased from 2 to 4. Orbital parameters of the Earth can be chosen optionally, using either those obtained from precise orbit determination for present-day climate or, for paleoclimatic applications, those obtained from solving the Kepler equation.

In the standard model configuration (without chemistry), ozone is prescribed as a function of month, latitude and height as constructed from ozone sonde profiles and satellite data (Fortuin and Kelder, 1998).

A new scheme for stratiform clouds has been developed. It includes prognostic equations for cloud liquid water, cloud ice and for the higher order moments of the total water content. Cloud microphysics includes rain formation by coalescence processes (autoconversion, cloud collection by rain and snow), aggregation of ice crystals to snow flakes, accretion of cloud droplets by falling snow, gravitational settling of ice crystals, sublimation/evaporation of falling snow/rain and also freezing and melting. Most of these processes are formulated as in Lohmann and Roeckner (1996). Fractional cloudiness is calculated from a statistical model (Tompkins, 2002) using a probability density function (PDF) for total water as suggested from simulations with a cloud-resolving model. Variance and skewness of the PDF are related to the intensity of subgrid-scale processes such as turbulence and convection.

An implicit scheme is used for coupling the land surface and the atmosphere (Schulz et al., 2001). Also, the heat transfer in the soil is calculated by using an implicit scheme. In the presence of snow, the top of the snow layer is considered as the top of the soil model. The heat conductivity in all layers which are totally or partially filled with snow are modified accordingly.

A prognostic equation for the amount of snow on the canopy has been introduced. Snow changes on the canopy result from interception of snowfall, sublimation, melting and unloading due to wind (Roesch et al., 2001).

The grid-mean surface albedo depends on the specified background albedo, a specified snow albedo (function of temperature), the area of the grid cell covered with forest, the snow cover on the ground (function of snow depth and slope of terrain) and the snow cover on the canopy (Roesch et al., 2001).

A simple mixed-layer lake model is used for calculating the temperature of 'big' lakes (i.e., grid cells with land fraction less than 50%). Ice thickness is derived from a thermodynamic ice model including a snow layer on top of the ice. Lakes are either ice-free or totally covered with ice.

Surface fluxes of radiation, sensible heat, moisture and momentum are calculated separately for open water and ice.

A new scheme for the representation of subgrid-scale orographic effects is used (Lott, 1999; Lott and Miller, 1997).

A new set of land surface data (vegetation ratio, leaf area index, forest ratio, background albedo) has been derived from a global 1 km-resolution dataset (Hagemann, 2002).

In its standard configuration, the model has 19 or 31 vertical layers with the top level at 10 hPa. The middle-atmosphere version is currently available with either 39 or 90 layers (top level at 0.01 hPa). Horizontal resolutions employed so far are T21, T31, T42, T63, T85, T106 and T159. Results will be presented in Part II (Roeckner et al., 2003).

2. Model dynamics

2.1. Introduction

The climate model ECHAM5 has been developed from the ECMWF operational forecast model cycle 36 (1989) (therefore the first part of its name: EC) and a comprehensive parameterisation package developed at Hamburg (therefore the abbreviation HAM). The part describing the dynamics of ECHAM is based on the ECMWF documentation, which has been modified to describe the newly implemented features and the changes necessary for climate experiments. Since the release of the previous version, ECHAM4, the whole source code has been extensively redesigned in the major infrastructure and transferred to Fortran 95. ECHAM is now fully portable and runs on all major high performance platforms. The restart mechanism is implemented on top of netCDF and because of that absolutelly independent on the underlying architecture.

In this chapter the technical details of the adiabatic part of ECHAM are described. The first two sections present the governing equations, the coordinates and the discretization schemes used. Attention is concentrated on the representation of the explicitly resolved adiabatic processes. A derivation of the equations including terms requiring parametrization is included in Appendix A.

Detailed descriptions of the parametrizations themselves are given in chapters 4 - 11. The dynamical part of ECHAM is formulated in spherical harmonics. After the inter-model comparisons by Jarraud et al. (1981) and Girard and Jarraud (1982) truncated expansions in terms of spherical harmonics were adopted for the representation of dynamical fields. The transform technique developed by Eliasen et al. (1970), Orszag (1970), and Machenhauer and Rasmussen (1972) is used such that non-linear terms, including parameterizations, are evaluated at a set of almost regularly distributed grid points - the Gaussian grid.

In the vertical, a flexible coordinate is used, enabling the model to use either the usual terrain-following sigma coordinate (Phillips, 1957), or a hybrid coordinate for which upper-level model surfaces flatten over steep terrain, becoming surfaces of constant pressure in the stratosphere (Simmons and Burridge (1981) and Simmons and Strüfing (1981)). Moist processes are treated in a different way using a mass conserving algorithm for the transport (Lin and Rood, 1996) of the different water species and potential chemical tracers. The transport is determined on the Gaussian grid.

First, in section 2.2 the continuous form of the governing equations is presented. Sections 2.3 and 2.4 give details of the spectral representation and of the vertical coordinate and its associated vertical finite difference scheme. The temporal finite-difference scheme, which includes not only a conventional semi-implicit treatment of gravity-wave terms (Robert et al., 1972), but also a semi-implicit treatment of the advection of vorticity (Jarraud et al., 1982), is described in section 2.5.1.

2.2. The continuous equations

Although the model has been implemented for one particular form of a vertical coordinate, which is introduced in section 2.4, it is convenient to introduce the equations and their spectral representation for a general pressure-based terrain-following vertical coordinate $\eta(p, p_s)$, which must be a monotonic function of pressure p, and depends as well on the surface pressure p_s, in such a way that

$$\eta(0, p_s) = 0 \qquad \text{and} \qquad \eta(p_s, p_s) = 1$$

For such a coordinate, the continuous formulation of the primitive equations for a dry atmosphere may be directly derived from their basic height coordinate forms following Kasahara (1974).

During the design of the model, a detailed derivation of the corresponding equations for a moist atmosphere, including a separation into terms to be represented explicitly in the subsequent discretized form of the equations and terms to be parameterized, was carried out. It is shown in Appendix A that under certain approximations, the momentum, thermodynamic and moisture equations may be written:

$$\frac{\partial U}{\partial t} - (f+\xi)V + \dot{\eta}\frac{\partial U}{\partial \eta} + \frac{R_d T_v}{a}\frac{\partial \ln p}{\partial \lambda} + \frac{1}{a}\frac{\partial(\phi + E)}{\partial \lambda} = P_U + K_U \tag{2.1}$$

$$\frac{\partial V}{\partial t} + (f+\xi)U + \dot{\eta}\frac{\partial V}{\partial \eta} + \frac{R_d T_v}{a}(1-\mu^2)\frac{\partial \ln p}{\partial \mu} + \frac{(1-\mu^2)}{a}\frac{\partial(\phi + E)}{\partial \mu} = P_V + K_V \tag{2.2}$$

$$\frac{\partial T}{\partial t} + \frac{U}{a(1-\mu^2)}\frac{\partial T}{\partial \lambda} + \frac{V}{a}\frac{\partial T}{\partial \mu} + \dot{\eta}\frac{\partial T}{\partial \eta} - \frac{\kappa T_v \omega}{(1+(\delta-1)q_v)p} = P_T + K_T \tag{2.3}$$

$$\frac{\partial q_i}{\partial t} + \frac{U}{a(1-\mu^2)}\frac{\partial q_i}{\partial \lambda} + \frac{V}{a}\frac{\partial q_i}{\partial \mu} + \dot{\eta}\frac{\partial q_i}{\partial \eta} = P_{q_i} \tag{2.4}$$

where q_i are the mixing ratios of the different water species.

The continuity equation is

$$\frac{\partial}{\partial \eta}\left(\frac{\partial p}{\partial t}\right) + \nabla \cdot \left(\vec{v}_h \frac{\partial p}{\partial \eta}\right) + \frac{\partial}{\partial \eta}\left(\dot{\eta}\frac{\partial p}{\partial \eta}\right) = 0 \tag{2.5}$$

and the hydrostatic equation takes the form

$$\frac{\partial \phi}{\partial \eta} = -\frac{R_d T_v}{p}\frac{\partial p}{\partial \eta} \tag{2.6}$$

The pressure coordinate vertical velocity is given by

$$\omega = \vec{v}_h \nabla p - \int_0^\eta \nabla \cdot \left(\vec{v}_h \frac{\partial p}{\partial \eta}\right) d\eta \tag{2.7}$$

and explicit expressions for the rate of change of surface pressure, and for $\dot{\eta}$, are obtained by integrating equation 2.5, using the boundary conditions $\dot{\eta} = 0$ at $\eta = 0$ and $\eta = 1$:

$$\frac{\partial p_s}{\partial t} = -\int_0^1 \nabla \cdot \left(\vec{v}_h \frac{\partial p}{\partial \eta} \right) d\eta \tag{2.8}$$

and

$$\dot{\eta} \frac{\partial p}{\partial \eta} = -\frac{\partial p}{\partial t} - \int_0^\eta \nabla \cdot \left(\vec{v}_h \frac{\partial p}{\partial \eta} \right) d\eta \tag{2.9}$$

equation 2.8 may also be written

$$\frac{\partial \ln p_s}{\partial t} = -\frac{1}{p_s} \int_0^1 \nabla \cdot \left(\vec{v}_h \frac{\partial p}{\partial \eta} \right) d\eta \tag{2.10}$$

Following the derivation given in Appendix A, the terms P_U, P_V, P_T, and P_{q_i} are written:

$$P_U = -g \cos\theta \left(\frac{\partial p}{\partial \eta} \right)^{-1} \frac{\partial J_U}{\partial \eta} \tag{2.11}$$

$$P_V = -g \cos\theta \left(\frac{\partial p}{\partial \eta} \right)^{-1} \frac{\partial J_V}{\partial \eta} \tag{2.12}$$

$$P_T = \frac{1}{c_p} \left[Q_R + Q_L + Q_D - g \left(\frac{\partial p}{\partial \eta} \right)^{-1} \left(\frac{\partial J_S}{\partial \eta} - c_{pd} T (\delta - 1) \frac{\partial J_{q_v}}{\partial \eta} \right) \right] \tag{2.13}$$

$$P_{q_i} = S_{q_i} - g \left(\frac{\partial p}{\partial \eta} \right)^{-1} \frac{\partial J_{q_i}}{\partial \eta} \tag{2.14}$$

where

$$c_p = c_{pd}(1 + (\delta - 1) q_v)$$

In equations 2.11 - 2.14, J_U, J_V, J_S, and J_{q_i} represent net parametrized vertical fluxes of momentum, dry static energy ($c_p T + \phi$), moisture and cloud species. They include fluxes due to convection and boundary-layer turbulence. Q_R, Q_L, and Q_D represent heating due to radiation, phase changes and to internal dissipation of kinetic energy associated with the P_U and P_V terms, respectively. S_{q_i} denotes the rates of change of q_i due to phase changes and precipitation formation. Details of the calculation of these terms are given in section 10.

The K terms in equations 2.1 - 2.4 represent the influence of unresolved horizontal scales. Their treatment differs from that of the P terms in that it does not involve a physical model of subgrid scale processes, but rather a numerically convenient form of scale selective diffusion of a magnitude determined empirically to ensure a realistic behaviour of resolved scales. These terms are specified in section 4.

In order to apply the spectral method, equations 2.1 and 2.2 are written in vorticity and divergence form following Bourke (1972). They become

$$\frac{\partial \xi}{\partial t} = \frac{1}{a(1-\mu^2)}\frac{\partial (F_V + P_V)}{\partial \lambda} - \frac{1}{a}\frac{\partial (F_U + P_U)}{\partial \mu} + K_\xi \tag{2.15}$$

$$\frac{\partial D}{\partial t} = \frac{1}{a(1-\mu^2)}\frac{\partial (F_U + P_U)}{\partial \lambda} + \frac{1}{a}\frac{\partial (F_V + P_V)}{\partial \mu} - \nabla^2 G + K_D \tag{2.16}$$

where

$$F_U = (f+\xi)V - \dot{\eta}\frac{\partial U}{\partial \eta} - \frac{R_d T_v}{a}\frac{\partial \ln p}{\partial \lambda} \tag{2.17}$$

$$F_V = -(f+\xi)U - \dot{\eta}\frac{\partial V}{\partial \eta} - \frac{R_d T_v}{a}(1-\mu^2)\frac{\partial \ln p}{\partial \lambda} \tag{2.18}$$

and

$$G = \phi + E \tag{2.19}$$

We also note that a streamfunction ψ and velocity potential χ may be introduced such that

$$\begin{aligned} U &= \frac{1}{a}\left[-(1-\mu^2)\frac{\partial \psi}{\partial \mu} + \frac{\partial \chi}{\partial \lambda}\right] \\ V &= \frac{1}{a}\left[\frac{\partial \psi}{\partial \lambda} + (1-\mu^2)\frac{\partial \chi}{\partial \mu}\right] \end{aligned} \tag{2.20}$$

and

$$\begin{aligned} \xi &= \nabla^2 \psi \\ D &= \nabla^2 \chi \end{aligned} \tag{2.21}$$

2.3. Horizontal discretization

2.3.1. Spectral representation

The basic prognostic variables of the model are ξ, D, T, q_i, and $\ln p_s$. While q_i are represented in grid point space, the other variables, and the surface geopotential ϕ_s, are represented in the horizontal by truncated series of spherical harmonics:

$$X(\lambda, \mu, \eta, t) = \sum_{m=-M}^{M} \sum_{n=m}^{N(M)} X_n^m(\eta, t) P_n^m(\mu)\, \mathrm{e}^{im\lambda} \tag{2.22}$$

where X is any variable, m is the zonal wave number and n is the meridional index. The P_n^m are the Associated Legendre Functions of the first kind, defined here by

$$P_n^m(\mu) = \sqrt{(2n+1)\frac{(n-m)!}{(n+m)!}}\frac{1}{2^n n!}(1-\mu^2)^{\frac{m}{2}}\frac{d^{(n+m)}}{d\mu^{(n+m)}}(\mu^2-1), \quad (m \geq 0) \tag{2.23}$$

and

$$P_n^{-m}(\mu) = P_n^m(\mu)$$

This definition is such that

$$\frac{1}{2}\int_{-1}^{1} P_n^m(\mu)P_s^m(\mu)d\mu = \delta_{ns} \tag{2.24}$$

where δ_{ns} is the Kronecker delta function. The X_n^m are the complex-valued spectral coefficients of the field X and given by

$$X_n^m(\eta,t) = \frac{1}{4\pi}\int_{-1}^{1}\int_{0}^{2\pi} X(\lambda,\mu,\eta,t)P_n^m(\mu)\ \mathrm{e}^{-im\lambda}d\lambda d\mu \tag{2.25}$$

Since X is real

$$X_n^{-m} = (X_n^m)^* \tag{2.26}$$

is valid, where $(\ )^*$ denotes the complex conjugate. The model thus deals explicitly only with the X_n^m for $m \geq 0$.

The Fourier coefficients of X, $X_m(\mu,\eta,t)$ are defined by

$$X_m(\mu,\eta,t) = \frac{1}{2\pi}\int_{0}^{2\pi} X(\lambda,\mu,\eta,t)\ \mathrm{e}^{-im\lambda}d\lambda \tag{2.27}$$

or using equation 2.22, by

$$X_m(\mu,\eta,t) = \sum_{n=m}^{N(m)} X_n^m(\eta,t)P_n^m(\mu) \tag{2.28}$$

with

$$X(\lambda,\mu,\eta,t) = \sum_{m=-M}^{M} X_m(\mu,\eta,t)\ \mathrm{e}^{im\lambda} \tag{2.29}$$

Horizontal derivatives are given analytically by

$$\left(\frac{\partial X}{\partial \lambda}\right)_m = imX_m \quad \text{and} \quad \left(\frac{\partial X}{\partial \mu}\right)_m = \sum_{n=m}^{N(m)} X_n^m \frac{dP_n^m}{d\mu} \tag{2.30}$$

where the derivative of the Legendre Function is given by the recurrence relation:

$$(1-\mu^2)\frac{dP_n^m}{d\mu} = -n\varepsilon_{n+1}^m P_{n+1}^m + (n+1)\varepsilon_n^m P_{n-1}^m \quad \text{with} \quad \varepsilon_n^m = \sqrt{\frac{n^2-m^2}{4n^2-1}} \tag{2.31}$$

An important property of the spherical harmonics is the algebraic form of the Laplacian:

$$\nabla^2(P_n^m(\mu)\ \mathrm{e}^{im\lambda}) = -\frac{n(n+1)}{a^2} P_n^m(\mu)\ \mathrm{e}^{im\lambda} \tag{2.32}$$

Relationships 2.20 and 2.21 may thus be used to derive expressions for the Fourier velocity coefficients, U_m and V_m in terms of the spectral coefficients ξ_n^m and D_n^m. It is convenient for later reference to write these expressions in the form

$$U_m = U_{\xi m} + U_{Dm} \quad \text{and} \quad V_m = V_{\xi m} + V_{Dm} \tag{2.33}$$

where

$$U_{\xi m} = -a \sum_{n=m}^{N(m)} \frac{1}{n(n+1)} \xi_n^m H_n^m(\mu) \tag{2.34}$$

$$U_{Dm} = -a \sum_{n=m}^{N(m)} \frac{im}{n(n+1)} D_n^m P_n^m(\mu) \tag{2.35}$$

$$V_{\xi m} = -a \sum_{n=m}^{N(m)} \frac{im}{n(n+1)} \xi_n^m P_n^m(\mu) \tag{2.36}$$

$$V_{Dm} = -a \sum_{n=m}^{N(m)} \frac{1}{n(n+1)} D_n^m H_n^m(\mu) \tag{2.37}$$

with

$$H_n^m(\mu) = -(1-\mu^2)\frac{dP_n^m}{d\mu} \tag{2.38}$$

The H_n^m can be computed from the recurrence relation 2.31. In ECHAM5 only triangular truncations can be used which is the preferred type of truncations for resolutions larger than T21. This restriction is implied by the parallelization of the spectral part of the model. The triangular truncation is completely defined by the three parameters illustrated in figure 2.1.

The triangular truncations are special cases of the pentagonal one in which $M = J = K$.

The summation limit, $N(m)$ is given by

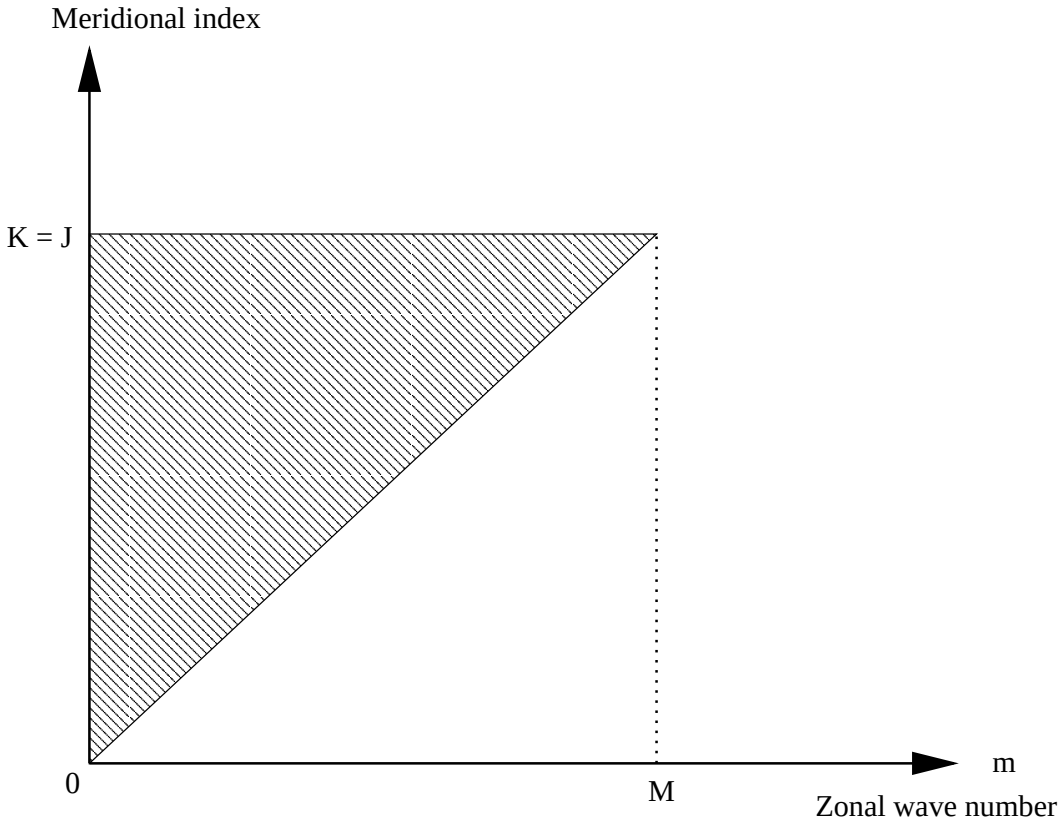

Figure 2.1.: Triangular truncation

$$N = J + |m| \quad \text{if} \quad J + |m| \leq K \quad \text{and} \quad N = K \quad \text{if} \quad J + |m| > K$$

The standard truncations used in ECHAM5 are at wave numbers 21, 31, 42, 63, 85, 106, or 159.

2.3.2. Spectral/grid-point transforms, and the evaluation of spectral tendencies

The general form of the equations follow that of the early multi-level spectral models described by Bourke (1974) and Hoskins and Simmons (1975), although the present model differs in its use of an advective form for the equations 2.15, 2.16, 2.3, and 2.10. Equations for the corresponding spectral coefficients are obtained by multiplying each side of these equations by $P_n^m(\mu)\ \mathrm{e}^{-im\lambda}$ and integrating over the sphere. This yields, from 2.25,

$$\frac{\partial \xi_n^m}{\partial t} = \frac{1}{4\pi a}\int_{-1}^{1}\int_{0}^{2\pi}\left(\frac{1}{1-\mu^2}\frac{\partial(F_V+P_V)}{\partial\lambda} - \frac{\partial(F_U+P_U)}{\partial\mu}\right)P_n^m(\mu)\ \mathrm{e}^{-im\lambda}d\lambda d\mu + (K_\xi)_n^m \tag{2.39}$$

$$\frac{\partial D_n^m}{\partial t} = \frac{1}{4\pi a}\int_{-1}^{1}\int_{0}^{2\pi}\left(\frac{1}{1-\mu^2}\frac{\partial(F_U+P_U)}{\partial\lambda} + \frac{\partial(F_V+P_V)}{\partial\mu}\right)P_n^m(\mu)\ \mathrm{e}^{-im\lambda}d\lambda d\mu - \frac{1}{4\pi}\int_{-1}^{1}\int_{0}^{2\pi}(\nabla^2 G)P_n^m(\mu)\ \mathrm{e}^{-im\lambda}d\lambda d\mu + (K_D)_n^m \tag{2.40}$$

$$\frac{\partial T_n^m}{\partial t} = \frac{1}{4\pi}\int_{-1}^{1}\int_{0}^{2\pi}(F_T+P_T)P_n^m(\mu)\ \mathrm{e}^{-im\lambda}d\lambda d\mu + (K_T)_n^m \tag{2.41}$$

$$\frac{\partial(\ln p_s)_n^m}{\partial t} = \frac{1}{4\pi}\int_{-1}^{1}\int_{0}^{2\pi}F_P P_n^m(\mu)\ \mathrm{e}^{-im\lambda}d\lambda d\mu \tag{2.42}$$

where F_U, F_V and G are given by 2.17 - 2.19, and

$$F_T = -\frac{U}{a(1-\mu^2)}\frac{\partial T}{\partial\lambda} - \frac{V}{a}\frac{\partial T}{\partial\mu} - \dot{\eta}\frac{\partial T}{\partial\eta} + \frac{\kappa T_\nu \omega}{(1+(\delta-1)q_v)p} \tag{2.43}$$

$$F_P = -\frac{1}{p_s}\int_0^1 \nabla\cdot(\vec{v}_h\frac{\partial p}{\partial\eta})d\eta \tag{2.44}$$

Equations 2.41 - 2.42 are in the form used in the model. The corresponding forms for the vorticity and divergence equations are obtained from 2.39 and 2.40 by integration by parts and use of 2.32:

$$\frac{\partial \xi_n^m}{\partial t} = \frac{1}{4\pi a}\int_{-1}^{1}\int_{0}^{2\pi}\frac{1}{1-\mu^2}[im(F_V+P_V)P_n^m(\mu)-(F_U+P_U)H_n^m(\mu)]\,\mathrm{e}^{-im\lambda}d\lambda d\mu + (K_\xi)_n^m \tag{2.45}$$

$$\frac{\partial D_n^m}{\partial t} = \frac{1}{4\pi a}\int_{-1}^{1}\int_{0}^{2\pi}\frac{1}{1-\mu^2}[im(F_U+P_U)P_n^m(\mu)+(F_V+P_V)H_n^m(\mu)]\,\mathrm{e}^{-im\lambda}d\lambda d\mu + \frac{n(n+1)}{4\pi a^2}\int_{0}^{1}\int_{0}^{2\pi} GP_n^m(\mu)\,\mathrm{e}^{-im\lambda}d\lambda d\mu + (K_D)_n^m \tag{2.46}$$

where $H_n^m(\mu)$ is given by 2.38.

An outline of the model's computation of spectral tendencies may now be given. First, a grid of points covering the sphere is defined. Using the basic definition of the spectral expansions 2.22 and equations 2.33 - 2.37, values of ξ, D, U, V, T, and $\ln p_s$ are calculated at the gridpoints, as are the derivatives

$$\frac{\partial T}{\partial \lambda}, \frac{\partial T}{\partial \mu}, \frac{\partial \ln p_s}{\partial \lambda} \text{and} \frac{\partial \ln p_s}{\partial \mu}$$

using 2.30. The resulting gridpoint values are sufficient to calculate gridpoint values of F_U, F_V, F_T, F_p and G, together with the parametrized tendencies P_U, P_V, and P_T, since prognostic surface fields associated with the parametrization are defined and updated on the same grid. The integrands of the prognostic equations 2.45, 2.46, 2.41 - 2.42 are thus known at each gridpoint, and spectral tendencies are calculated by numerical quadrature.

The grid on which the calculations are performed is chosen to give an exact (given the spectral truncation of the fields, and within round-off error) contribution to spectral tendencies from quadratic non-linear terms. The integrals with respect to λ involve the product of three trigonometric functions, and as shown by Machenhauer and Rasmussen (1972) they may be evaluated exactly using a regularly-spaced grid of at least $3 \cdot M + 1$ points. For the latitudinal integrals, Eliasen et al. (1970) showed that quadratic nonlinear terms lead to integrands which are polynomials in μ of a certain order.

They may thus be computed exactly using Gaussian quadrature (e.g. Krylov (1962), with points located at the (approximately equally-spaced) latitudes which satisfy $P_{N_G}^0(\mu) = 0$, for sufficiently large integer N_G. These latitudes form what are referred to as the Gaussian latitudes.

In order to find the necessary number of Gaussian latitudes for the triangular truncation, and from the exactness condition for the Gaussian integration it may be shown that the number of Gaussian latitudes N_G must fulfil the following condition:

$$N_G \geq \frac{3 \cdot K + 1}{2}$$

The associated number of Gaussian latitudes with respect to the given spectral resolution in ECHAM5[1] is given in table 2.1.

[1] Note: Since change of the ECMWF forecast model to the Semi-Lagrangian advection for the dynamics this model uses a linear truncation denoted T_L. This means that the number of Gaussian latitudes is smaller than in ECHAM5; e.g. T_L159 has 160 latitudes and 320 langitudes while the spectral truncation corresponding to this grid-point resolution for ECHAM5 is T106.

Truncation	No. of Longitudes	No. of Latitudes
T21	64	32
T31	96	48
T42	128	64
T63	192	96
T85	256	128
T106	320	160
T159	480	240

Table 2.1.: Truncation and associated number of Gaussian latitudes (and longitudinal number of gridpoints).

An asymptotic property of the Legendre Functions which may be derived directly from the definition 2.23 is

$$P_n^m(\mu) \sim (1-\mu^2)^{m/2} \text{ as } (\mu \rightarrow \pm 1).$$

Thus for large m the functions become vanishingly small as the poles are approached, and the contributions to the integrals 2.39 - 2.42 from polar regions become less than the unavoidable round-off error for sufficiently large zonal wavenumbers.

2.4. Vertical discretization

2.4.1. The hybrid vertical representation

To represent the vertical variation of the dependent variables ξ, D, and T the atmosphere is divided into layers as illustrated in table 2.2. These layers are defined by the pressures of the interfaces between them (the"half levels"), and these pressures are given by

$$p_{k+1/2} = A_{k+1/2} + B_{k+1/2} \;\; p_s \tag{2.47}$$

for $k = 0, 1, 2 \ldots NLEV$. The $A_{k+1/2}$ and $B_{k+1/2}$ are constants whose values effectively define the vertical coordinate. Necessary values are

$$A_{1/2} = B_{1/2} = A_{NLEV+1/2} = 0 \;\; \text{and} \;\; B_{NLEV+1/2} = 1 \tag{2.48}$$

The usual sigma coordinate is obtained as the special case

$$A_{k+1/2} = 0 \;, \;\; k = 0, 1, \ldots, NLEV \tag{2.49}$$

This form of hybrid coordinate has been chosen because it is particularly efficient from a computational viewpoint. It also allows a simple direct control over the "flattening" of coordinate surfaces as pressure decreases, since the $A's$ and $B's$ may be determined by specifying the distribution of half-level pressures for a typical sea-level surface pressure and for a surface pressure typical of the lowest expected to be attained in the model. Coordinate surfaces are surfaces of constant pressure at levels where $B_{k+1/2} = 0$.

The prognostic variables ξ, D, T and q_i are represented by their values at intermediate (full-level) pressures, p_k. Values for p_k are not explicitly required by the model's vertical finite-difference scheme, which is described in the following section, but they are required by parameterization schemes, in the creation of initial data, and in the interpolation to pressure levels that forms part of the post-processing. Alternative forms for p_k have been discussed by Simmons and Burridge (1981) and Simmons and Strüfing (1981). Little sensitivity has been found, and the simple form

$$p_k = \frac{1}{2}(p_{k+1/2} + p_{k-1/2}) \tag{2.50}$$

has been adopted, where half-level values are as given by 2.47. The explicit relationship between p and p_s defined for model half levels implicitly determines a vertical coordinate η. The model formulation is in fact such that this coordinate need not be known explicitly, as demonstrated in the following section. However, it is computationally convenient to define η for the radiative parametrization and for the vertical interpolation used in the post-processing. The half-level values are given by

$$\eta_{k+1/2} = \frac{A_{k+1/2}}{p_0} + B_{k+1/2} \tag{2.51}$$

where p_0 is constant pressure. From 2.47 it is seen that this coordinate is identical to the usual σ when $A_{k+1/2} = 0$, and in general equals σ when $p_0 = p_s \cdot \eta = p/p_0$ at levels where coordinate surfaces are surfaces of constant pressure. Values of η between half-levels are given by linear interpolation :

$$\eta = \eta_{k+1/2} + \frac{(p - p_{k+1/2})(\eta_{k+1/2} - \eta_{k-1/2})}{(p_{k+1/2} - p_{k-1/2})} \quad \text{for} \quad (p_{k-1/2} \leq p \leq p_{k+1/2} \tag{2.52}$$

A 19-layer version is used for the T21, T31, and T42 horizontal resolution. For resolutions starting from T63 31 layers are recommended. The value of p_0 used for the definition of η is the reference sea-level pressure of 101325 Pa.

2.4.2. The vertical finite-difference scheme

The vertical finite-difference scheme is a generalization to the hybrid coordinate with form 2.47 of the scheme adopted in the first operational ECMWF model (Burridge and Haseler, 1977), apart from a small modification concerned with the conservation of angular momentum. The generalized scheme has been discussed by Simmons and Burridge (1981) and Simmons and Strüfing (1981), and the presentation here is restricted to a prescription of the finite-difference forms of the various terms of the continuous equations that involve η.

2.4.3. The surface-pressure tendency

The finite-difference analogue of 2.10 is

$$\frac{\partial \ln p_s}{\partial t} = -\frac{1}{p_s} \sum_{k=1}^{NLEV} \nabla \cdot (\vec{v}_k \Delta p_k) \tag{2.53}$$

k	$A_{k+\frac{1}{2}}$ $[Pa]$	$B_{k+\frac{1}{2}}$	$A_{k+\frac{1}{2}}$ $[Pa]$	$B_{k+\frac{1}{2}}$
0	0.000000	0.0000000000	0.00000000	0.00000000
1	2000.000000	0.0000000000	2000.00000000	0.00000000
2	4000.000000	0.0000000000	4000.00000000	0.00000000
3	6046.110595	0.0003389933	6000.00000000	0.00000000
4	8267.927560	0.0033571866	8000.00000000	0.00000000
5	10609.513232	0.0130700434	9976.13671875	0.00039086
6	12851.100169	0.0340771467	11820.53906250	0.00291970
7	14698.498086	0.0706498323	13431.39453125	0.00919413
8	15861.125180	0.1259166826	14736.35546875	0.02031916
9	16116.236610	0.2011954093	15689.20703125	0.03697486
10	15356.924115	0.2955196487	16266.60937500	0.05948764
11	13621.460403	0.4054091989	16465.00390625	0.08789498
12	11101.561987	0.5249322235	16297.62109375	0.12200361
13	8127.144155	0.6461079479	15791.59765625	0.16144150
14	5125.141747	0.7596983769	14985.26953125	0.20570326
15	2549.969411	0.8564375573	13925.51953125	0.25418860
16	783.195032	0.9287469142	12665.29296875	0.30623537
17	0.000000	0.9729851852	11261.23046875	0.36114502
18	0.000000	0.9922814815	9771.40625000	0.41820228
19	0.000000	1.0000000000	8253.21093750	0.47668815
20			6761.33984375	0.53588659
21			5345.91406250	0.59508425
22			4050.71777344	0.65356457
23			2911.56933594	0.71059442
24			1954.80517578	0.76540524
25			1195.88989258	0.81716698
26			638.14892578	0.86495584
27			271.62646484	0.90771586
28			72.06358337	0.94421321
29			0.00000000	0.97298521
30			0.00000000	0.99228150
31			0.00000000	1.00000000

Table 2.2.: Vertical-coordinate parameters of the 19- and 31-layer ECHAM5 model

where the subscript k denotes a value for the k-th layer, and

$$\Delta p_k = p_{k+1/2} - p_{k-1/2} \tag{2.54}$$

From 2.47 we obtain

$$\frac{\partial \ln p_s}{\partial t} = - \sum_{k=1}^{NLEV} \left\{ \frac{1}{p_s} D_k \Delta p_k + (\vec{v}_k \cdot \nabla \ln p_s) \Delta B_k \right\} \tag{2.55}$$

where

$$\Delta B_k = B_{k+1/2} - B_{k-1/2} \tag{2.56}$$

2.4.4. The continuity equation

Equation 2.9 gives

$$\left(\dot{\eta}\frac{\partial p}{\partial \eta}\right)_{k+1/2} = -\frac{\partial p_{k+1/2}}{\partial t} - \sum_{j=1}^{k} \nabla \cdot (\vec{v}_j \Delta p_j) \tag{2.57}$$

and from 2.47

$$\left(\dot{\eta}\frac{\partial p}{\partial \eta}\right)_{k+1/2} = -p_s \left[B_{k+1/2}\frac{\partial \ln p_s}{\partial t} + \sum_{j=1}^{k} \left\{ \frac{1}{p_s} D_j \Delta p_j + (\vec{v}_j \cdot \nabla \ln p_s)\Delta B_j \right\} \right] \tag{2.58}$$

where $\frac{\partial \ln p_s}{\partial t}$ is given by 2.55.

2.4.5. Vertical advection

Given $\left(\dot{\eta}\frac{\partial p}{\partial \eta}\right)_{k+1/2}$ computed from 2.58, vertical advection of a variable is given by

$$\left(\dot{\eta}\frac{\partial X}{\partial \eta}\right)_{k} = \frac{1}{2\Delta p_k} \left\{ \left(\dot{\eta}\frac{\partial p}{\partial \eta}\right)_{k+1/2} (X_{k+1} - X_k) + \left(\dot{\eta}\frac{\partial X}{\partial \eta}\right)_{k-1/2} \cdot (X_k - X_{k-1}) \right\} \tag{2.59}$$

This form ensures that there is no spurious source or sink of kinetic and potential energy due to the finite-difference representation of vertical advection.

2.4.6. The hydrostatic equation

The form chosen for the finite-difference analogue of 2.6 is

$$\Phi_{k+1/2} - \Phi_{k-1/2} = -R_d \cdot (T_v)_k \cdot \ln\left(\frac{p_{k+1/2}}{p_{k-1/2}}\right) \tag{2.60}$$

which gives

$$\Phi_{k+1/2} = \Phi_S + \sum_{j=k+1}^{NLEV} R_d \cdot (T_v)_j \cdot \ln\left(\frac{p_{j+1/2}}{p_{j-1/2}}\right) \tag{2.61}$$

Full level values of geopotential are given by

$$\Phi_k = \Phi_{k+1/2} + \alpha_k \cdot R_d \cdot (T_v)_k \ , \tag{2.62}$$

where

$$\alpha_1 = \ln 2 \tag{2.63}$$

and, for $k > 1$,

$$\alpha_k = 1 - \frac{p_{k-1/2}}{\Delta p_k} \cdot \ln\left(\frac{p_{k+1/2}}{p_{k-1/2}}\right) \tag{2.64}$$

Reasons for this particular choice of the α_k are given below.

2.4.7. The pressure gradient term

It is shown by Simmons and Strüfing (1981) that if the geopotential is given by 2.62, the form

$$R_d \cdot (T_v \cdot \nabla \ln p)_k = \frac{R_d \cdot (T_v)_k}{\Delta p_k} \left\{ \left(\ln \frac{p_{k+1/2}}{p_{k-1/2}}\right) \cdot \nabla p_{k-1/2} + \alpha_k \cdot \nabla(\Delta p_k) \right\} \tag{2.65}$$

for the pressure-gradient term ensures no spurious source or sink of angular momentum due to vertical differencing. This expression is adopted in the model, but with the α_k given by 2.64 for all k. This ensures that the pressure-gradient term reduces to the familiar form $R_d(T_v)_k \nabla \ln p_s$ in the case of sigma coordinates, and the angular momentum conserving property of the scheme still holds in the case in which the first half-level below $p = 0$ is a surface of constant pressure. The choice $\alpha_1 = 1$ in the hydrostatic equation would have given angular momentum conservation in general, but a geopotential Φ_1 inappropriate to the pressure-level $p = p_1 = \Delta p/2$. If, alternatively, Φ_1 were to be interpreted not as a value for a particular level, but rather the mass-weighted layer-mean value, then the choice α_1 would be appropriate.

It is shown by Simmons and Chen (1991) that the form 2.65 can be significantly improved, with benefit particularly in regions of steep terrain, if T_v is replaced by its deviation from a reference state,

$$\tilde{T}_v = T_v - T_0 \left(\frac{p}{p_0}\right)^{\beta} \tag{2.66}$$

where $\beta = \gamma \cdot \frac{R_d}{g}$, $p_0 = 1013.25$ hPa, $T_0 = 288$ K and $\gamma = 6.5$ K/km. The reference temperature 2.66 is based on the tropospheric part of the ICAO (1964) standard atmosphere with a uniform lapse rate γ.

Using the form 2.47 for the half-level pressures 2.65 may be written

$$R_d \cdot (\tilde{T}_v \cdot \nabla \ln p)_k = \frac{R_d \cdot (\tilde{T}_v)_k}{\Delta p_k} \left\{ \Delta B_k + C_k \cdot \frac{1}{\Delta p_k} \cdot \left(\ln \frac{p_{k+1/2}}{p_{k-1/2}}\right) \right\} \nabla p_s \tag{2.67}$$

where

$$C_k = A_{k+1/2} \cdot B_{k-1/2} - A_{k-1/2} \cdot B_{k+1/2} \tag{2.68}$$

The modified form 2.67 finally requires a reformulation of the surface geopotential according to

$$\Phi_S = g \cdot z_S + \frac{R_d \cdot T_0}{\beta} \cdot \left(\frac{p_s}{p_0}\right)^{\beta} \tag{2.69}$$

2.4.8. Energy-conversion term

To obtain a form for the term $\kappa \cdot T_v \cdot \omega/(1+(\delta-1)q_v)$ in 2.3 we use 2.7 to write

$$\left(\frac{\kappa \cdot T_v \cdot \omega}{(1+(\delta-1)q_v)p}\right)_k = \frac{\kappa \cdot (T_v)_k}{1+(\delta-1)(q_v)_k}\left(\frac{\omega}{p}\right)_k \tag{2.70}$$

where

$$\left(\frac{\omega}{p}\right)_k = -\frac{1}{p}\int_0^{\eta_k} \nabla \cdot \left(\vec{v} \cdot \frac{\partial p}{\partial \eta}\right) d\eta + (\vec{v} \cdot \nabla \ln p)_k \tag{2.71}$$

An expression for $\left(\frac{\omega}{p}\right)_k$ is then determined by the requirement that the difference scheme conserves the total energy of the model atmosphere for adiabatic, frictionless motion. This is achieved by

- evaluating the first term on the right-hand side of 2.71 by

$$-\frac{1}{\Delta p_k}\left\{\left(\ln \frac{p_{k+1/2}}{p_{k-1/2}}\right) \cdot \sum_{k=1}^{k-1} \nabla \cdot (\vec{v}_j \cdot \Delta p_j) + \alpha_k \nabla \cdot (\vec{v}_k \cdot \Delta p_k)\right\} \tag{2.72}$$

  where the α_k are as given by 2.63 and 2.64, and as in 2.55 and 2.57

$$\nabla \cdot (\vec{v}_k \cdot \Delta p_k) = D_k \cdot \Delta p_k + p_s \cdot (\vec{v}_k \cdot \nabla \ln p_s) \cdot \Delta B_k \tag{2.73}$$

- using the form of 2.67 to evaluate the second term on the right-hand side of 2.71

$$(\vec{v} \cdot \nabla \ln p)_k = \frac{p_s}{\Delta p_k} \cdot \left\{\Delta B_k + C_k \cdot \frac{1}{\Delta p_k} \cdot \left(\ln \frac{p_{k+1/2}}{p_{k-1/2}}\right)\right\} \cdot \vec{v}_k \cdot \nabla \ln p_s \tag{2.74}$$

2.5. Time integration scheme

A semi-implicit time scheme is used for equations of divergence, temperature and surface pressure, based on the work of Robert et al. (1972). The growth of spurious computational modes is inhibited by a time filter (Asselin, 1972). In addition, a semi-implicit method for the zonal advection terms in the vorticity equation is used, following results obtained by Robert (1981, 1982). He showed that in a semi-implicit shallow water equation model the time-step criterion was determined by the explicit treatment of the vorticity equation. Facilities also exist for selective damping of short model scales to allow use of longer timesteps. These are incorporated within the horizontal diffusion routines of the model, and are described in section 2.6. The semi-implicit schemes are formally given by:

$$\delta_t \xi = ZT - \frac{1}{2a}\beta_Z \frac{U_r(\mu)}{1-\mu^2}\frac{\partial \Delta_{tt}\xi}{\partial \lambda} \tag{2.75}$$

$$\delta_t D = DT - \nabla^2 G - \frac{1}{2}\beta_{DT}\nabla^2\{\gamma\delta_{tt}T + R_d T_r \Delta_{tt} \ln p_s\} \tag{2.76}$$

$$\delta_t T = TT - \frac{1}{2}\beta_{DT}\tau\Delta_{tt}D \tag{2.77}$$

$$\delta_t \ln p_s = PT - \frac{1}{2}\beta_{DT}\nu\Delta_{tt}D \tag{2.78}$$

Here the terms ZT, DT, G, TT and PT represent those on the right-hand sides of equations 2.15, 2.16, 2.3 and 2.10, apart from the diffusion terms, which are neglected here. Adiabatic components are evaluated at the current time, t, and parametrized components are generally evaluated using values of fields at the previous timestep, $t - \Delta t$. The treatment of diffusion terms is described in section 4.

The remaining terms on the right-hand sides of 2.75 - 2.78 are corrections associated with the semi-implicit time schemes, and are discussed in more detail below. The operators δ_t and Δ_{tt} are given by

$$\delta_t X = \frac{(X^+ - X_f^-)}{2\Delta t} \tag{2.79}$$

$$\Delta_{tt} X = X^+ + X_f^- - 2X \tag{2.80}$$

where X represents the value of a variable at time t, X^+ the value at time $t + \Delta t$, and X_f^- a filtered value at time $t - \Delta t$. A further operator that will be used is

$$\tilde{\Delta}_{tt} X = X_f^- - 2X \tag{2.81}$$

The time filtering is defined by

$$X_f = X + \epsilon_f (X_f^- - 2X + X^+) \tag{2.82}$$

and it is computationally convenient to split it into two parts;

$$\tilde{X}_f = X + \epsilon_f (X_f^- - 2X) \tag{2.83}$$

$$X_f = \tilde{X}_f + \epsilon_f X^+ \tag{2.84}$$

The timestep Δt depends on resolution, while $\epsilon_f = 0.1$ is independent of the resolution.

2.5.1. The semi-implicit treatment of vorticity

Referring to equation 2.75, an explicit treatment of the vorticity equation is obtained by setting $\beta_Z = 0$. Otherwise $\beta_Z = 1$ and $U_r(\mu)$ is a zonally-uniform reference zonal velocity, multiplied by $\cos\theta$. Terms describing advection by this reference velocity are represented implicitly by the

arithmetic mean of values at times $t + \Delta t$ and $t - \Delta t$, while the remainder of the tendencies are represented explicitly by values at time t. $U_r(\mu)$ may vary in the vertical.

For the vorticity equation, 2.15 is used to write

$$ZT = \frac{1}{\alpha(1-\mu^2)}\frac{\partial(F_V + P_V)}{\partial\lambda} - \frac{1}{a}\frac{\partial(F_U + P_U)}{\partial\mu} \tag{2.85}$$

where the horizontal diffusion term has for convenience been neglected. Transforming into Fourier space gives:

$$\xi_m^+ = b_m(\mu) = \left[\left(\xi_f^- + \frac{2\ im\Delta t}{a(1-\mu^2)}(F_V + P_V)\right)_m - 2\ im\Delta t\alpha(\mu)\tilde{\Delta}_{tt}\xi_m - \frac{2\Delta t}{a}\frac{\partial(F_U + P_U)_m}{\partial\mu}\right] \tag{2.86}$$

The factor $b_m(\mu)$ renders the right-hand side of this equation unsuitable for direct integration by parts, but a suitable form is found from the relation

$$b_m(\mu)\frac{\partial(F_U + P_U)}{\partial\mu} = \frac{\partial\{b_m(\mu)(F_U + P_U)\}}{\partial\mu} - c_m(\mu)(F_U + P_U) \tag{2.87}$$

where

$$c_m(\mu) = \frac{\partial\{b_m(\mu)\}}{\partial\mu} \tag{2.88}$$

This gives

$$\xi_m^+ = \tilde{Z}_{\lambda m}(\mu) + \frac{\partial\tilde{Z}_{\mu m}(\mu)}{\partial\mu} \tag{2.89}$$

where

$$\tilde{Z}_{\lambda m}(\mu) = b_m(\mu)(\xi_f^-)_m + 2\Delta t\left(imb_m(\mu)\left[\frac{(F_V + P_V)_m}{a(1-\mu^2)} - \alpha(\mu)\tilde{\Delta}_{tt}\xi_m\right] + \frac{1}{a}c_m(\mu)(F_U + P_U)_m\right)$$

and

$$\tilde{Z}_{\lambda m}(\mu) = -\frac{2\Delta t}{a}b_m(\mu)(F_U + P_U)_m \tag{2.90}$$

New values $(\xi_n^m)^+$ are obtained from 2.89 by Gaussian quadrature, using integration by parts as illustrated by 2.39 and 2.45 for the continuous form of the equations.

$U_r(\mu)$ is the arithmetic mean of the maximum and minimum velocities multiplied by $cos\theta$, as computed for each latitude and model level at timestep $t - \Delta t$. Different values are thus used for different levels. In ECHAM5, $\beta_Z = 1$ is used.

2.5.2. The semi-implicit treatment of divergence, temperature and surface pressure

Referring to equations 2.76 - 2.78, an explicit treatment of the divergence, temperature and surface pressure equations is obtained by setting $\beta_{DT} = 0$. For $\beta_Z = 1$, the nature of the semi-implicit correction is such that gravity wave terms for small amplitude motion about a basic state with isothermal temperatue T_r and surface pressure p_r are treated implicitly by the arithmetic mean of values at times $t + \Delta t$ and $t - \Delta t$, while the remainder of tendencies are represented explicitly by values at time t. The choice of an isothermal reference temperature is governed by considerations of the stability of the semi-implicit time scheme (Simmons et al., 1978), while the appropriate choice of p_r for the hybrid vertical coordinate is discussed by Simmons and Burridge (1981) and Simmons and Strüfing (1981).

γ, τ and ν in equations 2.76 - 2.78 are operators obtained from linearizing the finite-difference forms specified in section 2.4 about the reference state $(T_r,\ p_r)$. Their definitions are

$$(\gamma T)_k = \alpha^r_k R_d T_k + \sum_{j=k+1}^{NLEV} R_d T_j \ln\left(\frac{p^r_{j+1/2}}{p^r_{j-1/2}}\right) \tag{2.91}$$

$$(\tau D)_k = \kappa T_r \left\{ \frac{1}{\Delta p^r_k} \ln\left(\frac{p^r_{j+1/2}}{p^r_{j-1/2}}\right) S^r_{k-1/2} + \alpha^r_k D_k \right\} \tag{2.92}$$

and

$$\nu D = \frac{S^r_{NLEV+1/2}}{p^r} \tag{2.93}$$

where

$$\begin{aligned} p^r_{k+1/2} &= A_{k+1/2} + p_r B_{k+1/2} \\ \Delta p^r_k &= p^r_{k+1/2} - p^r_{k-1/2} \\ S^r_{k+1/2} &= \sum_{j=1}^{k} D_j \Delta p^r_j \end{aligned} \tag{2.94}$$

and the α^r_k are defined by 2.63 and 2.64 , but with half-level pressures replaced by reference values $p^r_{k+1/2}$.

Expanding 2.76 - 2.78 using 2.79 and 2.80, and writing l to denote $\ln p'_S$, we obtain

$$\begin{aligned} D^+ &= D^-_f + 2\Delta t(DT) - 2\Delta t \nabla^2 \{G + \frac{\beta_{DT}}{2}[\gamma(T^+ + T^-_f - 2T) \\ &\quad + R_d T_r (l^+ + l^-_f - 2l)]\} \end{aligned} \tag{2.95}$$

$$T^+ = T_1 - \Delta t \beta_{DT} \tau D^+ \tag{2.96}$$

and

$$l^+ = l_1 - \Delta t \beta_{DT} \nu D^+ \tag{2.97}$$

where

$$T_1 = T_f^- + 2\Delta t(TT) - \Delta t \beta_{DT} \tau \tilde{\Delta}_{tt} D \tag{2.98}$$

and

$$l_1 = l_f^- + 2\Delta t(PT) - \Delta t \beta_{DT} \nu \tilde{\Delta}_{tt} D \tag{2.99}$$

Substituting 2.96 and 2.97 into 2.95 then gives

$$(1 - \Gamma \nabla^2) D^+ = DT' \tag{2.100}$$

where

$$\begin{aligned} \Gamma &= (\beta_{DT})^2 (\Delta t)^2 (\gamma\tau + R_d T_r \nu) && (2.101) \\ DT' &= D_f^- + 2\Delta t(DT) + \nabla^2 R = \tilde{D}_\lambda + \tilde{D}_\mu + \nabla^2 R && (2.102) \end{aligned}$$

with

$$\begin{aligned} \tilde{D}_\lambda &= D_f^- + \frac{2\Delta t}{a(1-\mu^2)} \frac{\partial (F_U + P_U)}{\partial \lambda} && (2.103) \\ \tilde{D}_\mu &= \frac{2\Delta t}{a} \frac{\partial (F_V + P_V)}{\partial \mu} && (2.104) \end{aligned}$$

and

$$R = -2\Delta t \left\{ G + \frac{B_{DT}}{2} (\gamma T_2 + R_d T_r l_2) \right\} \tag{2.105}$$

Here

$$\begin{aligned} T_2 &= T_1 + T_f^- - 2T && (2.106) \\ l_2 &= l_1 + l_f^- - 2l && (2.107) \end{aligned}$$

The sequence of these semi-implicit calculations in the model is thus as follows. The expressions 2.98, 2.99 and 2.105 - 2.107 are computed on the Gaussian grid to form the gridpoint values of R. The spectral expansion of DT' is then derived by Gaussian quadrature, using integration by parts as illustrated by 2.40 and 2.46 for the continuous form of the equations. Since

$$\{(1 - \Gamma \nabla^2) D^+\}_n^m = \left(1 + \frac{n(n+1)}{a^2} \Gamma\right) (D^+)_n^m, \tag{2.108}$$

the spectral coefficients of divergence at time $t + \Delta t$ are given from 2.40 by

$$(D^+)_n^m = \left(1 + \frac{n(n+1)}{a^2}\Gamma\right)^{-1} (DT')_n^m, \tag{2.109}$$

where this operation involves, for each (m, n), multiplication of the vector of $NLEV$ values of $(DT')_n^m$ by a pre-computed $NLEV \times NLEV$ matrix whose elements are independent of time and determined by writing the operators γ, τ and ν in matrix and vector form. Finally, 2.96 and 2.97 are applied in spectral space to compute spectral coefficients of T and $\ln p'_S$ at time $t + \Delta t$ in terms of the spectral coefficients of T_1 and l_1 (again determined by Gaussian quadrature) and those of D^+. In ECHAM5, $\beta_{DT} = 0.75$, $T_r = 300$ K and $p_r = 800$ hPa.

3. Tracer advection

The flux form semi-Lagrangian scheme employed in ECHAM5 for passive tracer transport has been introduced by Lin and Rood (1996). This type of advection scheme combines typical features of Eulerian, flux form schemes (i.e., exact mass conservation to machine precision) with the unconditional stability for all Courant numbers typical of standard (non conservative) semi-Lagrangian schemes. For Courant numbers smaller than one, the Lin-Rood schemes reverts to a multidimensional flux form scheme which takes properly into account transverse fluxes, such as those developed by Colella, LeVeque, Leonard and others (see references in Lin and Rood (1996)). In the constant velocity case at Courant number smaller than one, it is in fact identical with the Colella *Corner Transport Upwind* scheme. The scheme is described here for application to incompressible flows, its generalization to compressible fluids is described in Lin and Rood (1996).

Consider the conservative formulation of passive advection in an incompressible fluid

$$\frac{\partial Q}{\partial t} + \nabla \cdot (\mathbf{v}Q) = 0, \tag{3.1}$$

where Q is the tracer concentration and the continuity equation is given by

$$\nabla \cdot \mathbf{v} = 0. \tag{3.2}$$

It is to be remarked that there is an inherent coupling of (3.1) to the continuity equation, since in the case of constant tracer concentration (3.1) reduces to (3.2). This property should be also guaranteed by the discretization of (3.1).

Assuming a C-type grid staggering in which normal velocity components are defined at the grid sides and scalar quantities (to be interpreted as cell averages) are defined at the cell center, a flux form discretization of (3.1) is given by

$$Q_{i,j}^{n+1} = Q_{i,j}^{n} - \left(\mathcal{X}_{i+\frac{1}{2},j} - \mathcal{X}_{i-\frac{1}{2},j}\right) - \left(\mathcal{Y}_{i,j+\frac{1}{2}} - \mathcal{Y}_{i,j-\frac{1}{2}}\right) \tag{3.3}$$

where $\mathcal{X}_{i+\frac{1}{2},j}\mathcal{Y}_{i,j+\frac{1}{2}}$ and $\mathcal{X}_{i-\frac{1}{2},j}\mathcal{Y}_{i,j-\frac{1}{2}}$ are approximations of the Q fluxes in the E-W and N-S directions, respectively, integrated in time over the time step Δt. In order to achieve unconditional stability, in the Lin-Rood scheme the fluxes are computed as the sum of an *integer* and a *fractional* flux

$$\mathcal{X}_{i-\frac{1}{2},j} = \mathcal{X}^{int}_{i-\frac{1}{2},j} + \mathcal{X}^{fr}_{i-\frac{1}{2},j}.$$

The integer fluxes represent the contribution to the flux that arises in case of Courant numbers larger than one at the cell side $i - \frac{1}{2}$. More specifically, defining

$$C^{x}_{i-\frac{1}{2},j} = \frac{\Delta t u^{n+\frac{1}{2}}_{i-\frac{1}{2},j}}{\Delta x} = K^{x}_{i-\frac{1}{2},j} + c^{x}_{i-\frac{1}{2},j}$$

$$K^x_{i-\frac{1}{2},j} = INT(C^x_{i-\frac{1}{2},j}) \qquad I = INT(i - C^x_{i-\frac{1}{2},j})$$

(where INT has the same meaning as the corresponding *Fortran95* intrinsic function) and assuming e.g. a positive velocity, the integer flux is defined as

$$\mathcal{X}^{int}_{i-\frac{1}{2},j} = \sum_{k=1}^{K^x_{i-\frac{1}{2},j}} Q^n_{i-k,j}.$$

Thus, the integer flux represents the mass transport through all the cells crossed completely by a Lagrangian trajectory ending at $(i-\frac{1}{2},j)$ at timestep $n+1$ during a time interval Δt.

The fractional flux is defined as the Van Leer flux

$$\mathcal{X}^{fr}_{i-\frac{1}{2},j} = c^x_{i-\frac{1}{2},j}\left[Q^g_{I,j} + \frac{Q^g_{I+1,j} - Q^g_{I-1,j}}{4}\Big(SIGN(1, c^x_{i-\frac{1}{2},j}) - c^x_{i-\frac{1}{2},j}\Big)\right] \tag{3.4}$$

where $SIGN$ has the same meaning as the corresponding *Fortran95* intrinsic function.

The intermediate value $Q^g_{i,j}$ used in the computation of the Van Leer flux can be interpreted as a first order finite difference approximation of

$$\frac{\partial Q}{\partial t} + v\frac{\partial Q}{\partial y} = 0,$$

advanced in time $\Delta t/2$ from timestep n along the Lagrangian trajectory ending at $(i-\frac{1}{2},j)$ at timestep $n+1$.

More precisely,

$$Q^g_{i,j} = \frac{\Big(Q^n_{i,J} + Q^n_{i,j}\Big)}{2} + \frac{|c^y_{i,j}|}{2}\Big(Q^n_{i,J^*} - Q^n_{i,J}\Big)$$

where

$$C^y_{i,j} = \frac{\Delta t}{2\Delta y}\Big(v^{n+\frac{1}{2}}_{i,j-\frac{1}{2}} + v^{n+\frac{1}{2}}_{i,j+\frac{1}{2}}\Big)$$

$$c^y_{i,j} = C^y_{i,j} - INT(C^y_{i,j}) \qquad J = j - INT(C^y_{i,j}) \qquad J^* = J - SIGN(1, C^y_{i,j}).$$

The Lin and Rood scheme satisfies some fundamental requirements for a tracer advection algorithm:

- mass conservation: by construction, since it is formulated in flux form;
- consistency with the discretization of the continuity equation: setting $q = 1$ yields a discretization of (3.2) by the same scheme,

- monotonicity of the 1D advection schemes: if a flux limiter is applied to the centered difference $Q^g_{I+1,j} - Q^g_{I-1,j}$ in (3.4) (see references in Lin and Rood (1996)), the one dimensional flux operators are guaranteed to be monotonic, although this in general does not ensure that the full multidimensional scheme is monotonic as well;

- preservation of linear tracer correlations: if q_1, q_2 are the concentrations of two different tracers such that $q_2^n = \alpha q_1^n + \beta$, with α, β two constants, then the values q_1^{n+1}, q_2^{n+1} obtained by time update with the Lin and Rood scheme still satisfy $q_2^{n+1} = \alpha q_1^{n+1} + \beta$.

4. Horizontal diffusion

Unlike the other physical parameterizations which are computed in grid point space, the horizontal diffusion can conveniently be formulated in spectral space. Moreover, the treatment of horizontal diffusion differs from that of the other processes in that it does not involve a physical model of subgrid-scale processes, but rather a numerically convenient form of scale selective diffusion with coefficients determined empirically to ensure a realistic behavior of the resolved scales. As in many other models, the horizontal diffusion tendency is expressed in the form of a hyper-Laplacian,

$$\frac{\partial \chi}{\partial t} = -(-1)^q K_\chi \nabla^{2q} \chi \tag{4.1}$$

where χ is vorticity, divergence or temperature (no horizontal diffusion is applied to water components or trace constituents), K_χ is a constant diffusion coefficient for the respective variable, and $q > 0$ is an integer. The time rate of change of spectral component χ_n is given by

$$\frac{\partial \chi_n}{\partial t} = -K_\chi \left\{ n(n+1)a^{-2} \right\}^q \chi_n \tag{4.2}$$

where a is the Earth's radius and n is wavenumber. For convenience, K_χ can be replaced by the e-folding damping time τ of the highest resolvable wavenumber n_0

$$\tau(n_0) \equiv \tau_0 = K_\chi^{-1} \left\{ n_0(n_0+1)a^{-2} \right\}^{-q} \tag{4.3}$$

so that (4.2) can be expressed in terms of the order of the scheme, $2q$, and damping time τ_0. The scale selectivity of the scheme increases with increasing q. Both damping time and order depend on the horizontal resolution. Furthermore, in order to avoid spurious wave reflection at the upper boundary of the model, the diffusion is enhanced in the upper layers by gradually decreasing the order of the scheme (Table 4.1).

Level	T21 ($\tau_0 = 6$)	T31 ($\tau_0 = 12$)	T42 ($\tau_0 = 9$)	T63 ($\tau_0 = 7$)	T85 ($\tau_0 = 5$)	T106 ($\tau_0 = 3$)	T159 ($\tau_0 = 2$)
1	2	2	2	2	2	2	2
2	4	2	2	2	2	2	2
3	6	2	2	2	2	2	2
4	8	4	4	4	4	4	4
5	12	6	6	6	6	6	6
6	16	8	8	8	8	8	6
≥ 7	20	10	10	8	8	8	6

Table 4.1.: Damping time τ_0 in hours (independent of model level) and order, $2q$, of horizontal diffusion scheme applied at different model levels

5. Surface fluxes and vertical diffusion

The turbulent flux of a variable χ at the surface is obtained from the bulk transfer relation

$$\left(\overline{w'\chi'}\right)_S = -C_\chi |V_L|(\chi_L - \chi_S) \tag{5.1}$$

where C_χ is the transfer coefficient. The subscripts L and S refer to values at the lowest model level (representing the top of the surface layer) and the surface, respectively, and V_L is the horizontal wind vector at level L. The transfer coefficients are obtained from Monin-Obukhov similarity theory by integrating the flux-profile relationships over the lowest model layer. Approximate analytical expressions, similar to those suggested by Louis (1979), are employed for momentum and heat (subscripts m and h for all scalars), respectively,

$$C_{m,h} = C_N f_{m,h}\left(Ri_B, \frac{z_L}{z_{0m}} + 1, \frac{z_L}{z_{0h}} + 1\right) \tag{5.2}$$

$$C_N = \frac{k^2}{ln\left(\frac{z_L}{z_{0m}} + 1\right) ln\left(\frac{z_L}{z_{0h}} + 1\right)} \tag{5.3}$$

where C_N is the neutral transfer coefficient, k the von Kármán constant, z_L the height of the lowest model level, z_{0m} and z_{0h} are the roughness lengths for momentum and heat, and Ri_B is the 'moist' bulk Richardson number of the surface layer defined in terms of cloud conservative variables (total water content and liquid water potential temperature; e.g. Brinkop and Roeckner (1995). The stability functions for momentum and heat, f_m and f_h, representing the ratio of $C_{m,h}$ to their respective values under neutral conditions, are defined similar to Louis (1979) for unstable conditions ($Ri_B < 0$)

$$f_{m,h} = 1 - \frac{a_{m,h} Ri_B}{1 + 3c^2 C_N \sqrt{-Ri_B\left(\frac{Z_L}{Z_{0m}} + 1\right)}} \tag{5.4}$$

where $c = 5$, $a_m = 2c$, $a_h = 3c$,

and for stable and neutral conditions ($Ri_B \geq 0$)

$$f_m = \frac{1}{1 + a_m Ri_B / \sqrt{1 + Ri_B}} \tag{5.5}$$

$$f_h = \frac{1}{1 + a_m Ri_B \sqrt{1 + Ri_B}}. \tag{5.6}$$

Over land, z_{0m} and z_{0h} are specified as functions of subgrid-scale orography and vegetation with an upper limit $z_{0h} \leq 1$ m. For snow covered land, z_{0h} is set to 10^{-3} m. If the grid-cell is partially

covered with snow, a grid-cell mean z_{0h} is obtained from the blending height concept by averaging the respective neutral drag coefficients instead of the roughness lengths (e.g., Claussen (1991)). Over open water, the aerodynamic roughness length z_{0m} is computed from the formula (Charnock, 1955)

$$z_{0m} = \max(0.018u_*^2/g, 1.5 \cdot 10^{-5}m) \tag{5.7}$$

where u_* is the friction velocity and g the acceleration of gravity. Over sea ice, a constant value of 10^{-3} m is prescribed for both z_{0m} and z_{0h}. For the transfer of heat and water vapour over sea, the Charnock relation is modified slightly. Unlike the momentum transfer which is affected by pressure fluctuations in the turbulent wakes behind the roughness elements, heat and water vapour must be transferred by molecular diffusion across the interfacial sublayer. Observational data (Large and Pond, 1982) suggest that the transfer coefficients for heat and water vapour are largely independent of wind speed. In the model, these empirical results are taken into account by a suitable reduction of the aerodynamic roughness length over sea (5.7) according to

$$z_{0h} = z_{0m} \exp\left\{2. - 86.276 z_{0m}^{0.375}\right\}. \tag{5.8}$$

For low wind speed, free convection conditions must prevail. Therefore, in unstable conditions over sea, an empirical interpolation is used between the free convection limit and the neutral approximation (Miller et al., 1992).

$$C_h = C_N \left(1 + C_R^{\gamma}\right)^{1/\gamma} \tag{5.9}$$

$$C_R = \beta \frac{(\Delta\Theta_v)^{1/3}}{C_N |V_L|} \tag{5.10}$$

with $\beta = 0.001$ and $\gamma = 1.25$. $\Delta\Theta_v$ represents the virtual potential temperature difference between the surface and the lowest model level L.

Although the surface fluxes are calculated for three surface types in each grid-cell, i.e. land, water and ice, the area weighting does currently not include fractional land/sea coverages. The only exception are sea points which may partially be covered with ice. In this case, the respective water/ice fluxes enter into the vertical diffusion calculation.

Above the surface layer, the eddy diffusion method is applied, i.e. the vertical turbulent fluxes are related to the gradient of the respective variable according to

$$\overline{w'\chi'} = -K_\chi \frac{\partial \chi}{\partial z} \tag{5.11}$$

where K_χ is the vertical eddy diffusion coefficient. Analogous to the surface layer, different coefficients are used for momentum and heat. The eddy viscosity K_m and eddy diffusivity K_h are parameterized in terms of the turbulent kinetic energy E (e.g., Garratt (1992)).

$$K_{m,h} = \Lambda_{m,h}\sqrt{E} \tag{5.12}$$

with $E = \left(u'^2 + v'^2 + w'^2\right)/2$ and length scales $\Lambda_{m,h} = lS_{m,h}$, where $l = kz(1 + kz/\lambda)^{-1}$ is the mixing length (Blackadar, 1962). The asymptotic mixing length λ is set constant (150 m) for

both heat and momentum throughout the atmospheric boundary layer. In the free atmosphere, λ is assumed to decrease exponentially with height, approaching 1 m in the lower stratosphere. Analogous to the transfer coefficients in the surface layer, the functions $S_{m,h}$ are defined as a product of neutral coefficients S_{Nm}, S_{Nh} for momentum and heat, respectively, and stability functions $g_{m,h}$,

$$S_m = S_{N,m} \cdot g_m \tag{5.13}$$
$$S_h = S_{N,h} \cdot g_m \tag{5.14}$$

where the neutral coefficients are defined according to Mellor and Yamada (1982)

$$S_{Nh} = 3A_2\gamma_1\sqrt{2} \tag{5.15}$$
$$\frac{S_{Nm}}{S_{Nh}} = \frac{A_1}{A_2}\left\{\frac{\gamma_1 - C_1}{\gamma_1}\right\} \tag{5.16}$$

with $A_1 = 0.92$, $A_2 = 0.74$, $B_1 = 16.6$, $C_1 = 0.08$ and $\gamma_1 = 1/3 - 2A_1/B_1$.

The stability functions $g_{m,h}$ are defined consistently with $f_{m,h}$ in the surface layer. In unstable conditions ($Ri < 0$), the stability functions are defined as

$$g_{m,h} = 1 - \frac{a_{m,h}Ri}{1 + 3c^2l^2\left[\left(\frac{\Delta z}{z}+1\right)^{1/3} - 1\right]^{3/2}\left[\frac{\sqrt{-Ri}}{(\Delta z)^{3/2}\sqrt{z}}\right]} \tag{5.17}$$

where z is height, Δz the layer thickness, and Ri is the 'moist' Richardson number at the respective model layer. In stable conditions ($Ri > 0$), the stability functions are defined as

$$g_m = \frac{1}{1 + a_m Ri/\sqrt{1+Ri}} \tag{5.18}$$
$$g_h = \frac{1}{1 + a_m Ri\sqrt{1+Ri}} \tag{5.19}$$

A simplified form of the turbulent kinetic equation is solved, as described by Brinkop and Roeckner (1995), with advection of E neglected,

$$\frac{\partial E}{\partial t} = -\frac{\partial}{\partial z}\left(\overline{w'E} + \overline{w'p'}/\rho\right) - \overline{u'w'}\frac{\partial u}{\partial z} - \overline{v'w'}\frac{\partial v}{\partial z} + \frac{g}{\Theta_v}\overline{w'\Theta_v'} - \epsilon \tag{5.20}$$

All turbulent fluxes in (5.20) are computed from (5.11), with coefficients according to (5.12). $K_E = K_m$ is used for computing the turbulent transport of E (first term, where $w'p'/\rho$ is the pressure correlation term and ρ is density), for computing the shear terms as well as for the buoyancy flux $g(\overline{w'\Theta_v'})/\Theta_v$ which is formulated in terms of total water content and liquid water potential temperature (Brinkop and Roeckner, 1995). As usual, the dissipation rate is set $\epsilon = E^{3/2}/\Lambda_1$ with a dissipation length of $\Lambda_1 = S_{Nm}^{-3}l$. The solution of (5.20) requires the specification of a surface boundary condition for E. Here, the formulation of Mailhot and Benoit (1982) is adopted, i.e. the turbulent kinetic energy close to the surface is defined as

$$E_0 = 3.75u_*^2 \quad \text{(stable surface layer)} \tag{5.21}$$

$$E_0 = S_{Nm}^{-2}u_*^2 + 0.2w_*^2 + (-z_L/L_{MO})^{2/3}u_*^2 \quad \text{(unstable surface layer)} \tag{5.22}$$

where $w^* = \left\{gH(\overline{w'\Theta'_v})_s/\Theta_{vs}\right\}^{1/3}$ is a convective velocity scale, L_{MO} the Monin-Obukhov length, and H the height of the boundary layer. The surface buoyancy flux $\left(\overline{w'\Theta'_v}\right)$ is computed according to (5.1)-(5.10).

6. Surface processes

6.1. Heat budget of the soil

6.1.1. Land surface temperature

The surface energy balance is the link between the atmosphere and the underlying surface, with the surface temperature T_s as the key variable. The interface between the land surface and the atmosphere can be understood as a 'layer' at the surface which is in contact with the atmosphere. The surface energy balance for this layer can then be written as

$$C_L \frac{\partial T_s}{\partial t} = R_{net} + LE + H + G \tag{6.1}$$

where C_L is the heat capacity of the layer [$\mathrm{Jm^{-2}K^{-1}}$], H is the sensible heat flux, LE the latent heat flux (L is the latent heat of vaporization or sublimation of water, respectively), G is the ground heat flux and R_{net} the net radiation consisting of the following components,

$$R_{net} = (1 - \alpha_s)R_{sd} + \epsilon R_{ld} - \epsilon\sigma T_s^4 \tag{6.2}$$

where α_s is the surface albedo, R_{sd} the downwelling solar radiation, R_{ld} the downwelling longwave radiation, ϵ the surface emissivity, and α the Stefan-Boltzmann constant. Note that in (6.1) downward (upward) fluxes are positive (negative). Due to the strong coupling between the surface and the atmosphere, the numerical solution of (6.1) is closely linked to the vertical heat transfer within the atmosphere (c.f. section 5). In ECHAM5, an implicit coupling scheme is used (Schulz et al., 2001) which is unconditionally stable and allows to synchronously calculate the prognostic variables and the surface fluxes. In order to avoid iterations, the nonlinear terms appearing in the flux formulations are replaced by truncated Taylor expansions. These terms are the upward longwave radiation (i.e. the last term in (6.2))

$$\epsilon\sigma(T_s^{n+1})^4 \approx \epsilon\sigma(T_s^n)^4 + 4\epsilon\sigma(T_s^n)^3(T_s^{n+1} - T_s^n) \equiv \epsilon\sigma(T_{rad}^{n+1})^4, \tag{6.3}$$

where T_{rad}^{n+1} is an effective 'radiative temperature' used in the radiation scheme to close the energy balance, and the saturated specific humidity

$$q_s(T_s^{n+1}) \approx q_s(T_s^n) + \left.\frac{\partial q_s}{\partial T_s}\right|_{T_s^n} (T_s^{n+1} - T_s^n) \tag{6.4}$$

where n is the time level. With these linearizations, an expression for T_s^{n+1} is obtained which implicitly includes the surface fluxes at time level $n+1$, and T_s^{n+1}, on the other hand, is used in the vertical diffusion scheme for calculating new fluxes and atmospheric profiles of temperature

and humidity. This ensures energy conservation in the coupled system because the atmosphere receives the same surface fluxes as applied in the land surface scheme.

6.1.2. Soil temperatures

The temperature profile within the soil is calculated from the thermal diffusion equation

$$C_s \frac{\partial T}{\partial t} = -\frac{\partial G}{\partial z} = -\frac{\partial}{\partial z}\left(-\lambda_s \frac{\partial T}{\partial z}\right) \tag{6.5}$$

where $C_s = \rho_s c_s$ is the volumetric heat capacity of the soil, [$\mathrm{Jm^{-3}K^{-1}}$], ρ_s the soil density [$\mathrm{kgm^{-3}}$], c_s the soil specific heat [$\mathrm{Jkg^{-1}K^{-1}}$], G is the thermal heat flux (positive downward), $\lambda_s = \rho_s c_s k_s$ is the thermal conductivity [$\mathrm{Wm^{-1}K^{-1}}$], κ_s the thermal diffusivity [$\mathrm{m^2s^{-1}}$] and z the depth [m]. For the numerical solution of (6.5), the upper 10 m of the soil are divided into 5 unevenly spaced layers with thicknesses, from top to bottom, according to 0.065, 0.254, 0.913, 2.902, and 5.700 [m]. An implicit time integration scheme is applied where the finite difference form of (6.5) is reduced to a system of the type:

$$T_{k+1}^{n+1} = A_k^n + B_k^n T_k^{n+1} \tag{6.6}$$

where n is the time level and k the layer index. The coefficients A_k^n and B_k^n include the vertical increments Δz, the time step Δt, the volumetric heat capacity C_s, the thermal conductivity λ_s and the temperature at time level n in A_k^n. The coefficients A and B are obtained by integrating upward from bottom to top, assuming vanishing heat flux at the bottom of the lowest layer. The solution of (6.6) proceeds from top to bottom by using

$$T_1^{n+1} = T_s^{n+1} \tag{6.7}$$

as the upper boundary condition. For snow-free land, spatially varying C_s and κ_s are prescribed for ice sheets/glaciers and for five soil types according to the FAO soil map. For snow covered land, the solution method remains unchanged, except that a mass-weighted mixture of soil and snow is applied to determine the properties ρ_s, c_s, κ_s. For example, if the snow fills the top soil layer completely, and the next one partially, the respective properties for snow are used for the top layer and a mass-weighted mixture is used for the next one.

6.2. Water budget

Budget equations are formulated for the following water reservoirs (depth in m)

- Snow h_{snc} (water equivalent) intercepted by the canopy
- Snow h_{sn} (water equivalent) at the surface
- Rain water h_{wc} intercepted by the canopy
- Soil water h_{ws}

6.2.1. Interception of snow by the canopy

The snow interception scheme (Roesch et al., 2001) accounts for the effects of snowfall ($c_v S$, where $c_v = 0.25$ is an interception parameter and S the snowfall rate), sublimation of snow from the canopy ($E_{snc} < 0$), or deposition ($E_{snc} > 0$), and unloading of snow due to slipping and melting $U(T_c)$ and wind $U(v_c)$, where T_c and v_c are temperature and wind speed in the canopy, respectively,

$$\rho_w \frac{\partial h_{snc}}{\partial t} = c_v S + E_{snc} - \rho_w h_{snc}[U(T_c) + U(v_c)]. \tag{6.8}$$

The accumulation of snow on the canopy is limited by the capacity of the interception reservoir, $h_{snc} \leq h_{cin}$, where the interception reservoir, h_{cin}, is a function of the leaf area index, LAI,

$$h_{cin} = h_0 LAI \tag{6.9}$$

with $h_0 = 2 \cdot 10^{-4}$ m. The unloading processes are parameterized according to

$$U(T_c) = (T_c - c_1)/c_2 \geq 0 \tag{6.10}$$

$$U(v_c) = v_c/c_3 \geq 0 \tag{6.11}$$

with $c_1 = (T_0 - 3)$, where T_0 is the freezing temperature of water [K], $c_2 = 1.87 \cdot 10^5$ Ks and $c_3 = 1.56 \cdot 10^5$ m. Because T_c and v_c are not available in the model, the respective values at the lowest model level are used instead. Consistent with this assumption, the snow melt parameterized according to (6.10) results in a cooling of the lowest model layer

$$\frac{\partial T_c}{\partial t} = -\rho_w h_{snc} U(T_c) \frac{L_f}{c_p} \frac{g}{\Delta p} \tag{6.12}$$

where Δp is the pressure thickness of the lowest model layer.

6.2.2. Snow at the surface

The snow budget at the surface is given by

$$\rho_w \frac{\partial h_{sn}}{\partial t} = (1 - c_v) S + E_{sn} - M_{sn} + \rho_w h_{snc} U(v_c). \tag{6.13}$$

Here, $E_{sn} < 0$ is the sublimation of snow, $E_{sn} > 0$ the deposition, and M_{sn} is the snow melt

$$M_{sn} = \frac{C_s}{L_f} \left(\frac{T^* - T_0}{\Delta t} \right) \tag{6.14}$$

where C_s is the heat capacity of the snow layer, ρ_w the density of water, L_f the latent heat of fusion, and T^* is the surface temperature obtained from the surface energy balance equation (6.1)

without considering snow melt. The 'final' surface temperature, i.e. including the cooling due to snow melt, is given by

$$T_s = T^* - \frac{L_f}{C_s}(M_{sn}\Delta t) = T_0. \tag{6.15}$$

For the special case of complete melting during one time step $M_{sn}\Delta t$ is limited by the available snow amount $\rho_w h_{sn}$ so that $T^* > T_s \geq T_0$. Over ice sheets and glaciers, snow processes are neglected, i.e. $h_{sn} = h_{snc} = 0$. However, a melting term analogous to (6.14) is diagnosed for $T^* > T_0$ and T_s is set to T_0 in this case.

6.2.3. Interception of rain by the canopy

Analogous to snowfall, a fraction $c_v R$ of the incoming rain R is intercepted in the canopy with an upper limit defined by the capacity of the interception reservoir, h_{cin}, analogous to the interception of snowfall

$$\rho_w \frac{\partial h_{wc}}{\partial t} = c_v R + E_{wc} + \rho_w h_{snc} U(T_c) \tag{6.16}$$

where $E_{wc} < 0$ is the evaporation and $E_{wc} > 0$ the dew deposition. Melting of h_{snc} according to (6.8) and (6.10) contributes to h_{wc} unless the capacity of the interception reservoir is exceeded. In that case, the excess water would contribute to the soil water budget through the term M_{snc} in (6.17).

6.2.4. Soil water

Changes in soil water h_{ws} due to rainfall, evaporation, snow melt, surface runoff and drainage are calculated for a single bucket with geographically varying maximum field capacity h_{cws}

$$\rho_w \frac{\partial h_{ws}}{\partial t} = (1 - c_v)R + E_{ws} + M_{sn} + M_{snc} - R_s - D \tag{6.17}$$

where $E_{ws} < 0$ includes the effects of bare-soil evaporation and evapotranspiration, and $E_{ws} > 0$ the dew deposition. M_{sn} is the snow melt at the surface according to (6.14), M_{snc} the excess snow melt in the canopy, R_s the surface runoff and D the drainage. Runoff and drainage are calculated from a scheme which takes into account the heterogeneous distribution of field capacities within a grid-cell (Dümenil and Todini, 1992). The storage capacity of the soil is not represented by a unique value, as in the traditional bucket scheme, but by a set of values with a probability density function $F(h_{ws})$. Then, a 'storage capacity distribution curve' can be defined, which represents the fraction f_{ws} of the grid-cell in which the storage capacity is less or equal to h_{ws}

$$f_{ws} = 1 - (1 - h_{ws}/h_{cws})^b \tag{6.18}$$

where b is a shape parameter that defines the sub-grid scale characteristics of the basin or grid-cell. By integrating over one time step all fluxes in (6.17) contributing to the total water input

$$Q = \frac{\Delta t}{\rho_w}[(1 - c_v)R + M_{sn} + M_{snc} + \max(0, E_{ws})], \tag{6.19}$$

the surface runoff can be expressed as

$$\frac{\Delta t}{\rho_w} R_s = Q - (h_{cws} - h_{ws}) + \left[\left(1 - \frac{h_{ws}}{h_{cws}} \right)^{1/(1+b)} - \frac{Q}{(1+b)h_{cws}} \right]^{1+b} \tag{6.20}$$

provided that the soil is not brought to saturation during one time step (i.e. $[\cdots] > 0$). In this case, $Q > 0$ will always result in $R_s > 0$ due to the contribution from sub-grid scale areas that become saturated. If, on the other hand, Q and h_{ws} are large enough for generating saturation of the whole grid-cell so that $[\cdots] \leq 0$, the traditional bucket approach is applied, i.e. the surface runoff is given by the excess of water above the maximum value

$$\frac{\Delta t}{\rho_w} R_s = Q - (h_{cws} - h_{ws}). \tag{6.21}$$

The infiltration of water into the soil during one time step can be expressed as $I = Q - R_s \Delta t / \rho_w$. No infiltration is allowed in frozen soil, so that $R_s \Delta t / \rho_w = Q$ in this case. The shape parameter b in (6.18) and (6.20) is parameterized as a function of the steepness of the sub-grid scale terrain, or standard deviation of height σ_z in the grid-cell, according to

$$b = \frac{\sigma_z - \sigma_0}{\sigma_z + \sigma_{max}} \tag{6.22}$$

where $\sigma_0 = 100$ m is a threshold value below which a small constant, $b = 0.01$, is applied, and σ_{max} is a resolution dependent maximum value so that $b \to 0.5$ for $\sigma_z \to \sigma_{max}$. Drainage occurs independently of the water input Q if the soil water h_{ws} is between 5% and 90% of the field capacity h_{cws} ('slow drainage') or between 90% and 100% of h_{cws} ('fast drainage'):

$$D = 0 \text{ for } \{h_{ws} \leq h_{min}\} \tag{6.23}$$

$$D = d_{min} \left(\frac{h_{ws}}{h_{cvs}} \right) \text{ for } \{h_{min} < h_{ws} \leq h_{dr}\} \tag{6.24}$$

$$D = d_{min} \left(\frac{h_{ws}}{h_{cws}} \right) + (d_{max} - d_{min}) \left[\frac{h_{ws} - h_{dr}}{h_{cws} - h_{dr}} \right]^d \text{ for } \{h_{ws} > h_{dr}\} \tag{6.25}$$

with

$$\begin{aligned} d_{min} &= 2.8 \cdot 10^{-7} \text{kg/(m}^2\text{s)} \\ d_{max} &= 2.8 \cdot 10^{-5} \text{kg/(m}^2\text{s)} \\ d &= 1.5 \\ h_{min} &= 0.05 \cdot h_{cws} \\ h_{dr} &= 0.9 \cdot h_{cws}. \end{aligned}$$

6.3. Lake model

A simple scheme is used for calculating the water temperature, ice thickness and ice temperature of lakes, with water/ice fraction of 100% assigned to all non-coastal land points with land fraction $f_l \leq 50\%$. For $f_l > 50\%$, the water/ice fraction is set to zero. The temperature T_w of a constant-depth mixed layer ($h_m = 10$ m) is estimated from the heat budget equation by neglecting both

horizontal heat fluxes and those at the bottom of the layer. Thus, T_w is uniquely determined by the net surface heat flux, H, which represents the sum of all radiative and turbulent flux components,

$$C_w \frac{\partial T_w}{\partial t} = H \tag{6.26}$$

where $C_w = c_w \rho_w h_m$ is the heat capacity of the layer and c_p the specific heat of water at constant pressure. Ice formation may occur if T_w falls below the freezing point T_0. However, for numerical reasons, ice formation is suppressed until the cooling, during a time step, becomes large enough to form a slab of ice with thickness $h_i \geq h_{min}$ and $h_{min} = 0.1$ m. Therefore, the finite difference form of (6.26) includes a residual term ($R_f \leq 0$; see below) which takes into account 'unrealized freezing' from the previous time step in the case $0 < h_i \leq h_{min}$

$$\frac{C_w(T^* - T_w^n)}{\Delta t} = H + R_f \tag{6.27}$$

where n is the time level and T^* a preliminary water temperature.

Cases:

i. $T^* \geq T_0$. Here, the new temperature is given by $T_w^{n+1} = T^*$. Moreover, $h_i^{n+1} = 0$ and $R_f = 0$.

ii. $T^* < T_0$ but $C_w(T^* - T_0)/\Delta t > -(\rho_i L_f h_{min})/\Delta t$, where ρ_i is the ice density and L_f the latent heat of fusion. In this case of 'unrealized ice formation', the cooling is not large enough to form a slab of ice with $h_i \geq h_{min}$, so that $h_i^{n+1} = 0$ and $T_w^{n+1} = T_0$, while

$$R_f = \frac{C_w(T^* - T_0)}{\Delta t} < 0 \tag{6.28}$$

is used in (6.27) at the next time step. Assuming, for example, a constant $H < 0$ in (6.27), R_f will steadily decrease in the course of the integration until the following conditions are fulfilled:

iii. $T^* < T_0$ and $R_f \leq -(\rho_i L_f h_{min})/\Delta t$. In this case, the cooling is large enough to form a slab of ice with $h_i \geq h_{min}$ so that $T_w^{n+1} = T_0$, $R_f = 0$ and

$$h_i^{n+1} = -\left(\frac{C_w}{\rho_i L_f}\right)(T^* - T_0). \tag{6.29}$$

Once a slab of ice is formed (note that partial ice cover is not taken into accout, i.e. a lake is either ice-free or totally covered with ice), changes in ice thickness may result from freezing at the bottom, through conductive heat fluxes (H_c), melting (M_i) at the surface, sublimation of ice ($E_i < 0$) or deposition ($E_i > 0$):

$$\rho_i \frac{\partial h_i}{\partial t} = \frac{(H_c - M_i)}{L_f} + E_i. \tag{6.30}$$

M_i is calculated together with the ice temperature, and H_c is defined as

$$H_c = -\frac{\kappa_i}{h_{eff}}(T_i - T_0) \tag{6.31}$$

where $T_i \leq T_0$ is the surface temperature of the ice layer, κ_i the thermal conductivity of ice and h_{eff} an effective ice thickness which takes into account the effect of a snow layer (with depth h_{sni}) on the conductive heat flux

$$h_{eff} = h_i + \left(\frac{\kappa_i}{\kappa_s}\right) h_{sni} \tag{6.32}$$

where κ_s is the thermal conductivity of snow. The finite difference form of (6.30) involves the calculation of a preliminary ice thickness h^*, analogous to T^* in (6.27),

$$\rho_i \frac{(h^* - h_i^n)}{\Delta t} = \frac{(H_c - M_i)}{L_f} + E_i \tag{6.33}$$

Cases:

i. $h^* \geq h_{min}$ so that $h_i^{n+1} = h^*$.

ii. $0 < h^* < h_{min}$. In this case of 'unrealized melting', part of the available heat is used to decrease the ice thickness to the minimum value $h_i^{n+1} = h_{min}$, while the residual flux

$$R_m = \frac{\rho_i L_f (h_{min} - h^*)}{\Delta t} > 0 \tag{6.34}$$

is used for the calculation of the surface temperature (see below).

iii. $h^* \leq 0$. In this case of complete melting, $h_i^{n+1} = 0$, and the residual heat (if $h^* < 0$) is used to increase the water temperature according to

$$C_w \frac{(T_w^{n+1} - T_w^n)}{\Delta t} = \frac{-\rho_i L_f h^*}{\Delta t} \tag{6.35}$$

with $T_w^n = T_0$.

The surface temperature is calculated from the heat budget of a thin slab of ice with thickness h_0= 0.1 m

$$C_i \frac{\partial T_i}{\partial t} = H + H_c \tag{6.36}$$

where $C_i = \rho_i c_i h_0$ is the heat capacity of the slab and c_i the specific heat of ice. H is the net surface heat flux (sum of all radiative and turbulent flux components) and the conductive heat flux is defined in (6.31). The finite difference form of (6.36) includes the residual term defined in (6.34), which is non-zero (positive) for the case of 'unrealized melting'

$$C_i \frac{(T^* - T_i^n)}{\Delta t} = H + R_m - \frac{\kappa_i}{h_{eff}}(T^* - T_0) \tag{6.37}$$

or, equivalently,

$$\left(\frac{C_i}{\Delta t}+\frac{\kappa_i}{h_{eff}}\right)T^*=H+R_m+\frac{C_i}{\Delta t}T_i^n+\frac{K_i}{h_{eff}}T_0 \tag{6.38}$$

where T^* is a preliminary temperature.

Cases:

i. $T^* \leq T_0$. In this case, the new surface temperature is given by $T_i^{n+1}=T^*$.

ii. $T^* > T_0$. In this case, the new surface temperature is set to the freezing point $T_i^{n+1}=T_0$ and the residual heat flux, i.e. the ice melt

$$M_i=\left(\frac{C_i}{\Delta t}+\frac{\kappa_i}{h_{eff}}\right)(T^*-T_0), \tag{6.39}$$

is used in (6.33) for calculating h_i at the next time step.

The snow depth on lake-ice (h_{sni} in m) is obtained from the following budget equation

$$\rho_w\frac{\partial h_{sni}}{\partial t}=S+E_{sni}-M_{sni} \tag{6.40}$$

where S is the snowfall rate, $E_{sni}<0$ the sublimation, $E_{sni}>0$ the deposition, and M_{sni} the snow melt calculated analogous to (6.39). Note that no melting of ice is allowed unless the snow has vanished completely.

6.4. Sea-ice

Sea-ice concentration, f_{si}, is interpolated in time from monthly observations while sea-ice thickness, h_{si}, is prescribed according to $h_{si}=2$ m (1 m) for the northern (southern) hemisphere, respectively, if $f_{si}>0.01$. Otherwise, $f_{si}=0$ and $h_{si}=0$. Sea-ice temperature is calculated analogous to lake-ice temperature (c.f. (6.36) to (6.38)). The only difference is that the freezing temperature of freshwater ($T_0=0$℃) is replaced by the freezing temperature of saline water, T_{0s} = -1.77℃. Furthermore, a residual heat flux analogous to M_i in (6.39) is calculated for diagnostic purposes (note that h_{si} is not calculated but prescribed) and snow on sea-ice is not taken into account.

6.5. Coupling to mixed layer ocean

As an option, the sea surface temperature, SST, and sea-ice thickness, h_i, can be calculated in a way analogous to the lake model (see section 6.3). The main differences are (i) that the mixed layer depth is assumed to be larger ($h=50$ m) and (ii) that the ocean heat transport has to be taken into account. The heat budget of a constant-depth mixed layer can be written as

$$C_m\frac{\partial T_m}{\partial t}=H-Q \tag{6.41}$$

where $T_m = SST$, H = net surface heat flux (including all radiative and turbulent fluxes), Q = ocean heat transport and C_m is the heat capacity of the slab. While Q is unkown, its monthly climatology, Q_{clim}, can be derived from (6.41) by replacing T_m by the observed SST climatology, T_{clim}, and H by its climatology, H_{clim}. For consistency, H_{clim} has to be computed from the uncoupled AGCM with T_{clim} used as lower boundary forcing, resulting in

$$Q_{clim} = H_{clim} - C_m \frac{\partial T_{clim}}{\partial t}. \tag{6.42}$$

This simple approach of approximating Q in (6.41) by its monthly climatology has the main advantage that systematic errors in simulated SST are practically avoided while SST variability is captured through the variability of H. The main limitation is that variability of ocean heat transports is neglected. The flux (6.42) is applied also, with appropriate area weighting, in those regions where sea-ice is observed, according to climatology, except when the observed ice fraction is larger than 0.9. In order to avoid excessive ice formation in the southern ocean, a constant heat flux of 20 W/m^2 is applied to the sea-ice equation in those regions.

6.6. Surface albedo

For snow-free land surfaces, an annual mean background albedo α_{bg} has been derived from satellite data and values allocated to a high-resolution global distribution of major ecosystem complexes (Hagemann, 2002). For most surfaces, the albedo of snow and ice is assumed to be a linear function of surface temperature, ranging between a minimum value at the melting point $T_s = T_0$ and a maximum value for 'cold' temperatures $T_s \leq T_0 - T_d$:

$$\alpha_{sn} = \alpha_{sn,min} + (\alpha_{sn,max} - \alpha_{sn,min}) f(T_s) \tag{6.43}$$

where

$$f(T_s) = \min \left\{ \max \left[\left(\frac{T_0 - T_s}{T_0 - T_d} \right), 0 \right], 1 \right\} \tag{6.44}$$

with $T_d = T_0 - 1$ for sea-ice and lake-ice (with or without snow) and $T_d = T_0 - 5$ for snow on land and ice sheets.

The minimum and maximum values of snow/ice albedos are assigned as given in table 6.1.

Surface type	$a_{sn,min}$	$a_{sn,max}$
land	0.30	0.80
canopy	0.20	0.20
land ice	0.60	0.80
sea ice	0.50	0.75
lake ice	0.50	0.75
snow on lake ice	0.60	0.80

Table 6.1.: Snow and ice albedos for different surface types

Over snow-covered land, the grid-mean albedo depends on a number of parameters such as the fractional forest area, the leaf area index, the bare-soil albedo, the snow albedo according to

(6.43), and the fractional snow cover of both the ground and the canopy (Roesch et al., 2001). The fractional snow cover at the ground is a function of snow depth (h_{sn} in m water equivalent) and slope of terrain approximated by the subgrid-scale standard deviation of height σ_z

$$f_{sn} = \gamma_1 \tanh(100 h_{sn}) \sqrt{\frac{1000 h_{sn}}{1000 h_{sn} + \gamma_2 \sigma_z + \epsilon}} \tag{6.45}$$

where γ_1=0.95, γ_2= 0.15 and ϵ is a small number used to avoid division by zero for totally flat and snow-free grid-cells. The fractional snow cover of the canopy is defined as

$$f_{snc} = \min\left(1, \frac{h_{snc}}{h_{cin}}\right) \tag{6.46}$$

where h_{snc} is the snow depth at the canopy and h_{cin} the interception capacity. As in the Canadian Land Surface Scheme (CLASS; Verseghy (1991)), the albedo of snow-covered forests is related to a sky view factor (SVF) which describes the degree of canopy closure. The SVF is related to the leaf area index LAI by an exponential function according to

$$SVF = e^{-(rLAI)} \tag{6.47}$$

with $r = 1$ for both needleleaf and broadleaf trees. The total forest albedo is computed as

$$\alpha_{for} = SVF\alpha_g + (1 - SVF)\alpha_{can} \tag{6.48}$$

where α_g is the albedo of the ground

$$\alpha_g = f_{sn}\alpha_{sn} + (1 - f_{sn})\alpha_{bg} \tag{6.49}$$

and α_{can} the albedo of the canopy

$$\alpha_{can} = f_{snc}\alpha_{snc} + (1 - f_{snc})\alpha_{sfr} \tag{6.50}$$

where $\alpha_{snc} = 0.2$ is the albedo of the snow-covered part of the canopy and α_{sfr} the albedo of the snow-free canopy. The grid-mean albedo is finally given by

$$\alpha_{surf} = f_{for}\alpha_{for} + (1 - f_{for})\alpha_g \tag{6.51}$$

where f_{for} is the fractional forest area. To be consistent with the definition of the background albedo α_{bg} (Hagemann, 2002), we set $\alpha_{sfr} = \alpha_{bg}$ so that $\alpha_{surf} = \alpha_{bg}$ for a snow-free grid-cell.

Over water surfaces (lake, ocean), the albedo is set to a constant value $\alpha_{sea} = 0.07$. When a grid-cell is partially covered with sea ice, the grid-mean albedo is defined as a weighted average

$$\alpha_{surf} = f_{sea}\alpha_{sea} + f_{ice}\alpha_{sn} \tag{6.52}$$

where f_{sea} and f_{ice} are the respective fractional areas and α_{sn} is given by (6.43). Note that the land fraction is either 1 (100% land) or zero, so that (6.51) applies to all land points while (6.52) is used for all grid points covered with water and/or ice.

7. Subgrid scale orography parameterization

7.1. Introduction

The Subgrid Scale Orographic Parameterization (hereafter SSOP) developed by Lott and Miller (1997) and Lott (1999) that has been implemented in the ECHAM5 model is aimed at representing the effects of orographic variations on scales smaller than the typical horizontal resolution of a climate model.

The orography may affect the atmospheric flow in many ways. The SSOP considered in ECHAM5 takes into account two main mechanisms of interaction between the orography and the atmospheric flow:

1. momentum transfer from the earth to the atmosphere accomplished by orographic gravity waves and
2. the drag exerted by the subgrid scale mountains when the air flow is blocked at low levels.

The part of the SSOP concerning the propagation and dissipation of the orographic gravity waves follows the formulation of Palmer et al. (1986) and Miller et al. (1989). In addition, the SSOP has options for including the effects of low level trapped lee waves and of subgrid scale orographic lift (Lott, 1999).

Concerning the specification of the gravity wave forcing, the SSOP includes a relatively detailed description of the subgrid scale orography (based on the work of Baines and Palmer (1990) in order to take into account anisotropic orography and directional effects.

7.2. Representation of the subgrid scale orography

At one gridpoint, it is assumed that the subgrid scale orography can be described by seven parameters: the standard deviation μ, the anisotropy γ, the slope σ, the orientation θ, the minimum Z_{min}, the maximum Z_{max}, and the mean Z_{mea} elevation of the orography.

These parameters are evaluated offline for each gridpoint from the US Navy (10'x10') topographic dataset. The last three parameters are taken directly from the US Navy data set (for each horizontal model resolution considered), while the first four parameters are derived from topographic gradients relationships as formulated by Baines and Palmer (1990). In order to derive relationships between the low level flow and the orientation of the orography, it is assumed that the subgrid scale orography has the shape of an elliptical mountain. Thereafter, in each gridbox a typical number of elliptical mountains is considered. For a brief description and additional references see Lott and Miller (1997).

Concerning the large scale flow, it is assumed that the model mean orography is the optimal representation (eg, the so-called envelope orography used sometimes in low resolution models is excluded).

7.3. Low level drag and gravity wave stress

In case that the subgrid scale mountains are high enough, the vertical motion of the air is limited and part of the low level flow (below the mountain top) is blocked and a drag should be provided at the model levels that intersect the subgrid scale orography (the so-called low level drag). Given a non-dimensional height of the mountain: $H_n = NH/U$, where H is the maximum elevation of the mountain, U the wind speed and N the Brunt-Väisäla frequency, it can be shown theoretically that part of the low level flow is blocked for $H_n >> 1$. For $H_n << 1$ all the flow goes over the mountain and gravity waves are generated by the vertical motion of the air (Lott and Miller, 1997).

In the parameterization, it is distinguished between the incident flow, flowing above the mountain and forcing the gravity waves, and the blocked flow, associated with the low level drag. The incident flow is defined as the average of the wind speed, the Brunt-Väisäla frequency, and the fluid density between the model ground, Z_{mea}, and the mountain peak, Z_{max}. This flow is referenced as U_H, N_H, and ρ_H, respectively. Concerning the blocked flow, the parameter of interest is the height of the blocked flow, Z_b defined as the highest level that satisfies the condition:

$$\int_{Z_b}^{Z_{max}} \frac{N}{U_p} dz \leq H_{NC} \tag{7.1}$$

where the wind speed U_p is calculated by resolving the wind $\overrightarrow{U}$ in the direction of the incident flow. The parameter H_{NC} tunes the depth of the blocked flow layer and is of order one.

The low level drag for each layer below Z_b is given by:

$$\overrightarrow{D}_b(z) = -\rho C_d max\left(2 - \frac{1}{r}, 0\right) \frac{\sigma}{2\mu} \left(\frac{Z_b - z}{Z_b - Z_{mea}}\right) \left(B\cos^2\psi_H + C\sin^2\psi_H\right) \frac{\overrightarrow{U}\left|\overrightarrow{U}\right|}{2} \tag{7.2}$$

where ψ_H is the angle between the incident flow and the normal orographic ridge direction, the constants B and C are functions of the anisotropy, and r is the aspect ratio of the ridge as seen by the incident flow (see Lott and Miller (1997) and Lott (1999)).

If there is low level flow blocking, it is therefore assumed that the effective height, Z_{eff}, of the orography seen by the atmospheric flow is reduced to $Z_{max} - Z_b$. In case that there is no low level flow blocking, $Z_{max} - Z_{min}$ is instead used as effective height.

Taking into account the difference in orientation between a orographic ridge and the incident flow and the typical number of ridges within a gridbox, the gravity wave stress at the source level is given by:

$$\tau = \rho_H G U_H N_H Z_{eff}^2 \frac{\sigma}{4\mu} \left|\overrightarrow{P}\right| \tag{7.3}$$

where the parameter G tunes the gravity wave stress amplitude and is of order one. The directional vector $\overrightarrow{P}$ is given by:

$$\overrightarrow{P} = (B\cos^2\psi_H + C\sin^2\psi_H; (B-C)\sin\psi_H\cos\psi_H) \tag{7.4}$$

7.4. Gravity wave drag

Above the source level the gravity wave stress is constant, except when the waves encounter a critical level or when they break. Given that the gravity wave drag is the vertical derivative of the gravity wave stress, the gravity waves produce a drag on the resolved flow only when a critical level is reached or when they become unstable and break, in agreement with wave-mean flow theory.

A critical level is encountered when the background wind turns with height so that it becomes zero in the plane of the low level stress. If this happens, the gravity wave stress is set to zero at that level.

The part of the SSOP that concerns gravity wave breaking follows the original formulation of Palmer et al. (1986), that uses a breaking condition based on the Richardson number and the Lindzen (1981) saturation hypothesis to determine the stress at the breaking level.

At each model level a minimum Richardson number that includes the gravity wave influence on the static stability and wind shear is evaluated:

$$Ri_{min} = Ri\frac{1-(N\delta h/U)}{\left\{1+Ri^{1/2}(N\delta hU)\right\}^2} \tag{7.5}$$

where $Ri = (N/(dU/dz))^2$ is the background (resolved) flow Richardson number, N the background static stability, U the background wind speed (derived from the projection of the wind vector in the plane of the low level stress), and δh is the amplitude of the vertical displacement induced by the gravity waves. δh is derived following a steady two dimensional model of gravity waves and is given by:

$$\delta h^2 = G\frac{\rho_H N_H U_H}{\rho N U} Z_{eff}^2 \tag{7.6}$$

Ri_{min} is a lower bound (hence 'minimum') to the Richardson number, in the sense that it is the minimum value that can be anticipated from a steady two dimensional model of gravity wave propagation (Palmer et al., 1986).

It is assumed that instability occurs if $Ri_{min} < Ri_c$, where Ri_c is the critical Richardson number equal to 0.25. This condition takes into account the occurrence of both convective overturning and shear instability.

If the critical Richardson number is reached, the waves are assumed to saturate: their amplitude is limited to the value at which instability occurs (Lindzen, 1981). The wave vertical displacement is therefore computed from the Ri_{min} equation with $Ri_{min} = Ri_c$. This vertical displacement, ε, is thereafter used in the gravity wave stress at the breaking height, the saturation stress:

$$\tau_s = \rho\frac{U^3}{N}\varepsilon^2\frac{\sigma}{2\mu} \tag{7.7}$$

The equation for the saturation stress is obtained following Lindzen (1981). Thereafter, above the breaking level, the gravity wave stress remains constant and equal to the saturation stress, if the condition for instability is not reached again.

In the parameterization, the calculation of the gravity wave stress proceeds from the bottom to the top of the vertical column. The procedure of evaluating the Richardson number and the search for instability is therefore applied from the bottom up, and can produce more than one breaking level.

8. Parameterization of the momentum flux deposition due to a gravity wave spectrum

8.1. Introduction

The parameterization of the effects of a gravity wave spectrum is based on the Doppler spread theory of propagation and dissipation of a gravity wave spectrum as formulated by Hines (1991a,b,c, 1993). The simplifications to the Doppler spread theory necessary for developing the parameterization are discussed in Hines (1997a,b). Here the version of the parameterization formulated following Hines (1997a,b) that has been implemented in the middle atmosphere (MA) version of ECHAM5. The impact of the Doppler spread parameterization in the middle atmosphere of the previous model cycle (MAECHAM4) has been discussed by Manzini et al. (1997) and Manzini and McFarlane (1998).

8.2. Hines Doppler spread theory

During the last decades, an increasing number of observations by a variety of techniques has contributed to the current characterization of atmospheric gravity waves (among others, Allen and Vincent (1995); Eckermann et al. (1994); Hamilton (1991); Smith et al. (1987); Dewan and Good (1986); Hirota (1984)). The forcing mechanisms generating the gravity waves are most likely located in the troposphere, and may include convective activity, shear instabilities, frontal systems, transient flow over topography. In the middle atmosphere, the gravity waves appear to propagate predominantly upward from their tropospheric source regions and they appear to form a broad background spectrum of waves.

On the basis of these observations, the Hines Doppler spread theory (henceforth, HDST) assumes an interacting and upward propagating gravity wave spectrum with tropospheric sources. The HDST does not directly deal with the forcing mechanisms of the gravity waves. The HDST considered in the current parameterization only assumes that the variety of the forcing mechanisms gives rise to a broad band and continuous spectrum. Within this framework, quasi monochromatic waves cannot be take into account, although extensions are possible (Hines, 1997b).

Evidence that the vertically propagating gravity waves are dissipating and therefore interacting with the large scale flow has been derived form the observations that the amplitude of the spectrum at high vertical wavenumbers tends not to change with height, in spite of the growth expected in response to the decrease in atmospheric density, a behavior usually termed saturation (Smith et al., 1987; Dewan and Good, 1986). A variety of processes can be responsible for saturation (see Fritts (1984, 1989) for reviews). According to the HDST, as the gravity waves propagate upwards from the troposphere to the mesosphere, an essential role in the saturation process is played be the nonlinear advective interaction exerted on each wave component of the spectrum by the gravity wave wind field induced by the other waves.

The HDST builds upon gravity wave theory for small amplitude waves propagating in a mean flow that is uniform horizontally and temporally and slowly varying in altitude (for a review of gravity wave theory see Andrews et al. (1987)). The core aspects of the Hines Doppler spread theory (Hines, 1991a,b,c, 1993) are here briefly summarized:

1. The effects of the wind field induced by the other waves on each wave component of the spectrum at a given height are assumed to be approximately determined by treating the wave induced wind field as a background horizontal wind field, slowly varying in altitude while horizontally and temporally uniform. As the waves propagate upward, their vertical wavenumber spectrum is therefore modified, and in turn the spectral characteristics of the wave induced wind field are also modified. In a statistical sense, the modification induced by the advective nonlinear interaction is found to be a Doppler spreading of the vertical wavenumber spectrum towards high wavenumbers.

2. In conformity with wave theory, wave action density is conserved as the waves propagate upwards, until the gravity wave spectrum as a whole becomes unstable and the waves at high vertical wavenumbers break down into turbulence. For parameterization purposes the transition to turbulence is taken to occur at a specific vertical wavenumber, the *maximum permissible vertical wavenumber* m_M, and the breaking waves (with $m > m_M$) are removed from the spectrum. Within the HDST it is possible to assume a more complex and smooth transition to turbulence. The momentum carried by the waves that have been removed is deposited into the large scale background flow.

3. In agreement with wave-mean flow interaction theory (Andrews et al., 1987), within the HDST formulation the background large scale flow has the effect of producing Doppler shifts of the vertical wavenumber. In the presence of a background large scale flow, differential momentum flux deposition (hence forcing of the large scale flow) can therefore occur also for an isotropic gravity wave spectrum. Consequently, it becomes necessary to take into account the variations in the azimuth of wave propagation. Note that in the absence of a background large scale flow and for an isotropic gravity wave spectrum, the momentum flux would be deposited isotropically and no *net* deposition of momentum flux would occur.

4. An aspect of the Hines formulation crucial to the practical development of a parameterization is that at any given height, the spectral characteristics of the gravity waves are determined by a modification of the gravity wave spectrum at a specified low altitude. The calculation of the spectral evolution with altitude is therefore by-passed in the parameterization, by keeping track of the portion of the gravity wave spectrum at the specified low altitude which continue to propagate upward. The largest vertical wavenumber of the spectrum at the specified low altitude that continues to propagate upward at the current height of interest is called the *cutoff vertical wavenumber* m_C. The vertical evolution of m_C is the key computation of the parameterization. A drastic reduction of the gravity wave quantities describing the vertical evolution of the gravity wave spectrum is therefore achieved, a requirement for any parameterization of practical use in a general circulation model.

8.3. The Hines Doppler Spread Parameterization (HDSP)

The quantity that has to be evaluated is the deposition of the horizontal momentum transferred by the vertically propagating gravity waves (what is referred to as momentum flux deposition). As commonly done in a general circulation model, only vertical propagation is considered, assuming that a gridbox is large enough that oblique propagation (outside the vertical column) can

be neglected. For each gridbox, the dependence in the azimuth of wave propagation must be discretized: the total number of azimuths considered is defined to be J. It is assumed (although not necessary) that the J azimuths are equally spaced around the azimuth circle.

Within this framework, the HDSP requires the specification of the input gravity wave spectrum at some low altitude (within the forcing region). Thereafter, the momentum flux deposition is determined in function of the large scale flow and buoyancy frequency, the input gravity wave spectrum at a specified low altitude, and a limited number of height varying gravity wave related quantities, the most important being the horizontal wind variance and the cutoff vertical wavenumber. These quantities are defined and derived below.

At any given height, the broad band gravity wave spectrum is characterized by the power spectral density H_j^2 of the horizontal winds associated with the gravity waves at that height in the j-th azimuth. The power spectral density is a function of horizontal wavenumber k (a directional wavenumber in the j-azimuth) and vertical wavenumber m. The spectrum is assumed to be separable in k and m. For convenience, k and m are made positive for upward propagating waves.

The *horizontal wind variance* at the height of interest that is contributed by the waves propagating in the j-th azimuth is the integral over all positive horizontal and vertical wavenumbers of the power spectral density:

$$s_j^2 = \int_0^{m_M} \int_0^{\infty} H_j^2 dk dm \tag{8.1}$$

The integral in the vertical wavenumber is limited by the maximum permissible vertical wavenumber m_M (see point 2 in section 8.2). The s_j^2 are derived in section 8.3.2.

At any given height, the *total rms horizontal wind speed* σ_T is contributed by gravity waves propagating in all azimuths:

$$\sigma_T = \left(\sum_{j=1}^{J} s_j^2 \right)^{1/2} \tag{8.2}$$

At any given height, the *total rms horizontal wind speed σ_j in the j-th azimuth* depends on the variance from waves in the j-th azimuth and in all other azimuths, non-orthogonal to the j-th direction. These contributions must be added up, and they are found by projecting the s_j^2 wind variances on the azimuth of interest. The total rms horizontal wind speed σ_j in the j-th azimuth is:

$$\sigma_j = \left(\sum_{p=1}^{J} s_p^2 \cos(\alpha_p - \alpha_j)^2 \right)^{1/2} \tag{8.3}$$

where α_p and α_j are respectively the p- and j-th azimuth.

The height where the gravity wave spectrum is specified is defined to be the *initial (or launching) height*, and any gravity wave quantity at the initial height is given the subscript I.

8.3.1. Cutoff vertical wavenumber

At any given height, the dispersion relation for an individual gravity wave with azimuth j in a background flow that is horizontally and temporally uniform, is:

$$\omega/k = N/m + V_j + v_j \tag{8.4}$$

where k is the horizontal wavenumber, m the vertical wavenumber, ω the ground based frequency, N the buoyancy frequency, and V_j and v_j are respectively the large scale background flow and the wave induced wind field in the j-th azimuth. For convenience, k, ω and m are made positive for upward propagating waves. Given that ω and k are height independent, from the combination of equation (8.4) as written for the initial height and for some overlying height of interest, it is obtained:

$$N/m = N_I/m_I + V_{jI} - V_j - v_j \tag{8.5}$$

assuming that the induced wave field at the initial height is negligible. Equation (8.5) expresses the mapping between the vertical wavenumber m at the height of interest and the corresponding vertical wavenumber m_I at the initial height. In equation (8.5), N_I and V_{jI} are respectively the buoyancy frequency and the j-directed large scale background flow at the initial height.

Equation (8.5) shows that as $V_j + v_j$ increases, the vertical wavenumber m is Doppler shifted to infinity and into negative values. Before reaching negative values, at sufficiently large vertical wavenumbers, the spectrum is likely to become unstable and dissipative processes are likely to take place (the vertical wavelength is reduced, critical level conditions are approached). In practice, it is assumed that this transition occurs at a specific vertical wavenumber m_M (large, positive and less than infinity), the maximum permissible vertical wavenumber of the spectrum at the height of interest (already introduced, see point 2 in section 8.2). The waves with wavenumbers equal or larger than m_M are supposed to be dissipated and are removed from the spectrum. The vertical wavenumber m_M may be reached by a wave when the wave induced wind field v_j increases to the value:

$$v_{jM} = N_I/m_I - N/m_M + V_{jI} - V_j \tag{8.6}$$

The probability for the induced wind field to meet condition (8.6) was first derived in Hines (1993) for the case of no large scale background flow and m_M equal to infinity, in order to determine the cutoff vertical wavenumber m_C (see point 4 in section 8.2). In Hines (1993) it was found that the probability for a wave to survive to some height decreases rapidly as m_I enters a particular critical range. On the basis of this rapid transition and further approximations (Hines, 1997a), an expression for v_{jM} is found in order to evaluate a provisional (i.e., subject to two conditions expressed below) cutoff vertical wavenumber in the j-th azimuth for the general case of a positive and finite m_M and a nonzero background flow:

$$\{m_j\}_{TRIAL} = N_I(N/m_M + V_j - V_{jI} + \Phi_1\sigma_j)^{-1} \tag{8.7}$$

with v_{jM} expressed in terms of the total rms wind speed in the j-th azimuth σ_i. The coefficient Φ_1 that appears in (8.7) is a nondimensional factor that lays in the range: $1.2 < \Phi_1 < 1.9$, deduced in Hines (1993, 1997a). In (8.7) the cutoff vertical wavenumber m_C is a function of azimuth and is denoted m_j.

The maximum permissible wavenumber m_M was determined in Hines (1991b) by the condition of marginal instability of the total wave system. In Hines (1997a) the derivation is extended by approximation to the case of a nonzero background flow, so that:

$$N/m_M = \Phi_2 \sigma_T \tag{8.8}$$

where Φ_2 is a second nondimensional factor that lays in the range: $0.1 < \Phi_2 < 0.4$ deduced in Hines (1991b, 1997a). The limits of Φ_2 are intended to roughly correspond to 17% or 8% of space time being convectively unstable, with and additional 10% or 4 % being dynamically unstable. Inserting (8.8) in (8.7), the provisorial cutoff wavenumber in the j-th azimuth becomes:

$$\{m_j\}_{TRIAL} = N_I(\Phi_2 \sigma_T + V_j - V_{jI} + \Phi_1 \sigma_j)^{-1} \tag{8.9}$$

Equation (8.9) is the fundamental equation of the HDSP. The first term on the right-hand side of equation (8.9) represents the effect of instability of the spectrum as a whole at the height of interest. The $V_j - V_{jI}$ term represents the effect of Doppler shifting by the background winds, common for instance also to parameterizations based on **?**. The $\Phi_1 \sigma_j$ term (unique to this theory) represents the nonlinear effect of localized Doppler shifting on individual waves by all the other waves.

The two above mentioned conditions to be imposed on $\{m_j\}_{TRIAL}$ are: (1) the cutoff wavenumber must be monotonically non increasing with height, (2) the cutoff wavenumber must be positive. Equation (8.9) shows that these conditions can be achieved, because there always exists a positive m_j at the initial height, where $V_j - V_{jI}$ is zero.

8.3.2. Horizontal wind variance

At the height of interest and in the j-th azimuth, an elementary contribution of the power spectral density H_j^2 of the horizontal winds associated with the gravity waves to the horizontal wind variance is written:

$$H_j^2 dk dm = \rho^{-1} \rho_I s_{jI}^2 K_j(k) M_j(m) dk dm \tag{8.10}$$

where ρ is the atmospheric density and ρ_I is its value at the initial height. K_j and M_j are respectively the horizontal and vertical wavenumber spectra in the j-th azimuth (the spectrum is assumed to be separable in k and m). The integrals of $K_j dk$ and $M_j dm$ over all positive values are taken to be normalized to 1 at the initial height. As required by the definition of spectral density, the integral of the horizontal wind power spectral density at the initial height is therefore equal to s_{jI}^2, the horizontal wind variance at the initial height.

The theory and the parameterization as developed to date consider that the K_j spectrum is unchanging with height, while the M_j spectrum evolves in response to the background large scale flow, buoyancy frequency, and nonlinear interactions.

Thereafter, the conservation of the vertical flux of the horizontal momentum (or equivalently wave action, see point 2 in section 8.2) is used to compute the horizontal wind variance. Given that the vertical flux of the horizontal momentum transported by the waves that are not yet removed

from the spectrum is conserved, the portion of the spectra not removed at the height of interest and that at the initial height are related by:

$$(HW)_j dm = \rho^{-1} \rho_I (HW)_{jI} dm_I \tag{8.11}$$

where an elemental range dm_I of the initial spectrum is mapped into the range dm at the height of interest. $(HW)_j$ represents the covariance spectrum of the horizontal and vertical velocity fluctuations associated with the gravity waves, the vertical flux of horizontal momentum transferred by the waves, at the height of interest. $(HW)_{jI}$ is the covariance at the initial height.

Following gravity wave theory, the vertical velocity perturbation is in phase with the horizontal velocity perturbation and is given by k/m times the horizontal velocity, hence:

$$H_j^2 dm = \rho^{-1} \rho_I H_{jI}^2 (m/m_I) dm_I \tag{8.12}$$

the horizontal wavenumber k being constant with height.

The determination of the horizontal wind variance in the j-th azimuth at the height of interest can therefore be achieved by integration of the right-hand side of equation (8.12) over all positive m_I up to the cut off vertical wavenumber m_j. For this purpose, m on the right must be written as a function of m_I. This can be done by means of (8.5), with the induced wind field contribution v_j ignored, under the approximation that the spreading effect is significant only for waves at large vertical wavenumber, and that the contribution of those waves to the total wind variance is small Hines (1991a):

$$m/m_I = N/N_I (1 - (V_j - V_{jI}) m_I / N_I)^{-1} \tag{8.13}$$

Substituting (8.13) into (8.12) and integrating over all positive k and m, the horizontal wind variance at any height is obtained:

$$s_j^2 = \rho^{-1} \rho_I N N_I^{-1} s_{jI}^2 \int_0^{m_j} M_{jI}(m_I)(1 - N_I^{-1}(V_j - V_{Ji}) m_I)^{-1} dm_I \tag{8.14}$$

The determination of the evoluted M_j spectrum is therefore by-passed by the mapping between the spectrum at the current height and the initial spectrum. The initial spectrum M_{jI} and the cutoff vertical wavenumber m_j are all what is needed to compute the horizontal wind variance.

8.3.3. Momentum flux deposition

At any given height, the vertical flux density of the j-directed horizontal momentum that is transferred upward by the j-directed waves is:

$$F_j = \rho \int_0^{m_M} \int_0^{\infty} (HW)_j dk dm \tag{8.15}$$

where (HW) is the covariance spectrum of the horizontal and vertical velocity fluctuations associated with the gravity waves already introduced. Using again the conservation of horizontal

momentum for the portion of the spectra not removed, the j-directed flux density at the height of interest can be written in terms of the spectrum at the initial height:

$$F_j = \rho_1 s_{jI}^2 K^* \int_0^{m_j} M_{jI}(m_I) m_I^{-1} dm_I \tag{8.16}$$

Where K^* is obtained by the integration of $kK_j dk$ over all positive k, and by neglecting the dependence on azimuth for simplicity (although not necessary). K^* can be considered a weighted average of the directional horizontal wavenumber, and is called the *characteristic horizontal wavenumber*. In (8.16) the integral in vertical wavenumber m_I is limited by the m_j cutoff vertical wavenumber. Height variations in F_j are therefore expressed by the dependence in height of the m_j cutoff vertical wavenumber.

In order to compute the rate of horizontal momentum flux deposition at each gridpoint of the general circulation model, the momentum flux must be expressed in the cardinal eastward and northward azimuths, respectively. The rate of horizontal momentum flux deposition is thereafter given by the vertical convergence of the momentum flux in the cardinal directions.

8.4. Summary

The parameters that must be specified at the initial (launching) height are the total rms gravity wave wind speed σ_{TI}, the initial vertical wavenumber spectrum M_{jI}, and the s_{jI}^2 variances, which sum over the azimuths must be σ_{TI}^2, as defined in (8.2). In addition, the location of the initial height, the characteristic horizontal wavenumber K^*, and the nondimensional factors Φ_1 and Φ_2 must be specified.

Given that the current knowledge about the global and seasonal distributions of these gravity wave parameters is very limited, simple choices have been made so far, based on the generalization of observations of gravity wave variances and spectra, for instance Allen and Vincent (1995); Fritts and Nastrom (1992); Vincent et al. (1997).

The vertical wavenumber spectrum at the initial height is assumed to follow a power law form in the initial vertical wavenumber, extending from $m_I = 0$ to the cutoff vertical wavenumber m_{jI} at the initial height. Its integral must be normalized to 1 at the initial height, therefore:

$$M_{jI}(m_I) = (s+1) m_{jI}^{-s-1} m_I^s \tag{8.17}$$

where s is the slope. The cutoff vertical wavenumber m_{jI} at the initial height is computed from (8.9) with $V_j = V_{jI}$:

$$m_{jI} = N_I (\Phi_2 \sigma_{TI} + \Phi_1 \sigma_{jI})^{-1} \tag{8.18}$$

The computation of the cutoff vertical wavenumber m_j thereafter proceeds upward. At the first step upward and above the m_j is obtained by (8.9), subjected to the conditions of being monotonically non increasing with height and positive. In principle, above the initial height the horizontal wind variance at that vertical level should be used in (8.9). However, the horizontal wind variance at that vertical level depends in turn on the cutoff vertical wavenumber that has to be evaluated. An iteration procedure would therefore be required. As Hines (1997a) has suggested, in case the vertical resolution of the general circulation model is sufficiently high, the

iteration can be avoided by using in the computation of the m_j at any vertical level above the initial height the horizontal wind variance at the level immediately below. This approach is used in the parameterization implemented in the ECHAM5 model.

9. Cumulus convection

As in ECHAM4, a mass flux scheme (Tiedtke, 1989) is applied for cumulus convection with modifications for penetrative convection according to Nordeng (1994). The contribution of cumulus convection to the large scale budgets of heat, moisture and momentum is represented by an ensemble of clouds consisting of updrafts and donwdrafts in a steady state. The bulk equations for mass, heat, moisture, cloud water and momentum for an ensemble of cumulus updrafts are

$$\frac{\partial M_u}{\partial z} = E_u - D_u \tag{9.1}$$

$$\frac{\partial}{\partial z}(M_u s_u) = E_u \overline{s} - D_u s_u + L\overline{\rho} c_u \tag{9.2}$$

$$\frac{\partial}{\partial z}(M_u q_u) = E_u \overline{q} - D_u q_u - \overline{\rho} c_u \tag{9.3}$$

$$\frac{\partial}{\partial z}(M_u l_u) = -D_u l_u + \overline{\rho} c_u - \overline{\rho} P_u \tag{9.4}$$

$$\frac{\partial}{\partial z}(M_u u_u) = E_u \overline{u} - D_u u_u \tag{9.5}$$

$$\frac{\partial}{\partial z}(M_u v_u) = E_u \overline{v} - D_u v_u \tag{9.6}$$

where the subscript u denotes updraft variables and the overbar denotes large-scale variables. E is entrainment, D is detrainment, $s = c_p T + gz$ the dry static energy, ρ the air density, q is specific humidity, l the cloud water mixing ratio, c_u the release of latent heat from condensation, P_u the conversion of cloud water to precipition, and u and v are the components of the horizontal wind vector. A corresponding set of equations is used for the cumulus downdrafts which are assumed to originate from mixing of cloud air with environmental air which has been cooled to its wet bulb temperature by evaporation of precipitation generated in the updrafts. The cloud water detrainment in (9.4) is used as a source term in the stratiform cloud water/ice equations (10.2, 10.3).

9.1. Organized entrainment

In Tiedtke (1989), organized entrainment is consistent with the closure and is based on a moisture convergence hypothesis. Nordeng (1994), on the other hand, assumes organized entrainment to take place as inflow of air into the cloud when cloud parcels accelerate upwards, i.e. when the buoyancy is positive. Organized detrainment takes place where the air decelerates, i.e. when the buoyancy becomes negative. Organized entrainment and detrainment are therefore related to the cloud activity itself. Fractional entrainment and detrainment rates, ϵ_i and δ_i (Turner, 1963), are introduced so that for an individual updraft i, $E_i = M_i \epsilon_i$ and $D_i = M_i \delta_i$, and for the cloud

ensemble

$$E = M\epsilon = \sum_i M_i \epsilon_i = \sum_i E_i \tag{9.7}$$

$$D = M\delta = \sum_i M_i \delta_i = \sum_i D_i \tag{9.8}$$

where the cloud ensemble mass flux is defined as

$$M = \sum_i M_i = \sum_i \overline{\rho} \sigma_i w_i \tag{9.9}$$

with fractional area σ_i and vertical velocity w_i. Equation (9.1) can then be expressed as

$$\frac{1}{M}\frac{\partial M}{\partial z} = \epsilon - \delta \tag{9.10}$$

where the subscript u denoting the updraft has been omitted for convenience (in the following as well). According to Simpson and Wiggert (1969), the steady state vertical momentum equation for an individual updraft is given by

$$w_i \frac{\partial w_i}{\partial z} = b_i - \epsilon_i w_i^2 \tag{9.11}$$

where b_i is the buoyancy term which may include water loading and non-hydrostatic effects. Assuming that the fractional area σ_i of each individual updraft is constant with height (except in the ouflow part, see later), organized entrainment, according to (9.9) and (9.10), can be written as

$$\epsilon_i = \frac{1}{M_i}\frac{\partial M_i}{\partial z} = \frac{1}{w_i}\frac{\partial w_i}{\partial z} + \frac{1}{\overline{\rho}}\frac{\partial \overline{\rho}}{\partial z} \tag{9.12}$$

whenever the buoyancy is positive ($\delta_i = 0$). By integrating (9.11) upwards, starting at cloud base ($z = 0$), and using (9.7), (9.11) and (9.12), the organized entrainment rate of the cloud ensemble becomes

$$\epsilon = \frac{b}{2\left(w_0^2 + \int_o^z b dz\right)} + \frac{1}{\overline{\rho}}\frac{\partial \overline{\rho}}{\partial z} \tag{9.13}$$

with the ensemble buoyancy $b = \frac{g}{\overline{T}_v}(T_v - \overline{T}_v) - gl$.

9.2. Organized detrainment

Organized detrainment is defined as the loss of total massflux due to detrainment of those clouds which are losing their buoyancy, i.e.

$$D = E - \frac{\partial M}{\partial z} = \sum_i \overline{\rho}\sigma_i w_i \left(\frac{1}{w_i}\frac{\partial w_i}{\partial z} + \frac{1}{\overline{\rho}}\frac{\partial \overline{\rho}}{\partial z}\right) - \frac{\partial}{\partial z}\sum_i \overline{\rho}\sigma_i w_i = -\sum_i \overline{\rho} w_i \frac{\partial \sigma_i}{\partial z} \tag{9.14}$$

Since the fractional area of each individual member of the ensemble is assumed to be constant with height, except for the detrainment level, the only contribution to the sum in (9.14) comes from those members of the ensemble which detrain at this level (k), i.e.,

$$D = -\sum_k \overline{\rho} w_k \frac{\partial \sigma_k}{\partial z} \approx \frac{\overline{\rho} \sigma_k w_k}{\Delta z} = \frac{M_k}{\Delta z} \tag{9.15}$$

where Δz is the depth over which the detrainment takes place. Thus, organized detrainment is equal to the change of mass flux with height. Since the in-cloud vertical velocities are primarily a function of the height above cloud base and, hence, $w_k \approx w$, and due to the assumption that individual clouds do not change their area fraction before they start to detrain, the individual cloud cover change is equal to the total, i.e.,

$$\frac{\partial \sigma_k}{\partial z} = \frac{\partial \sigma}{\partial z} \tag{9.16}$$

so that, according to (9.15) and (9.16), the organized detrainment may be parameterized as

$$D = -\frac{M}{\sigma} \frac{\partial \sigma}{\partial z} \tag{9.17}$$

It remains to determine the variation of cloud cover with height. Having obtained the level where clouds start to detrain (z_d), an analytical function $\sigma = \sigma(z)$ is specified with boundary values $\sigma(z_d) = \sigma_0$ and $\sigma = (z_t) = \sigma_0$, where z_t is the highest possible cloud level obtained from undiluted ascent starting at cloud base. In the parameterization, the spectrum of clouds detraining at different levels is realized through the following function

$$\sigma(z) = \sigma_0 \cos\left[\frac{\pi}{2} \frac{(z - z_d)}{(z_t - z_d)}\right] \tag{9.18}$$

Except for being continuous at $z = z_d$, and satisfying the boundary conditions specified above, there is no physical reason for chosing this particular function.

9.3. Adjustment closure

The adjustment-type closure suggested by Nordeng (1994) relates the cloud base mass flux to convective instability. The dominant part of convective heating and drying, respectively, is due to compensating subsidence in the environment Fritsch and Chapell (1980)

$$\frac{\partial \overline{T}}{\partial t} \approx \frac{1}{\overline{\rho} c_p} M \frac{\partial \overline{s}}{\partial z} \tag{9.19}$$

$$\frac{\partial \overline{q}}{\partial t} \approx \frac{1}{\overline{\rho}} M \frac{\partial \overline{q}}{\partial z} \tag{9.20}$$

where M is the massflux.

Convective activity is expressed in terms of $CAPE$ (convective available potential energy) which is estimated from the parcel ascent incorporating the effects of water loading,

$$CAPE = \int_{base}^{top} \left(\frac{g}{\overline{T}_v} \left[T_v - \overline{T}_v \right] - gl \right) dz \tag{9.21}$$

where cloud ensemble values are used for T_v and l. The change of $CAPE$ due to convective heating/moistening is approximated by

$$\frac{\partial}{\partial t} CAPE \approx - \int_{base}^{top} \frac{g}{\overline{T}_v} \frac{\partial \overline{T}_v}{\partial t} dz = -M_B \int_{base}^{top} \left(\frac{[1 + \delta \overline{q}]}{c_p \overline{T}_v} \frac{\partial \overline{s}}{\partial z} + \delta \frac{\partial \overline{q}}{\partial z} \right) \eta \frac{g}{\overline{\rho}} dz \tag{9.22}$$

with normalized mass flux η defined as $M = M_B \cdot \eta(z)$ where M_B is the cloud base mass flux. By assuming that convection acts to reduce $CAPE$ towards zero over a specified time scale τ, the time rate of change is approximated by

$$\frac{\partial}{\partial t} CAPE \approx - \frac{CAPE}{\tau} \tag{9.23}$$

so that the cloud base mass flux can be obtained from (9.22) and (9.23) according to

$$M_B = \frac{CAPE}{\tau} \left\{ \int_{base}^{top} \left[\frac{(1 + \delta \overline{q})}{c_p \overline{T}_v} \frac{\partial \overline{s}}{\partial z} + \delta \frac{\partial \overline{q}}{\partial z} \right] \eta \frac{g}{\overline{\rho}} dz \right\}^{-1}. \tag{9.24}$$

Since η is not known before the total mass flux is known, $CAPE$ is estimated through a first guess $M_B = M_B^*$ obtained from first applying the moisture convergence scheme. Thus, the cloud base mass can finally be written as

$$M_B = \frac{CAPE}{\tau} = M_B^* \left\{ \int_{base}^{top} \left[\frac{(1 + \delta \overline{q})}{c_p \overline{T}_v} \frac{\partial \overline{s}}{\partial z} + \delta \frac{\partial}{\partial z} \overline{q} \right] M^* \frac{g}{\overline{\rho}} dz \right\}^{-1}. \tag{9.25}$$

Following Nordeng (1994), who argued that τ should be smaller (larger) with increasing (decreasing) horizontal resolution, we apply an algorithm similar to that used in the ECMWF model, $\tau[s] = \min(3 \cdot 3600, 2 \cdot 3600 \cdot 63/N)$, where N denotes the spectral resolution.

10. Stratiform cloud scheme

The scheme for the respresentation of stratiform clouds consists of prognostic equations for the vapor, liquid, and ice phase, respectively, a cloud microphysical scheme (Lohmann and Roeckner (1996); with some revisions), and a statistical cloud cover scheme including prognostic equations for the distribution moments (Tompkins, 2002).

10.1. Governing equations

The governing equations for the grid-cell mean mass mixing ratios of water vapor, $\bar{r_v}$, cloud liquid water, $\bar{r_l}$, and cloud ice, $\bar{r_i}$, are written in symbolic form as follows (units are $\mathrm{kgkg^{-1}s^{-1}}$)

$$\frac{\partial \bar{r}_v}{\partial t} = Q_{Tv} + Q_{evr} + Q_{evl} + Q_{sbs} + Q_{sbis} + Q_{sbi} - Q_{cnd} - Q_{dep} - Q_{tbl} - Q_{tbi} \quad (10.1)$$

$$\frac{\partial \bar{r}_l}{\partial t} = Q_{Tl} + Q_{mli} + Q_{mlis} + Q_{cnd} + Q_{tbl} - Q_{evl} - Q_{frh} - Q_{frs} - Q_{frc} - Q_{aut} - Q_{racl} - Q_{sacl} \quad (10.2)$$

$$\frac{\partial \bar{r}_i}{\partial t} = Q_{Ti} + Q_{sed} + Q_{dep} + Q_{tbi} - Q_{mli} - Q_{sbi} + Q_{frh} + Q_{frs} + Q_{frc} - Q_{agg} - Q_{saci} \quad (10.3)$$

with

Q_{Tv} Transport of $\overline{r}_v$ by advection (Q_{Av}), diffusion (Q_{Dv}) and changes due to convection

Q_{Tl} Transport of $\overline{r}_l$ by advection (Q_{Al}), diffusion (Q_{Dl}) and convective detrainment (Q_{Cl})

Q_{Ti} Transport of $\overline{r}_i$ by advection (Q_{Ai}), diffusion (Q_{Di}) and convective detrainment (Q_{Ci})

Q_{evr} Evaporation of rain falling into the respective layer

Q_{evl} Instantaneous evaporation of r_l transported into the cloud-free part of the grid cell

Q_{sbs} Sublimation of snow

Q_{sbis} Sublimation of r_i in the sedimentation flux

Q_{sbi} Instantaneous sublimation of r_i transported into the cloud-free part of the grid cell

Q_{cnd} Condensation of r_v (if $Q_{cnd} > 0$), or evaporation of r_l (if $Q_{cnd} < 0$)

Q_{dep} Deposition of r_v (if $Q_{dep} > 0$), or sublimation of r_i (if $Q_{dep} < 0$)

Q_{tbl} Generation ($Q_{tbl} > 0$) or dissipation ($Q_{tbl} < 0$) of r_l through turbulent fluctuations

Q_{tbi} Generation ($Q_{tbi} > 0$) or dissipation ($Q_{tbi} < 0$) of r_i through turbulent fluctuations

Q_{mli} Instantaneous melting of r_i if the temperature exceeds the freezing point

Q_{mlis} Melting of r_i in the sedimentation flux

Q_{frh} Homogeneous freezing of r_l

Q_{frs} Stochastical and heterogeneous freezing of r_l

Q_{frc} Contact freezing of r_l

Q_{aut} Autoconversion of r_l

Q_{racl} Accretion of r_l by rain

Q_{sacl} Accretion of r_l by snow

Q_{sed} Sedimentation of $\overline{r}_i$, including losses due to Q_{sbis} and Q_{mlis}

Q_{agg} Aggregation of r_i

Q_{saci} Accretion of r_i by snow

Note that the transport terms as well as the sedimentation of cloud ice is calculated from the respective grid-cell mean values (denoted by an overbar), while the microphysical processes are calculated from in-cloud values (without overbar). The phase changes sketched above result in the following temperature change

$$\left(\frac{\partial T}{\partial t}\right)_{ph} = \left(\frac{\partial T}{\partial t}\right)_{vapor\leftrightarrow liquid} + \left(\frac{\partial T}{\partial t}\right)_{vapor\leftrightarrow solid} + \left(\frac{\partial T}{\partial t}\right)_{liquid\leftrightarrow solid} \tag{10.4}$$

with

$$\left(\frac{\partial T}{\partial t}\right)_{vapor\leftrightarrow liquid} = \frac{L_v}{c_p}(Q_{cnd} + Q_{tbl} - Q_{evr} - Q_{evl}) \tag{10.5}$$

$$\left(\frac{\partial T}{\partial t}\right)_{vapor\leftrightarrow solid} = \frac{L_s}{c_p}(Q_{dep} + Q_{tbi} - Q_{sbs} - Q_{sbi} - Q_{sbis}) \tag{10.6}$$

$$\left(\frac{\partial T}{\partial t}\right)_{liquid\leftrightarrow solid} = \frac{L_f}{c_p}(Q_{frh} + Q_{frs} + Q_{frc} + Q_{sacl} - Q_{mli} - Q_{mlis} - Q_{mls}) \tag{10.7}$$

where L_v, L_s, L_f is the latent heat of vaporization, sublimation, and fusion, respectively, c_p is the specific heat of moist air at constant pressure, Q_{mls} is the melting of snow falling into the respective layer, and 'solid' refers to both cloud ice and snow.

10.2. Cloud cover

10.2.1. Cloud scheme framework

Cloud microphysical processes, and radiative transfer as well, depend crucially on the distribution of water within the grid-cell. In ECHAM5, the subgrid-scale distribution is derived within the framework of a statistical-dynamical approach (Tompkins, 2002). Neglecting temperature fluctuations, i.e. assuming that subgrid-scale cloud formation is caused solely by fluctuations in total water content, the fractional cloud cover can be expressed as

$$C = \int_{r_s}^{\infty} G(r_t)\, dr_t \tag{10.8}$$

where $G(r_t)$ is the probability density function (PDF) of $r_t = r_v + r_l + r_i$, and the saturation mixing ratio, r_s, is assumed to be constant within the respective grid-cell. Similarly, the cloud condensate, $r_c = r_l + r_i$, is given by

$$\overline{r}_c = \int_{r_s}^{\infty} (r_t - r_s) G(r_t) dr_t \tag{10.9}$$

where the overbar denotes the grid-cell average. The remaining task is to choose an appropriate PDF and to determine its moments. The choice of the PDF was guided by simulations with a cloud resolving model (CRM) which was run on a horizontal domain of about 90 km x 90 km and 21 km in the vertical (Tompkins, 2002). A good fit to the simulated distributions of r_t can be obtained by using the beta distribution. The beta distribution is determined by four parameters, two shape parameters, p and q, and the lower and upper bounds, a and b, respectively, or alternatively the first four moments. Its PDF is defined as

$$G(t) = \frac{1}{B(p,q)} \frac{(t-a)^{p-1}(b-t)^{q-1}}{(b-a)^{p+q-1}} \tag{10.10}$$

for $a \leq t \leq b$, $p > 0$, $q > 0$ and with $B(p,q) = \frac{\Gamma(p)\Gamma(q)}{\Gamma(p+q)}$ where Γ is the gamma function.

Although the distribution (10.10) can take various forms, such as J, U, or bell shapes, only the bell-shaped regime is allowed in the current scheme ($p > 1, q > 1$). Two additional simplifications are made by setting $p = \text{const}$ and assuming $q \geq p$ which limits the distribution to either normal ($q = p$) or positively skewed ($q > p$). A major advantage of the beta distribution is that it is bounded, as opposed to the Gaussian, log-normal, exponential or gamma distributions. Using $t = r_t$ in (10.10), the grid-cell mean total water content is given by

$$\overline{r}_t = \frac{1}{B(p,q)} \int_0^b \frac{r_t (r_t - a)^{p-1}(b - r_t)^{q-1}}{(b-a)^{p+q-1}} dr_t \tag{10.11}$$

and the grid-cell means of water vapor and cloud condensate, respectively, can be expressed as

$$\overline{r}_v = (b-a)\frac{p}{p+q} I_x(p+1, q) + (a - r_s) I_x(p,q) + r_s \tag{10.12}$$

$$\overline{r}_c = (b-a)\frac{p}{p+q} [1 - I_x(p+1, q)] + (a - r_s)[1 - I_x(p,q)] \tag{10.13}$$

where $x = (r_s - a)/(b - a)$. The incomplete beta function ratio I_x is defined as

$$I_x(p,q) = \frac{1}{B(p,q)} \int_0^x t^{p-1}(1-t)^{q-1} dt \tag{10.14}$$

and the fractional cloud cover is given by

$$C = 1 - I_x(p,q). \tag{10.15}$$

By combining (10.12) and (10.13), the mean of the beta distribution, equivalent to (10.11), is obtained

$$\overline{r}_t = (b-a)\frac{p}{p+q} + a. \tag{10.16}$$

As mentioned above, four parameters are required to define the beta distribution. In the current scheme, q is determined from a prognostic equation, p is set constant, and the remaining two parameters chosen are $\overline{r}_t$ and $\overline{r}_c$ which are computed in the model through solution of the prognostic equations (10.1) to (10.3). The distribution minimum, a, can then be determined by iteration (for details see Tompkins (2002)), and the upper bound, b, or the distribution width, $b - a$, can be diagnosed from (10.16). However, the system is not closed in clear sky conditions, $\overline{r}_c = 0$, and in overcast sky conditions, $\overline{r}_v = r_s$. In both cases, only three independent items of information are available, p, q, $\overline{r}_t$, leaving one degree of freedom to define. The solution we apply in these cases is to carry an additional quasi-prognostic equation for the distribution width, $b - a$. The terminology 'quasi- prognostic' is adopted since the predicted value is directly used only in clear sky or overcast conditions, otherwise it is always slaved to the value diagnosed by the iteration process mentioned above. The remaining task is to specify how subgrid-scale processes such as turbulence and convection affect the evolution of q and $b-a$. Note that the higher-order moments such as variance and skewness are uniquely determined by a, b, p, and q.

10.2.2. Distribution moments

The distribution moments, variance and skewness, are obtained from numerical solutions of the respective prognostic equations. The time rate of change of the total water content due to turbulent fluctuations (denoted by a prime) can be expressed as follows (e.g., Deardorff (1974))

$$\frac{\partial r_t'^2}{\partial t} = -\overline{2w'r_t'}\frac{\partial \overline{r}_t}{\partial z} - \frac{\partial \overline{w'r_t'^2}}{\partial z} - \epsilon\left(r_t'^2\right) \tag{10.17}$$

where w is the vertical velocity. Advective transport and contributions from fluctuations in horizontal wind components are neglected. Moreover, since turbulence can be considered to be isotropic, it does not contribute to the production of skewness. The first term on the r.h.s. of (10.17) represents the production of variance in the presence of a vertical gradient of r_t, the second term the vertical transport of variance by turbulent eddies, and the last term the dissipation of variance. The production term can easily be obtained from the vertical diffusion scheme which provides the turbulent fluxes of all water components (see section 5). The transport term is

parameterized analogous to the mean variables by relating the flux to the gradient of the variance according to

$$\overline{w' r_t'^2} = \Lambda_h \sqrt{E} \left(\frac{\partial \overline{r_t'^2}}{\partial z} \right) \tag{10.18}$$

where E is the turbulent kinetic energy and Λ_h a mixing length scale (see section 5, equations 5.11 to 5.20). The dissipation term consists of two parts representing the three-dimensional turbulence (dominant in the ABL) and the effect of two-dimensional eddies in the free atmosphere, respectively. The dissipation is parameterized as a Newtonian relaxation process, where τ_v and τ_h are time scales associated with vertical and horizontal dissipation, respectively,

$$\epsilon = r_t'^2 \left(\tau_v^{-1} + \tau_h^{-1} \right). \tag{10.19}$$

The vertical dissipation time scale is parameterized as usual (e.g., Deardorff (1974))

$$\tau_v^{-1} = \sqrt{E} / \Lambda_1 \tag{10.20}$$

with a dissipation length scale, $\Lambda_1 = S_{Nm}^{-3} l$, as applied also in the turbulent kinetic energy equation. The horizontal dissipation time scale is parameterized in terms of the wind shear as

$$\tau_h^{-1} = C_s^2 \sqrt{\left(\frac{\partial u}{\partial x} \right)^2 + \left(\frac{\partial v}{\partial y} \right)^2} \tag{10.21}$$

where C_s is a tunable constant. Since the mixing will also reduce the skewness of the distribution, tending toward a symmetric one, the same relaxation is applied to the skewness parameter q

$$\left(\frac{\partial q}{\partial t} \right)_{diss} = (q_0 - q) \left(\tau_v^{-1} + \tau_h^{-1} \right) \tag{10.22}$$

where q_0 defines the shape of the final distribution.

In contrast to turbulence, convection cannot be considered as isotropic because small-scale convective updrafts are balanced by large-scale subsidence. Deep convective towers directly detrain cloud condensate to form cirrus anvils with extensive stratiform cloud coverage. The cumulus convection scheme (section 8) already represents the convective transport of the mean quantities of water vapor and condensate, but it is clear that convective processes also increase the variance of water vapor by introducing localized perturbations (Liao and Rind, 1997). Moreover, the CRM data showed that since deep convective clouds detrain high mixing ratios of condensate, they also introduce a significant positive skewness into the distribution of cloud. Similarly, the presence of convective downdrafts that inject relatively dry air into the boundary layer resulted in a negative skewness of the distribution. However, in the current scheme, only positively skewed or symmetrical distributions are represented which allows to keep the parameter p constant. The simplest approach is to relate the increase in skewness parameter, q, to the detrainment of cloud condensate which is available from the cumulus convection scheme

$$\left(\frac{\partial q}{\partial t} \right)_{conv} = \frac{K}{\rho r_s} \left[\frac{\partial \left(M^{cu} r_t^{cu} \right)}{\partial z} \right] \tag{10.23}$$

where ρ is the air density, M^{cu} the updraft mass flux, r_t^{cu} the total water in the updrafts, and K is a tunable constant. Here, the implicit assumption is made that $r_t^{cu} \gg \overline{r}_t$.

For overcast sky, the effect of convective detrainment on the distribution width, $b-a$, should also be taken into account. Since the increase in $(b-a)$ is associated with increased skewness, the change in the distribution minimum, a, is much smaller than the change in the maximum, b. Therefore, under the simplifying assumption that $\Delta a = 0$, the new $(b-a)$ can be calculated by using (10.16) according to

$$\left[\frac{\partial(b-a)}{\partial t}\right]_{conv} = \frac{(r_t - a)(p+q+\Delta q_{conv})p^{-1} - (b-a)}{\Delta t} \tag{10.24}$$

where Δq_{conv} is the increase in q during a time step Δt as derived from integrating (10.23).

Further processes that should be considered are the microphysical pathways that are represented in the cloud scheme. If a cloud is heavily precipitating, for example, the loss of cloud water will reduce both the skewness and the variance. While the effect on the variance is already taken into account through changes in cloud condensate, the effect on the skewness must be explicitly considered. For this purpose, a simple approach has been developed which relates the change in distribution maximum due to cloud microphysics, Δb_{micro}, to the change in cloud condensate, $(\Delta \overline{r}_c)_{micro}$, resulting from all microphysical processes in (10.1) to (10.3) during a time step Δt according to the linear relationship

$$\Delta b_{micro} = \frac{(\Delta \overline{r}_c)_{micro}}{\overline{r}_c}(b - r_s). \tag{10.25}$$

For example, if microphysical processes remove all cloud within one time step, the change in b would simply be $\Delta b_{micro} = r_s - b$, and $b + \Delta b_{micro}$ accordingly be reduced to r_s. As for the convection source of variance (10.24), the assumption is made that for microphysical processes $|\Delta a| \ll |\Delta b|$, which allows the change in skewness to be expressed via (10.16) as

$$\left(\frac{\partial q}{\partial t}\right)_{micro} = \frac{1}{\Delta t}\left[\frac{(b + \Delta b_{micro} - a)p}{(r_t - a)} - (p+q)\right]. \tag{10.26}$$

In summary, the system is closed by two prognostic equations for the skewness parameter q

$$\frac{\partial q}{\partial t} = \left(\frac{\partial q}{\partial t}\right)_{conv} + \left(\frac{\partial q}{\partial t}\right)_{micro} + \left(\frac{\partial q}{\partial t}\right)_{diss} \tag{10.27}$$

where the individual contributions are defined by (10.22), (10.23) and (10.26), and for the distribution width, $b-a$, instead of the variance. The variance equation (10.17) has to be rewritten accordingly, so that the equation for $(b-a)$ can be expressed as

$$\frac{\partial(b-a)}{\partial t} = -\frac{\eta}{b-a}\overline{w'r_t'}\frac{\partial \overline{r}_t}{\partial z} - \Lambda_h\sqrt{E}\frac{\partial(b-a)}{\partial z} - (b-a)\left(\tau_v^{-1} + \tau_h^{-1}\right) + \left[\frac{\partial(b-a)}{\partial t}\right]_{conv} \tag{10.28}$$

with $\eta = (p+q)^2(p+q+1)(pq)^{-1}$ and the convective source term defined by (10.24). Note that advective transport of both q and $(b-a)$ is neglected because its effect was found to be small compared to the respective sources and sinks. The scheme has two tunable constants that appear

in (10.21) and (10.23). Currently, we use $C_s = 0.23$ and $K = 10$. Moreover, the parameter p of the beta distribution is currently not predicted but specified, $p = 2$, and $q_0 = p$ in (10.22) so that the mixing processes tend to relax the distribution toward a symmetric one.

10.3. Sedimentation and cloud microphysics

10.3.1. Sedimentation of cloud ice

Sedimentation of cloud ice is formally treated like vertical advection, i.e. the algorithm is applied to grid-cell mean values so that the flux divergence is given by

$$\left(\frac{\partial \overline{r}_i}{\partial t}\right)_{sed} = \frac{1}{\rho}\frac{\partial \overline{F}_i}{\partial z} = \frac{1}{\rho}\frac{\partial \left(\rho \overline{v}_i \overline{r}_i\right)}{\partial z} \tag{10.29}$$

where the fall velocity is parameterized as $\overline{v}_i = \alpha \left(\rho \overline{r}_i\right)^{\beta}$ with $\alpha = 3.29$ and $\beta = 0.16$ (Heymsfield and Donner, 1990). Equation (10.29) can be expressed in discrete form as

$$Q_{sed} \equiv \left(\frac{\partial \overline{r}_i}{\partial t}\right)_{sed} \approx \frac{1}{\rho \Delta z}\left(\overline{F}_i^{top} - \rho \overline{v}_i \overline{r}_i\right) \tag{10.30}$$

where $\overline{F}_i^{top}$ is the incoming sedimentation flux which has already been subject to sublimation and melting. By keeping $\overline{F}_i^{top}$ as well as $\overline{v}_i$ constant during a time step interval, (10.30) can be solved analytically (Rotstayn (1997); see also section 10.3.8). The flux leaving the respective layer, $\overline{F}_i^{bot}$, is obtained by integrating (10.30) over the layer, giving

$$\overline{F}_i^{bot} = \overline{F}_i^{top} - \rho \Delta z Q_{sed}. \tag{10.31}$$

As the integration proceeds from the top of the model down to the surface, the flux at the bottom of a layer can be used as incoming flux for the layer beneath. In the lowest model layer ($k = N$), the flux $\overline{F}_i^{bot}(k = N) \equiv \overline{F}_i(p_s)$, representing the ice sedimentation at the surface, where p_s is surface pressure, is added to the snow flux according to (10.62).

10.3.2. Condensation/evaporation, deposition/sublimation and turbulence effects

The cloud microphysical terms in the governing equations (10.1) to (10.3) are calculated from in-cloud values, r_l and r_i, respectively, which are related to the grid-cell mean values by $r_l = \overline{r}_l / C$ and $r_i = \overline{r}_i / C$, where C is fractional cloud cover defined by (10.15). To be consistent with this definition, any cloud liquid water or cloud ice that is transported into the clear-sky part of the grid-cell, $(1 - C)$, by advection, vertical diffusion, convective detrainment or sedimentation, is instantaneously removed by evaporation and/or sublimation. By assuming that the transport is distributed equally over the grid-cell, the respective budget terms in (10.1) to (10.3) are defined as

$$Q_{evl} = (1 - C) Q_{Tl} \tag{10.32}$$

$$Q_{sbi} = (1 - C)(Q_{Ti} + Q_{sed}). \tag{10.33}$$

The remaining fractions, $C \cdot Q_{Tl}$ and $C \cdot (Q_{Ti} + Q_{sed})$, are used to increase the in-cloud values r_l and r_i, respectively. On the other hand, r_l and/or r_i are diminished by transport divergence, while no change is allowed in that situation within the cloud-free part of the grid-cell.

Apart from convective detrainment which is included in (10.2) and (10.3) in the transport terms Q_{Tl} and Q_{Ti}, the most important cloud generation processes are condensation, $Q_{cnd} > 0$, and deposition, $Q_{dep} > 0$, of water vapor in the presence of moisture convergence and/or cooling. Oppositely, moisture divergence and/ or warming will result in cloud dissipation through evaporation, $Q_{cnd} < 0$, or sublimation, $Q_{dep} < 0$. The calculation of the respective terms has to be consistent with the PDF adopted for the total water content (see section 10.2.1). This implies that the shape factors p and q are not changed so that Q_{cnd} and Q_{dep} can be obtained from (10.11) to (10.14) by a simple translation of the PDF, including humidity changes, $\Delta\overline{r}_v$, due to advection and other processes, as well as changes in the saturation mixing, $\Delta\overline{r}_s$, due to temperature changes

$$Q_{cnd} = \frac{1}{\Delta t}\left[(b-a)\frac{p}{p+q}\{1 - I_x(p+1,q)\} - x(b-a)\{1 - I_x(p,q)\} - \overline{r}_l\right] \tag{10.34}$$

$$Q_{dep} = \frac{1}{\Delta t}\left[(b-a)\frac{p}{p+q}\{1 - I_x(p+1,q)\} - x(b-a)\{1 - I_x(p,q)\} - \overline{r}_i\right] \tag{10.35}$$

with $x = (r_s + \Delta r_s - a - \Delta\overline{r}_v) \cdot (b-a)^{-1}$. Depending on ambient temperature and the availability of cloud ice, either Q_{cnd} is calculated, using r_s and Δr_s with respect to liquid water, or Q_{dep}, using r_s and Δr_s with respect to ice. Depositional growth of ice crystals takes place at temperatures $T < -35$°C, and $Q_{cnd} = 0$ is assumed in this case. At temperatures $T \geq 0$°C, only condensational growth takes place, according to (10.34), and $Q_{dep} = 0$ is assumed in this case. In the temperature range -35°C$\leq T <$ 0°C, the Bergeron-Findeisen process is crudely represented by taking into account that the saturation water vapor pressure with respect to ice is smaller than with respect to liquid water. Therefore, supercooled droplets can form by condensational growth only if the cloud ice concentration is relatively small. On the other hand, depositional growth of ice crystals is favoured, i.e. $Q_{cnd} = 0$, if a certain cloud ice threshold, γ_{thr}, is exceeded. In case of cloud dissipation due to moisture divergence and/or heating, $\overline{r}_l$ and $\overline{r}_i$ are reduced, in proportion to their concentrations, by $Q_{cnd}(r_l/(r_l + r_i))$ and $Q_{dep}(r_i/(r_l + r_i))$, respectively, if $Q_{cnd} + Q_{dep} < 0$.

The changes $\Delta\overline{r}_v$ and Δr_s in (10.34) and (10.35) include contributions from all processes that have been calculated prior to condensation and deposition. This includes radiative heating/cooling, moisture transport by advection and vertical diffusion, instantaneous evaporation and sublimation, according to (10.32) and (10.33), of $\overline{r}_l$ and $\overline{r}_i$ that have been transported into the clear-sky part of a cell through advection, vertical diffusion, convective detrainment, and sedimentation of cloud ice. In addition, a few processes are included that will be discussed in the following like cloud generation/dissipation by turbulence, (10.38) and (10.39), evaporation of rain (10.57), sublimation of snow and falling ice (10.58), and melting of snow and falling ice (10.65).

Changes in skewness and variance due to turbulence, via (10.22) and (10.28), may result in phase changes through condensation/deposition or evaporation/sublimation which have to be taken into account in the water budget. The new humidity is obtained by integrating (10.22) and (10.28) forward by one time step Δt and using the new values of q and $(b-a)$ in (10.12) to obtain $\overline{r}_v^{n+1}$ with r_s assumed to remain constant. Thus, the humidity change associated with turbulent activity can be expressed as

$$\left(\frac{\partial\overline{r_v}}{\partial t}\right)_{turb} = \frac{\Delta\overline{r}_v}{\Delta t} = \frac{\overline{r}_v^{n+1} - \overline{r}_v^{n}}{\Delta t}. \tag{10.36}$$

Assuming that the total water content does not change, the change in humidity, in the presence of clouds, has to be balanced by a change in cloud condensate (sum of liquid and ice)

$$\left(\frac{\partial \overline{r}_c}{\partial t}\right)_{turb} = \frac{\Delta \overline{r}_c}{\Delta t} = -\frac{\Delta \overline{r}_v}{\Delta t}. \tag{10.37}$$

The changes in the liquid and ice phase are finally obtained by splitting the total condensate change, $\Delta \overline{r}_c$, in proportion to the respective mixing ratios according to

$$\left(\frac{\partial \overline{r}_l}{\partial t}\right)_{turb} \equiv Q_{tbl} = \frac{r_l \Delta \overline{r}_c}{(r_l + r_i)\Delta t} \tag{10.38}$$

$$\left(\frac{\partial \overline{r}_i}{\partial t}\right)_{turb} \equiv Q_{tbi} = \frac{r_i \Delta \overline{r}_c}{(r_l + r_i)\Delta t}. \tag{10.39}$$

10.3.3. Freezing of cloud liquid water and melting of cloud ice

At temperatures $T < -35$℃, the total amount of cloud liquid water freezes homogeneously and instantaneously, during one time step Δt, to cloud ice Levkov et al. (1992) so that

$$Q_{frh} = \frac{\overline{r}_l}{\Delta t}. \tag{10.40}$$

For stochastical and heterogeneous freezing in the temperature range -35℃ $\leq T <$ 0℃, we use the extrapolated equation by Bigg (1953) down to the cloud droplet size (Levkov et al., 1992; Murakami, 1990).

$$Q_{frs} = Ca_1\{\exp[b_1(T_0 - T)] - 1\}\frac{\rho r_l^2}{\rho_w N_l} \tag{10.41}$$

where the constants $a_1 = 100$ m^{3}s^{-1} and b_1=0.66 K^{-1} are taken from laboratory experiments, T_0 = 273.15 K is the freezing point, ρ_w = 1000 kgm^{-3} is the density of water, ρ the air density, T the grid-cell mean temperature, r_l the in-cloud liquid water mixing ratio, N_l is the cloud droplet number concentration, and C the fractional cloud cover. In the standard version of ECHAM5, N_l is prescribed within the atmospheric boundary layer (= $220 \cdot 10^6$ m^{-3} over land and $80 \cdot 10^6$ m^{-3} over sea, respectively). Above the boundary layer, N_l decreases exponentially to 50 m^{-3} in the upper troposphere over both land and ocean.

Brownian diffusion contact nucleation results from random collisions of aerosol particles with supercooled cloud droplets. It may be written as (e.g. Levkov et al. (1992))

$$Q_{frc} = Cm_{io}F_1 DF_{ar} \tag{10.42}$$

where $m_{io} = 10^{-12}$ kg is the initial mass of a nucleated ice crystal, $DF_{ar} = 1.4 \cdot 10^{-8}$ m^{-2}s^{-1} the aerosol diffusivity (Pruppacher and Klett, 1978), and $F_1 = (4\pi R_{vl} N_l N_a)/\rho$. The concentration of active contact nuclei is approximated as $N_a = \max[N_{a0}(T_0 - T - 3), 0]$, with $N_{a0} = 2 \cdot 10^5$ m^{-3}, and the mean volume droplet radius, R_{vl}, is obtained from

$$\frac{4}{3}\pi R_{vl}^3 N_l \rho_w = r_l \rho. \tag{10.43}$$

Following Levkov et al. (1992), cloud ice is assumed to melt completely when $T > T_0$, giving

$$Q_{mli} = \frac{\overline{r}_i}{\Delta t}. \tag{10.44}$$

10.3.4. Precipitation formation in warm clouds, cold clouds and in mixed-phase clouds

In warm clouds ($T > 0$°C) and also in mixed phase clouds (-35°C $\leq T < 0$°C), the cloud liquid water content can be diminished by autoconversion of cloud droplets, Q_{aut}, growth of rain drops by accretion of cloud droplets, Q_{racl}, and growth of snow crystals by accretion of cloud droplets, Q_{sacl}. The autoconversion rate is derived from the stochastic collection equation which describes the time evolution of a droplet spectrum changing by collisions among droplets of different size (Beheng, 1994) which gives

$$Q_{aut} = C\gamma_1 \left[a_2 n^{-b_2} \left(10^{-6} N_l\right)^{-b_3} \left(10^{-3} \rho r_l\right)^{b_4} \right] / \rho \tag{10.45}$$

where $a_2 = 6 \cdot 10^{28}$, $n = 10$ is the width parameter of the initial droplet spectrum described by a gamma distribution, $b_2 = 1.7$, $b_3 = 3.3$, $b_4 = 4.7$, and γ_1 is a tunable parameter which determines the efficiency of the autoconversion process and, hence, cloud lifetime.

Raindrops, once formed, continue to grow by accretion of cloud droplets. The accretion rate is derived from the stochastic collection equation (Beheng, 1994)

$$Q_{racl} = \min(C, C_{pr}) a_3 r_l \rho r_{rain} + \gamma_2 \rho Q_{aut} \Delta t \tag{10.46}$$

where r_{rain} is the mass mixing ratio of rain falling into a fraction C_{pr} of the respective grid-cell, and $a_3 = 6$ m^{3}kg^{-1}s^{-1}. The second term in the bracket is the local rainwater production during a time step by autoconversion, and γ_2 is a tunable parameter. The remaining precipitation process occurring in the cloud liquid water equation, Q_{sacl}, will be discussed below together with the analogous process for cloud ice, Q_{saci}.

The conversion rate from cloud ice to snow by aggregation of ice crystals has been adopted from Levkov et al. (1992), based on the work of Murakami (1990)

$$Q_{agg} = C\gamma_3 \frac{\rho r_i^2 a_4 E_{ii} X \left(\frac{\rho_0}{\rho}\right)^{1/3}}{-2\rho_i \log\left(\frac{R_{vi}}{R_{s0}}\right)^3} \tag{10.47}$$

where $a_4 = 700$ s^{-1} is an empirical constant, $E_{ii} = 0.1$ is the collection efficiency between ice crystals, $X = 0.25$ is the dispersion of the fall velocity spectrum of cloud ice, $\rho_0 = 1.3$ kgm^{-3} is a reference density of air, $\rho_i = 500$ kgm^{-3} is the density of cloud ice, R_{vi} is the mean volume ice crystal radius, $R_{so} = 10^{-4}$ m is the smallest radius of a particle in the snow class, and γ_3 is a tunable parameter. From simultaneous measurements of ρr_i, R_{vi} and the effective radius of ice crystals, R_{ei}, Moss (1996; personal communication) derived the following relationships

$$R_{ei} = a_5 \left(10^3 \rho r_i\right)^{b_5} \tag{10.48}$$

$$R_{ei}^3 = R_{vi}^3 \left(a_6 + b_6 R_{vi}^3\right) \tag{10.49}$$

with R_{ei}, R_{vi} in μm, $a_5 = 83.8$, $b_5 = 0.216$, $a_6 = 1.61$, $b_6 = 3.56 \cdot 10^{-4}$, so that after solving for (10.49)

$$R_{vi}[m] = 10^{-6} \left(\sqrt{2809 R_{ei}^3 + 5113188} - 2261 \right)^{1/3}. \tag{10.50}$$

The accretional growth of snow through riming and collecting of ice crystals is based on Lin et al. (1983) and Levkov et al. (1992). Snow crystals are assumed to be exponentially distributed (Gunn and Marshall, 1958)

$$n_s(D_s) = n_{0s} \exp(-\lambda_s D_s) \tag{10.51}$$

where $n_s(D_s)$ is the concentration of particles of diameters D_s per unit size interval, D_s is the diameter of the snow particle, $n_{0s} = 3 \cdot 10^6$ m^{-4} is the intercept parameter obtained from measurements (Gunn and Marshall, 1958), and λ_s is the slope of the particle size distribution and is written as (Potter, 1991)

$$\lambda_s = \left(\frac{\pi \rho_s n_{0s}}{\rho r_{snow}} \right)^{1/4} \tag{10.52}$$

where $\rho_s = 100$ kgm^{-3} is the bulk density of snow and r_{snow} is the mass mixing ratio of snow. Snow crystals settle through a population of supercooled cloud droplets, colliding and coalescing with them (riming). The rate of change in the snow mixing ratio is based on geometric sweep-out concept integrated over the size distribution (10.51)

$$Q_{sacl} = \min(C, C_{pr}) \gamma_4 \frac{\pi E_{sl} n_{0s} k_s r_l \Gamma(3 + b_7)}{4 \lambda_s^{3+b_7}} \left(\frac{\rho_0}{\rho} \right)^{1/2} \tag{10.53}$$

where $k_s = 4.83$ m^{2}s^{-1}, $b_7 = 0.25$, $E_{sl} = 1$ is the collection efficiency of snow for cloud droplets (Lin et al., 1983) and γ_4 is a tunable parameter. The accretion rate of ice crystals by snow is similar to (10.53) and is expressed as

$$Q_{saci} = \min(C, C_{pr}) \frac{\pi E_{si} n_{0s} k_s r_i \Gamma(3 + b_7)}{4 \lambda_s^{3+b_7}} \left(\frac{\rho_0}{\rho} \right)^{1/2} \tag{10.54}$$

where the collection efficiency of snow for cloud ice is assumed to be temperature dependent according to $E_{si} = \exp[-a_7(T_0 - T)]$ with $a_7 = 0.025$. Note that $r_i = 0$ for $T > T_0$ (c.f.,(10.44)) so that $Q_{saci} = 0$ in this case. Analogous to (10.46), ρr_{snow} used in (10.53) and (10.54) through (10.52) consists of two parts. The first one is a contribution from the snow flux into the respective grid-cell (c.f., section 10.3.7), and the second one, $\gamma_2 \rho Q_{agg} \Delta t$, is due to local snow generation through aggregation of ice crystals (10.47).

10.3.5. Evaporation of rain and sublimation of snow and ice

The evaporation of rain is obtained by integration of the evaporation for a single rain drop of diameter D_r over the Marshall-Palmer distribution (Marshall and Palmer, 1948). The rate of

change can then be expressed as

$$Q_{evr} = C_{pr} \frac{2\pi n_{0r} S_l}{\rho(A' + B')} \left[\frac{a_8}{\lambda_r^2} + \frac{b_8 S_c^{1/3}}{\lambda_r^{\delta_r/2}} \Gamma\left(\frac{\delta_r}{2}\right) \left(\frac{k_r \rho}{\mu}\right)^{1/2} \left(\frac{\rho_0}{\rho}\right)^{1/4} \right] \tag{10.55}$$

where $A' = L_v^2/(K_a R_v T^2)$, $B' = 1/(\rho r_{sl} D_v)$, K_a is the thermal conductivity of air, R_v is the gas constant for water vapor, D_v is the diffusivity of vapor in the air, $n_{0r} = 8 \cdot 10^6$ m^{-4} is the intercept parameter, r_{sl} is the saturation water vapor mixing ratio with respect to liquid water, $S_l = 1 - r_v/r_{sl}$ is the respective sub-saturation, $S_c = \mu/(\rho D_v)$ is the Schmidt number, μ is the dynamic viscosity of air, $\delta_r = 5.5$, $a_8 = 0.78$, $b_8 = 0.31$, $k_r = 141.4$ m^{2}s^{-1}, and the slope of the size distribution is defined as

$$\lambda_r = \left(\frac{\pi \rho_w n_{0r}}{\rho r_{rain}} \right)^{1/4}. \tag{10.56}$$

Instead of (10.55) we use a simplified form obtained after minor simplifications and evaluation of parameters after Rotstayn (1997)

$$Q_{evr} = C_{pr} \frac{a_9 S_l}{\rho^{1/2}(A' + B')} \left(\frac{P_r}{C_{pr}} \right)^{b_9} \tag{10.57}$$

where P_r is the rain flux [kgm^{-2}s^{-1}], $a_9 = 870$ and $b_9 = 0.61$.

Analogously, the sublimation of snow is obtained by integrating the sublimation for a single particle of diameter D_s over the Gunn-Marshall distribution (10.51). The time rate of change can then be expressed as

$$Q_{sbs} = C_{pr} \frac{2\pi n_{0s} S_i}{\rho(A'' + B'')} \left[\frac{a_8}{\lambda_s^2} + \frac{b_8 S_c^{1/3}}{\lambda_s^{\delta_s/2}} \Gamma\left(\frac{\delta_s}{2}\right) \left(\frac{k_s \rho}{\mu}\right)^{1/2} \left(\frac{\rho_0}{\rho}\right)^{1/4} \right], \tag{10.58}$$

where $A'' = L_s^2/K_a R_v T^2)$, $B'' = 1/(\rho_{si} D_v)$, r_{si} is the saturation water vapor mixing ratio with respect to ice, $S_i = 1 - r_v/r_{si}$ is the respective sub-saturation, $\delta_s = 5.25$ and $k_s = 4.83$ m^{2}s^{-1} (Levkov et al., 1992). The expression (10.58) is used for sublimation of both snowfall, Q_{sbs}, and falling ice, Q_{sbis}. Note that in Q_{sbis} the slope parameter λ_s (10.52) includes the ice mixing ratio, r_{ised}, instead of r_{snow} (see section 10.3.7).

10.3.6. Precipitation

The total amount of non-convective precipitation at a certain pressure level, p, is obtained by integrating the relevant processes from the top of the model ($p = 0$) to the respective pressure level. The fluxes of rain and snow [kgm^{-2}s^{-1}] can then be expressed as

$$P_{rain}(p) = \frac{1}{g} \int_0^p (Q_{aut} + Q_{racl} - Q_{evr} + Q_{mls})\, dp \tag{10.59}$$

$$P_{snow}(p) = \frac{1}{g} \int_0^p (Q_{agg} + Q_{sacl} + Q_{saci} - Q_{sbs} - Q_{mls})\, dp \tag{10.60}$$

with the snow melt, Q_{mls}, defined in (10.65). The sedimentation (see section 10.3.1) is given by

$$\bar{F}_i(p) = -\frac{1}{g}\int_0^p Q_{sed} dp \geq 0 \tag{10.61}$$

where Q_{sed} includes the effects of sublimation Q_{sbis}, and melting, Q_{mlis}. At the surface ($p = p_s$), the sedimentation is added to the snow fall so that the total snow flux is given by

$$P_{snow}(p_s) = \frac{1}{g}\int_0^{p_s} (Q_{agg} + Q_{sacl} + Q_{saci} - Q_{sbs} - Q_{mls})\, dp + \bar{F}_i(p_s). \tag{10.62}$$

Melting of falling ice and snow is calculated from the heat budget in case the air temperature exceeds the freezing point. The excess heat in the respective model layer with pressure thickness, Δp, is then used for melting all or part of the snow and/or ice sedimentation according to

$$f_m \frac{c_p\left(\tilde{T} - T_0\right)}{\Delta t}\frac{\Delta p}{g} = \max(L_f \hat{M}, 0) \tag{10.63}$$

where $\tilde{T}$ includes all processes except melting, $\hat{M}$ is a preliminary value, and $0 \leq f_m \leq 1$ is the fraction of the excess heat that can be used for melting. The actual amount of melting depends not only on the excess heat, according to (10.63), but also on the available snow fall, P_{snow}, and/or incoming sedimentation flux, $\bar{F}_i^{top}$. This can be expressed as

$$M_{snow,ice} = \begin{pmatrix} \hat{M} \left\{ P_{snow}, \bar{F}_i^{top} \geq \hat{M} \right\} \\ P_{snow}, \bar{F}_i^{top} \left\{ P_{snow}, \bar{F}_i^{top} < \hat{M} \right\} \end{pmatrix}. \tag{10.64}$$

In the first case, melting is limited by the excess heat, i.e. $f_m = 1$. In the second case, melting is limited by the available flux, i.e. only a fraction $f_m = (P_{snow}, \bar{F}_i^{top})/\hat{M} < 1$, of the excess heat is required for complete melting. The temperature change associated with melting (c.f., (10.7)) can be written as

$$\left(\frac{\partial T}{\partial t}\right)_{melt} = -\frac{L_f}{c_p}(Q_{mls} + Q_{mlis}) \tag{10.65}$$

with $Q_{mls} \equiv M_{snow} \cdot g/\Delta p$ and $Q_{mlis} \equiv M_{ice} \cdot g/\Delta p$ with M_{snow} and M_{ice} defined in (10.64).

The precipitation fluxes (10.59) - (10.62) represent grid-cell averages, while the accretion processes (10.46), (10.53) and (10.54) as well as evaporation of rain (10.57) and sublimation of snow (10.58) depend on the fractional area, C_{pr}, of a grid-cell covered with precipitation. Our approach for estimating C_{pr} is a slight modification of that employed by Tiedtke (1993), as defined in Jakob and Klein (1999)

$$C_{pr}^k = \max\left(\hat{C}_{pr}, \frac{C^k \Delta Pr^k + \hat{C}_{pr} Pr^{k-1}}{\Delta Pr^k + Pr^{k-1}}\right) \tag{10.66}$$

where Pr^{k-1} is the total precipitation flux, $P_{rain} + P_{snow}$, at model level $k-1$, ΔPr^k is the amount of precipitation produced locally in the layer beneath, C is the cloud cover (10.15) and

$$\hat{C}_{pr} = \begin{pmatrix} C^k \text{ for } \left(\Delta Pr^k \geq Pr^{k-1}\right) \\ C_{pr}^{k-1} \text{ for } \left(\Delta Pr^k < Pr^{k-1}\right) \end{pmatrix}. \tag{10.67}$$

According to (10.66) and (10.67), the vertical profile of C_{pr} is related to the profiles of both fractional cloud cover and precipitation. In case the local precipitation production exceeds the incoming flux, the precipitation fraction is given by $C_{pr}^k = C^k$. Note also that $C_{pr}^k = 0$ for $\Delta Pr^k + Pr^{k-1} = 0$.

10.3.7. Mixing ratios of rain, falling ice and snow

The mass mixing ratio of rain, r_{rain}, is related to the rain flux by

$$\rho r_{rain} = P_{rain}/(C_{pr} v_r) \tag{10.68}$$

where P_{rain}/C_{pr} is the rain flux within the fraction of the grid-cell covered with rain, and v_r is the mass-weighted fall velocity of rain drops parameterized according to Kessler (1969)

$$v_r = a_{10} \left(\frac{\rho r_{rain}}{n_{0r}}\right)^{1/8} \left(\frac{\rho_0}{\rho}\right)^{1/2} \tag{10.69}$$

with the intercept parameter $n_{0r} = 8 \cdot 10^6$ m^{-4} and $a_{10} = 90.8$. By using (10.69) in (10.68) we obtain

$$\rho r_{rain} = \left(\frac{P_{rain}}{C_{pr} a_{10} (n_{0r})^{-1/8} \sqrt{\rho_0/\rho}}\right)^{8/9}. \tag{10.70}$$

According to (10.29), the mass mixing ratio of falling ice can be obtained from

$$r_{ised} = \overline{F}_i^{top}/(\rho v_i) \tag{10.71}$$

where v_i is the fall velocity of cloud ice, $\overline{F}_i^{top}$is the grid-cell mean sedimentation flux and v_i parameterized as in (10.29) by employing the Heymsfield and Donner (1990) approach

$$v_i = a_{11} (\rho r_{ised})^{b_{10}} \tag{10.72}$$

with $a_{11} = 3.29$ and $b_{10} = 0.16$. By using (10.72) in (10.71) we obtain

$$\rho r_{ised} = \left(\frac{\overline{F}_i^{top}}{a_{11}}\right)^{1/(1+b_{10})}. \tag{10.73}$$

Analogously, the mass mixing ratio of snow within the fraction C_{pr} of the grid-cell covered with snow is obtained from the snow fall rate according to

$$\rho r_{snow} = \left(\frac{P_{snow}}{C_{pr} a_{11}} \right)^{1/(1+b_{10})} . \tag{10.74}$$

10.3.8. Solution method and parameter choice

The cloud microphysical terms are solved in a split manner, i.e. sequentially. In the following, a subscript n denotes the value of a variable before application of the respective process, while $n+1$ denotes the updated value after application of the process. A major part of the microphysics is solved analytically (Q_{frs}, Q_{aut}, Q_{agg}, Q_{racl}, Q_{sacl}, and Q_{saci}), and these terms can formally be written as

$$\frac{\partial \Psi}{\partial t} = -F_\Psi \Psi^z \tag{10.75}$$

where $F_\Psi > 0$ is kept constant during the respective time interval, Δt, and $z \geq 1$. In the linear case, i.e. for all accretion processes (Q_{racl}, Q_{sacl}, Q_{saci}), the solution of (10.75) is given by

$$\Psi_{n+1} = \Psi_n \exp(-F_\Psi \Delta t). \tag{10.76}$$

For $z > 1$, i.e. for $Q_{frs}(z = 2)$, $Q_{aut}(z = 4.7)$ and $Q_{agg}(z = 2)$, the solution of (10.75) is given by

$$\Psi_{n+1} = \Psi_n \left[1 + F_\Psi \Delta t (z-1) \Psi_n^{z-1} \right]^{1/(1-z)} . \tag{10.77}$$

Analytical solutions can also be obtained for the variance equation (10.17), but excluding the turbulent transport of variance, and also for the ice sedimentation (10.30). These equations can be written in the form

$$\frac{\partial \Psi}{\partial t} = A - B\Psi \tag{10.78}$$

where A and B are constants. The solution after one time step interval, Δt, is given by

$$\Psi_{n+1} = \Psi_n \exp(-B\Delta t) + \frac{A}{B}[1 - \exp(-B\Delta t)]. \tag{10.79}$$

In the sedimentation equation, $\overline{F}_i^{top}$ is included in A, while the fall velocity v_i is included in B. Both are assumed constant during the respective time step interval. In the variance equation, the production term, which is available from the vertical diffusion scheme, is set to A. According to (10.19), the dissipation is a linear function of the variance and $(\tau_v^{-1} + \tau_h^{-1})$ is replaced by B. The remaining term in (10.17), i.e. the turbulent transport of variance, is solved implicitly in the same way as the turbulent transport of the mean variables in the vertical diffusion scheme.

The microphysics scheme includes a large number of parameters, $(a_1, a_2, ..., a_{11})$ and $(b_1, b_2, ..., b_{10})$, which are kept constant as part of the parameterizations. On the other hand, $(\gamma_1, \gamma_2, \gamma_3, \gamma_4)$, in (10.45), (10.46), (10.47), and (10.53), respectively, are used as 'tuning' parameters. This can be justified to some extent because these parameterizations are based on detailed microphysical

models and cannot be applied to large-scale models without adjustment. The parameter γ_{thr} is a cloud ice threshold which decides on either condensational growth of supercooled cloud droplets or depositional growth of ice crystals (see (10.34) and (10.35)). The following values are used in ECHAM5: $\gamma_1 = 15$; $0 \leq \gamma_2 \leq 0.5$ depending on model resolution; $\gamma_3 = 95$; $\gamma_4 = 0.1$; $\gamma_{thr} = 5 \cdot 10^{-7}$ kgkg^{-1}.

11. Radiation

The integration of the general circulation requires heating/cooling rates within the atmosphere and energy fluxes at the surface and at the top of the atmosphere (TOA) related to the radiative transfer of solar shortwave and terrestrial longwave radiation. These forcing fields depend on the composition of the atmosphere, of the gaseous, the particulate as well as the condensed constituents, the orbit position of the Earth, the local solar zenith angle, as well as the thermal structure from the surface to the top of the atmosphere.

Due to the inherent complexity of the radiative transfer calculation some approximations and simplifications cannot be avoided in the practical realization of radiative computations within general circulation models (GCMs). The general assumptions used in the schemes described below are:

1. Plane parallel assumption
2. Gas constituents are homogeneously mixed within each cell
3. Gas constituents are in local thermodynamic equilibrium (LTE)

For efficiency reasons the radiative transfer computation in ECHAM5 is called less frequently than the dynamics and other parameterizations. Typically the radiation time step dt_{rad} is set to 2 hours. At each radiation time step t_{rad} the transfer calculation is executed at all grid points of the Gaussian grid used in the GCM. At each grid point the scheme provides profiles of the net radiative fluxes F_{SW} and F_{LW} in the shortwave and longwave spectrum, respectively, based on the profiles of absorber mixing ratios q_i and temperature T at the previous time step $t_{rad} - dt$. For the shortwave computation the radiative transfer calculation uses the effective solar zenith angle ϑ_{0eff} at time $t_{rad} + dt_{rad}/2$, i.e. halfway across the following radiation time interval, which includes a correction for high zenith angles that maintains a minimal irraditation for zenith angles exceeding 90°. This correction is necessary to provide non-zero fluxes in areas which are crossed by the day/night terminator during the radiation time interval.

$$F_{LW}(t_{rad}) = F_{LW}(q_i(t_{rad} - dt), T(t_{rad} - dt)) \tag{11.1}$$

$$F_{SW}(t_{rad}) = F_{SW}(q_i(t_{rad} - dt), T(t_{rad} - dt), \vartheta_{0eff}(t_{rad} + dt_{rad}/2)) \tag{11.2}$$

The resulting longwave fluxes $F_{net,LW}$ are kept constant over the whole radiation time interval, while the shortwave fluxes $F_{net,SW}$ are corrected for the local change in solar irradiation at the top of the atmosphere within the radiation time interval. The computation of the current shortwave flux is based on the local zenith angle at time t with a cut-off at 90° zenith angle.

$$F_{LW}(t_{rad} \leq t < t_{rad} + dt_{rad}) = F_{LW}(t_{rad}) \tag{11.3}$$

$$F_{SW}(t_{rad} \leq t < t_{rad} + dt_{rad}) = F_{SW}(t_{rad}) \cdot \frac{F_0(t\vartheta_0)}{F_0(\vartheta_{0eff})} \tag{11.4}$$

The heating rate Q_{rad} in a cell is computed from the difference of the total net flux $F_{rad} = F_{LW} + F_{SW}$ at the lower and upper boundary of a cell, the amount of air m and the specific heat c_p of moist air[1]. The mass of air is derived from the pressure difference between the lower and upper boundary of a cell, making use of the hydrostatic assumption.

$$F_{rad} = F_{LW} + F_{SW} \tag{11.5}$$

$$Q_{rad} = -(F_{rad}^{lower} - F_{rad}^{upper})/(m \cdot c_p) \tag{11.6}$$

$$c_p(t) = (1 - q_v(t)) \cdot c_{pd} + q_v(t) \cdot c_{pv} \tag{11.7}$$

$$m = (p^{lower} - p^{upper})/g \tag{11.8}$$

Temperature tendencies related to radiative processes are integrated explicitly.

11.1. Atmospheric composition

The radiative transfer calculation requires profiles of the active gases, of aerosols, and of cloud water and ice. Additionally the fractional cloud cover must be known.

11.1.1. Water vapour, cloud water, cloud ice, and cloud cover

Water vapour and cloud water and ice are prognostic variables, while cloud cover is a diagnostic variable (c.f., section 10). These variables vary in space and time.

11.1.2. Carbon dioxide

Carbon dioxide is prescribed with a constant mixing ratio. The default ratio is 348 ppmv.

11.1.3. Ozone

Ozone is prescribed following the climatology of Fortuin and Kelder (1998) which is based entirely on ozone observations over the period 1980-1991. The climatology contains zonal mean ozone values at 19 pressure levels from 1000 hPa to 0.3 hPa for each month of the year. The climatology $q_{O_3}^{clim}(m_{i=1...12})$ is linearly interpolated between the closest two months m_1 and m_2 to the current time step t_{rad}. The resulting climatology $q_{O_3}^{clim}(t_{rad})$ is interpolated to the vertical grid of the model and normalized such that the total column ozone amount on the model grid is equal to that on the grid of the climatology for the actual surface pressure.

[1] Within the radiation time interval the longwave cooling $Q_{LW}(t)$ in a cell of constant mass may vary slightly due to the time dependence of the water vapour mixing ratio $q_v(t)$. In dry air, as for instance above the troposphere, $Q_{LW}(t)$ is essentially constant over the radiation time interval.

11.1.4. Methane

By default methane is prescribed with a constant mixing ration of $q^{trop}_{CH_4} = 1.65$ ppmv. Optionally methane can be prescribed as a vertical profile with decreasing mixing ratios in the stratosphere for the middle atmosphere configuration of ECHAM5. This profile is assumed to be constant in time and to be independent of longitude and latitude. The transition to a mesospheric value $q^{meso}_{CH_4} = 0.125 \cdot q^{trop}_{CH_4} = 206$ ppbv is modeled by a tanh function with the node point at $p_{CH_4} = 6.83$ hPa and a dimensionless transition scale length $l_{CH_4} = 1.43$.

$$q_{CH_4}(p) = q^m_{CH_4} - q^d_{CH_4} \cdot \tanh\left(\frac{\ln(p_{CH_4}/p)}{l_{CH_4}}\right) \tag{11.9}$$

$$q^m_{CH_4} = \frac{1}{2} \cdot (q^{trop}_{CH_4} + q^{meso}_{CH_4}) \tag{11.10}$$

$$q^d_{CH_4} = \frac{1}{2} \cdot (q^{trop}_{CH_4} - q^{meso}_{CH_4}) \tag{11.11}$$

11.1.5. N_2O

By default N_2O is prescribed with a constant mixing ration of $q^{trop}_{N_2O} = 306$ ppbv. Optionally N_2O can be prescribed as a vertical profile with decreasing mixing ratios in the stratosphere for the middle atmosphere configuration of ECHAM5. This profile is assumed to be constant in time and to be independent of longitude and latitude. The transition to a mesospheric value $q^{meso}_{N_2O} = 0.012 \cdot q^{trop}_{N_2O} = 3.67$ ppbv is modeled by a tanh function with the node point at $p_{CH_4} = 13.95$ hPa and a dimensionless transition scale length $l_{CH_4} = 1.43$. The mixing ratio profile is computed analogous to that of methane.

11.1.6. $CFCs$

$CFC11$ and $CFC12$ are prescribed with constant mixing ratios of 0.280 ppbv and 0.484 ppbv, respectively. Other CFC species are currently not included.

11.1.7. Aerosols

Aerosol distributions are prescribed following Tanre et al. (1984). This climatology distinguishes time independent spatial distributions of the optical thickness of sea, land, urban, and desert aerosols, and well mixed tropospheric and stratospheric background aerosols.

The spatially varying sea, land, urban, and desert aerosols are described by a maximum optical thickness $\tau^{max}_{s,l,d,u}$ at 0.55μ, normalized horizontal distributions $r_{s,l,d,u}(\lambda, \theta)$, normalized vertical integrals $R_{s,l,d,u}(p)$, and a troposphere stratosphere discrimination factor $x_{ts}(p, T)$. The normalized horizontal distributions are obtained from T10 spectral distributions. The other factors are defined as follows:

$$\tau^{max}_{s,l,d,u} = \quad 0.05, \quad 0.2, \quad 1.9, \quad 0.1 \tag{11.12}$$

$$R_{s,l,d,u}(p) = \left(\frac{p}{p_0}\right)^{h_{s,l,d,u}}, \quad h_{s,l,u} = \frac{H}{1000m}, \quad h_d = \frac{H}{3000m}, \quad H = 8434m \tag{11.13}$$

$$x_{ts}(p,T) = \begin{cases} 1 & stratosphere + mesosphere \\ \left(\frac{T_{tr}}{T}\right)^{\kappa_{ts}} & troposphere \end{cases} \tag{11.14}$$

where T_{tr} is the local tropopause temperature. The tropopause is defined as the level below 10 hPa where the lapse rate changes sign going towards higher pressure. The exponent $\kappa_{ts} = 30$ leads to a fast decay of x_{ts} towards 0 for increasing tropospheric temperatures, e.g. $(200K/220K)^{\kappa_{ts}} = 0.06$. The optical thickness in a layer is then computed as follows:

$$\tau_{s,l,d,u} = (1 - x_{ts}) \cdot \tau^{max}_{s,l,d,u} \cdot r_{s,l,d,u} \cdot \Delta R \tag{11.15}$$

$$\Delta R_{s,l,d,u} = R_{s,l,d,u}(p^{lower}) - R_{s,l,d,u}(p^{upper}) \tag{11.16}$$

Background aerosols for the troposphere and stratosphere are specified by their optical thickness per mass of air and the troposphere stratosphere discrimination factor x_{ts}. The optical thickness in a layer is then computed as follows:

$$\tau_{trbg} = (1 - x_{ts}) \cdot \frac{\tau^{max}_{trbg}}{p_{trop}} \cdot \Delta p, \quad \tau_{stbg} = x_{ts} \cdot \frac{\tau^{max}_{stbg}}{p_{strat}} \cdot \Delta p \tag{11.17}$$

$$\tau_{trbg} = (1 - x_{ts}) \cdot \frac{\tau^{max}_{trbg}}{p_{trop}} \cdot \Delta p, \quad \tau^{max}_{trbg} = 0.03, \quad p_{trop} = 101325Pa - 19330Pa \tag{11.18}$$

$$\tau_{stbg} = x_{ts} \cdot \frac{\tau^{max}_{stbg}}{p_{strat}} \cdot \Delta p, \quad \tau^{max}_{stbg} = 0.045, \quad p_{strat} = 19330Pa \tag{11.19}$$

Optionally the model provides optical properties for 11 GADS type aerosols. If GADS type aerosol distributions are provided, the resulting optical properties is computed and provided to the radiative transfer schemes.

11.2. Solar irradiation

The solar irradiation at each time step t depends on the annular mean solar irradiation I_0 (the solar constant), the relative variation of the actual sun Earth distance $d_{se}(t)$ to the mean distance d_{se0} (see description of orbit), and the cosine μ_0 of the local solar zenith angle $\vartheta_0(\lambda, \theta, t)$.

$$I_0 = 1365W/m^2 \tag{11.20}$$

$$F(\lambda, \theta, t) = I_0 \cdot \left(\frac{d_{se0}}{d_{se}(t)}\right)^2 \cdot \mu_0(\lambda, \theta, t) \tag{11.21}$$

$$\mu_0 = \max\{0, \cos(\vartheta_0(\lambda, \theta, t))\} \tag{11.22}$$

The actual shortwave computation executed at the radiation time step t_{rad} is based on the effective solar zenith angle $\theta_{0eff} = cos^{-1}(\mu_{0eff})$ which accounts for curvature of the atmosphere and its effect on the length of the optical path of the direct solar beam with respect to a plane parallel atmosphere following Paltridge and Platt (1976). Altitude dependencies as well as refraction are disregarded.

$$\mu_{0eff} = \frac{r_{AE}}{\sqrt{\mu_0^2 + r_{AE} \cdot (2 + r_{AE})} - \mu_0} \tag{11.23}$$

$$r_{AE} = H/R_E = 0.001277 \tag{11.24}$$

The correction provided by μ_{0eff} is such that the effective solar zenith angle remains lower than 88.56°, so that the shortwave transfer calculation has a minimum irradiation of 2.5% of I_0, except for the variation due to the sun Earth distance. At zero solar zenith angle μ_{0eff} is identical to μ_0.

$$\mu_{0eff}(\vartheta_0 \to 90°) = \mu_{0eff}(\vartheta_0 \geq 90°) = \mu_0(\vartheta_{0effmax} = 88,55°) = 0.025 \tag{11.25}$$

$$\mu_{0eff}(\vartheta_0 = 0) = \mu_0(\vartheta_0 = 0) = 1 \tag{11.26}$$

11.3. Shortwave radiation

Solar radiation is the main energy source for the climate system. The irradiation is reflected back to space (planetary albedo), absorbed in the atmosphere or absorbed at the surface. The accurate determination of the solar energy input to the atmosphere and the soil or oceans is complicated by the simultaneous occurrence of scattering processes and absorption in the atmosphere by gases as well as by cloud and aerosol particles. The shortwave (SW) radiative transfer of ECHAM5 follows Fouquart and Bonnel (1980) as implemented in cycle 23 release 1 (CY23R1) of the IFS model of ECMWF. The scheme uses the Eddington approximation for the integration over the zenith and azimuth angles and the delta-Eddington approximation for the reflectivity of a layer. The scheme includes Rayleigh scattering, absorption by water vapour and ozone, both varying in time and space, and $CO_2 + N_2O + CO + CH_4 + O_2$ as uniformly mixed gas. Aerosols and cloud particles are effective by absorption and scattering.

Generally the radiative transfer equation for the radiance $L(\tau, \mu, \phi)$ in the direction with zenith angle ϑ with $\mu = \cos\vartheta$ and azimuth angle ϕ at normal optical depth τ and frequency υ in the solar spectrum may be formulated as:

$$\mu \cdot \frac{dL(\tau, \mu, \phi)}{d\tau} = L(\tau, \mu, \phi) - J_{diff}(\tau, \mu, \phi) - J_{dir}(\tau, \mu, \phi) \tag{11.27}$$

$$d\tau/\mu(p) = -\frac{dp}{g} \tag{11.28}$$

Here the zenith angle for upward radiance is positive by definition, i.e. μ is negative for downward radiance. The extinction of the radiance L is proportional to L. J_{diff} and J_{dir} represent the scattering of diffuse radiance from all solid angles and of the direct solar beam from the direction

(μ_0, ϕ_0) at depth τ to the angle (μ, ϕ). Using the scattering phase function $P(\mu, \phi; \mu', \phi')$ to describe the probability that a scattered photon with incident direction (μ', ϕ') radiates into the new direction (μ, ϕ) and the single scattering albedo $\widetilde{\omega}$ to describe the likelihood for scattering into direction (μ, ϕ) with respect to the extinction for photons with incident direction (μ', ϕ'), the source functions can be written as:

$$J_{diff}(\tau, \mu, \phi) = \widetilde{\omega} \cdot \frac{1}{2\pi} \int_0^{2\pi} d\phi' \cdot \frac{1}{2} \int_{-1}^{1} d\mu' \cdot L(\tau, \mu', \phi') \cdot P(\mu, \phi; \mu', \phi') \tag{11.29}$$

$$J_{dir}(\tau, \mu, \phi) = \frac{\widetilde{\omega}}{4\pi} \cdot F_0 \cdot \exp -\tau/\mu_0 \cdot P(\mu, \phi; -\mu_0, \phi_0) \tag{11.30}$$

The diffuse source term J_{diff} contributes photons of frequency υ which have been scattered at least once before. Generally each photon provided by J_{diff} has its own scattering history, and hence has passed an individual optical path. From a statistical point of view it is therefore useful to consider a probability density function $\Pi(\tau, u)$ of the absorber amount u passed by photons contributing to the radiance $L_{cons}(\tau, \mu, \phi)$ at normal optical depth τ in the case of a purely scattering atmosphere, i.e. if $\widetilde{\omega} = 0$. This closure separates the scattering processes from the absorption, so that, if $\Pi(\tau, u)$ and the conserved radiance $L_{cons}(\tau, \mu, \phi)$ are known, the radiances in the absorbing atmosphere is obtained from:

$$L(\tau, \mu, \phi) = L_{cons}(\tau, \mu, \phi) \cdot \int_0^{\infty} \Pi(\tau, u) \cdot \exp(-k_\upsilon u) \cdot du \tag{11.31}$$

Shortwave radiative transfer schemes for general circulation models solve the problem under a number of simplifications. Radiances are integrated over azimuth and zenith angle to obtain fluxes across the upper and lower boundaries of grid boxes. The integration is simplified by the two stream Eddington approximation. In spectral space, only a few bands can be considered, such that transfer functions t_b have to be employed which are accurate although the extinction varies across a spectral band and the band integral of the absorption depends on the temperature and pressure conditions. Such dependencies may be accounted for by using a scaled effective amount u_{eff} for specified reference conditions.

$$F_b(p) = F_{b,cons}(p) \cdot \int_0^{\infty} \Pi(p, u_{eff}) \cdot t_b(u_{eff}) \cdot du_{eff} \tag{11.32}$$

This relationship can be simplified if it is exploited that the band integrated fluxes can be derived from the transmission functions of photon path length weighted integrals of u and $\sqrt{u}$ for weak and strong absorbers, respectively,

$$F_b(p) = F_{b,cons}(p) \cdot t_b(\langle u \rangle) \quad weak\ absorber \tag{11.33}$$

$$F_b(p) = F_{b,cons}(p) \cdot t_b(\langle \sqrt{u} \rangle) \quad strong\ absorber \tag{11.34}$$

$$\langle f(x) \rangle = \int_0^{\infty} \Pi(x) \cdot f(x) \cdot dx \tag{11.35}$$

so that it is sufficient to determine an effective absorber amount U_e between $\langle u \rangle$ and $\langle \sqrt{u} \rangle$ by use of an effective absorption coefficient k_e estimated from the transmission through the atmosphere in clear sky conditions.

$$U_e = \ln(F_b / F_{b,cons}) / k_e \tag{11.36}$$

$$k_e = \frac{1}{u_{tot}/\mu_0} \cdot \ln(t_b(u_{tot}/\mu_0)) \tag{11.37}$$

The scheme of Fouquart and Bonnel expresses the transmissions for H_2O, CO_2, and O_3 in each band in form of Pade approximants with $N = 6$, where absorber amounts are given as effective amounts for reference conditions $T_{ref} = 296K$ and $p_{ref} = 1000hPa$.

$$t_{a,b}(u_{eff}) = \frac{\sum_{i=0}^{N} A_{a,b} \cdot u_{eff}^i}{\sum_{i=0}^{N+1} B_{a,b} \cdot u_{eff}^i} \tag{11.38}$$

The effective amounts are found by the scaling assumption accounting for the spreading of line widths with pressure and temperature.

$$u_{eff}(k) = \frac{1}{g} \int_{p_{top}(k)}^{p_{bot}(k)} \left(\frac{p}{p_{ref}}\right)^n \cdot \left(\frac{T}{T_{ref}}\right)^{-n/2} \cdot q \cdot dp \tag{11.39}$$

The scaling exponent is set to $n_{H_2O} = 0.9$ and $n_{CO_2} = 0.75$. For ozone, mostly a stratospheric constituent, the pressure scaling may be neglected, hence $n_{O_3} = 0$. Variations of the temperature and of the mixing ratios within layers are neglected so that the integral is solved analytically:

$$u_{eff}(k) \cong \frac{1}{n+1} \left(\frac{p_{bot}^{n+1}}{p_{ref}^n} - \frac{p_{top}^{n+1}}{p_{ref}^n}\right) \cdot \left(\frac{\overline{T}}{T_{ref}}\right)^{-n/2} \cdot \frac{\overline{q}}{g} \tag{11.40}$$

The SW scheme includes absorption and Rayleigh scattering by water vapour and ozone, both varying in time and space, and $CO_2 + N_2O + CO + CH_4 + O_2$ as uniformly mixed gases. Aerosols and cloud particles are effective by absorption and scattering. Interactions between scattering processes and absorption are considered for water vapour and the uniformly mixed gases, but not for ozone, because gas absorption is assumed to dominate in the stratosphere.

Transmission functions for H_2O, CO_2, and O_3 in each band are expressed in form of Pade approximants with $N = 6$, where absorber amounts are given as effective amounts for reference conditions (see above).

$$t_{a,b}(u) = \frac{\sum_{i=0}^{N} A_{a,b} \cdot u^i}{\sum_{i=0}^{N+1} B_{a,b} \cdot u^i} \tag{11.41}$$

The computation of transmissivities and reflectivities across the column is split into two separate calculations for the cloud free section and the cloudy section. For the downward flux the actual optical path in each cell is computed from the solar zenith angle for the area exposed to the direct beam and the diffusivity factor $r = 1.66$ for the area related to the diffuse flux. The latter area depends on Rayleigh and aerosol scattering and, in the cloudy part of the column only, on the

band	$\lambda\,[\mu m]$	type	$I_{0,b}\,[\%]$	gaseous absorption
1	0.25-0.69	vis+UV	45.9760	H_2O, O_3
2	0.69-1.19	near IR	32.6158	H_2O, UMG
3	1.19-2.38	near IR	18.0608	H_2O, UMG
4	2.38-4.00	near IR	3.3474	H_2O, UMG, O_3

Table 11.1.: Spectral intervals, band type, fraction of solar irradiation, and absorbers (UMG denotes uniformly mixed gases)

scattering by cloud particles in the layers above. The area of diffuse flux is computed assuming maximum random overlap (see below). For the upward flux the optical path is increased by the diffusivity factor r.

11.3.1. Spectral resolution

The scheme has 4 spectral bands, 1 for the visible+UV range and 3 for the near infrared range. The near infrared range is now resolved by 3 bands instead of 1 in ECHAM4 to account better for the wavelength dependencies of the optical properties of cloud particles or aerosols. The interaction of scattering processes and gaseous absorption is considered only in the near IR bands, but neglected in the visible band. The solar irradiation $I_{0,b}$ is distributed over the bands as indicated in table 11.1.

11.3.2. Cloud optical properties

For the shortwave part of the spectrum, the single scattering properties are determined on the basis of Mie calculations using idealized size distributions for both cloud droplets and spherical ice crystals (Rockel et al., 1991). The results are averaged over the relatively wide spectral ranges of the GCM with appropriate weighting by the Planck function. This procedure is employed for different effective radii, and suitable fits are derived which allow to express the single scattering properties in terms of the effective radii of cloud droplets, R_{el}, and ice crystals, R_{ei}, respectively. While the latter is defined in section 10.3.4, R_{el} is obtained from the mean volume radius, R_{vl} (as defined in section 10.3.3 by using the following empirical relationship (Johnson, 1993)

$$R_{vl}^3 = kR_{el}^3 \tag{11.42}$$

with $k = 0.67(0.80)$ for continental (maritime) clouds. The mass extinction coefficients for liquid water clouds, $\tau_l[m^2g^{-1}]$, and for ice clouds, τ_i, are parameterized as

$$\tau_{l,i} = a_0 R_{el,i}^{a_1} \tag{11.43}$$

with $R_{el,i}$ in (μm) and different coefficients a_0, a_1 for the liquid and ice phase, respectively (Table 11.2). The single scattering albedo is parameterized as

$$\omega_{l,i} = \sum_{n=0}^{2} b_n \left(\log R_{el,i}\right)^n , \tag{11.44}$$

except for the ice phase in band no. 4, where the following expression is employed

$$\omega_{i,4} = b_0 R_{ei}^{b_1} \tag{11.45}$$

with coefficients according to Table 11.3. The asymmetry factor is expressed as

$$\gamma_{l,i} = \sum_{n=0}^{4} c_n \left(\log R_{el,i}\right)^n , \tag{11.46}$$

with coefficients according to Tables 11.4 and 11.5. The optical depth of a cloud layer is defined as

$$\delta_l = \tau_l \cdot LWP \tag{11.47}$$
$$\delta_i = \tau_i \cdot IWP \tag{11.48}$$

where LWP [gm^{-2}] is the in-cloud liquid water path and IWP is the in-cloud ice water path in the respective model layer.

It is well known that Mie theory tends to overestimate the asymmetry factor for ice clouds (e.g., Stephens et al. (1990)). Therefore, a correction factor of 0.91 is applied, adjusting γ_i to a more realistic value of ≈ 0.80 (Francis et al., 1994) for a wide range of effective radii. In the mixed phase, the shortwave cloud optical depth δ_m, the single scattering albedo ω_m, and the asymmetry factor γ_m are defined as (Rockel et al., 1991)

$$\delta_m = \delta_l + \delta_i \tag{11.49}$$
$$\omega_m = \frac{\omega_l \delta_l + \omega_i \delta_i}{\delta_l + \delta_i} \tag{11.50}$$
$$\gamma_m = \frac{\omega_l \delta_l \gamma_l + \omega_i \delta_i \gamma_i}{\omega_l \delta_l + \omega_i \delta_i}. \tag{11.51}$$

In the current model version, no subgrid-scale variability of cloud, except for fractional cloudiness, is taken into account in the radiation code, i.e. clouds are treated as plane-parallel homogeneous (PPH) layers. For a given cloud water content this simplification leads to maximum cloud albedo compared to any other distribution. Since real clouds are never homogeneous, the calculated cloud albedo is systematically too high for 'realistic' values of the cloud water content. Several suggestions have been made to eliminate this so called PPH-bias. The most popular one is the 'effective thickness approach' (ETA) whereby cloud optical thickness is reduced by a factor which is either constant, e.g. $f = 0.7$ (Cahalan et al., 1994), or dependent on cloud type, for example Tiedtke (1996). More recently, statistical correction schemes have been developed from satellite data (e.g., Barker et al. (1996)) using idealized Γ-distributions of optical thickness.

In the standard ECHAM5, an ETA variant is used with correction factors defined differently for the liquid and ice phase, respectively. The total liquid water path in a vertical column, TLWP [gm^{-2}], is modified according to

$$TLWP^* = a(TLWP)^b \tag{11.52}$$

Spectral range [μm]	a_0 (liquid)	a_1 (liquid)	a_0 (ice)	a_1 (ice)
0.2 - 0.69	1.8362	-1.0665	1.9787	-1.0365
0.69 - 1.19	2.0731	-1.1079	2.1818	-1.0611
1.19 - 2.38	1.8672	-1.042	1.9608	-1.0212
2.38 - 4.0	1.0787	-0.79772	1.2558	-0.88622

Table 11.2.: Coefficients for mass extinction coefficient, see (11.43).

Spectral range [μm]	b_0 (liquid)	b_1 (liquid)	b_0 (ice)	b_1 (ice)	b_2 (ice)
0.2 - 0.69	1	-2.2217e-7	1	-1.143e-7	0
0.69 - 1.19	1	-1.6712e-5	0.99999	-7.923e-6	0
1.19 - 2.38	0.99936	-1.3632e-3	0.99975	-1.662e-3	6.9726e-6
2.38 - 4.0	0.90032	-0.091955	0.89779	-0.0802	-

Table 11.3.: Coefficients for single scattering albedo, see (11.44) and (11.45). Note that b_2 (liquid) = 0 for all bands.

Spectral range [μm]	c_0 (liquid)	c_1 (liquid)	c_2 (liquid)	c_3 (liquid)	c_4 (liquid)
0.2 - 0.69	0.78063	0.126	-0.042412	0	0
0.69 - 1.19	0.74102	0.16315	-0.050268	0	0
1.19 - 2.38	0.7073	0.18299	-0.045693	0	0
2.38 - 4.0	0.70554	0.88798	-1.8214	1.5775	-0.46293

Table 11.4.: Coefficients for the asymmetry factor γ_l, see (11.46)

Spectral range [μm]	c_0 (ice)	c_1 (ice)	c_2 (ice)
0.2 - 0.69	0.79602	0.10183	-0.028648
0.69 - 1.19	0.77176	0.11995	-0.030557
1.19 - 2.38	0.74691	0.13514	-0.02714
2.38 - 4.0	0.77614	0.15186	-0.031452

Table 11.5.: Coefficients for the asymmetry factor γ_i, see (11.46).

so that the correction factor can be obtained as

$$\frac{TLWP^*}{TLWP} \equiv f_l = a(TLWP)^{b-1} \tag{11.53}$$

for $TLWP > 1$ gm^{-2}, $f_l = 1$ for $TLWP \leq 1$ gm^{-2}, $a = 1$ and $b = 0.925$. Note that for $a = 0.7$ and $b = 1$, (11.52) and (11.53) result in $f_l = 0.7$ (Cahalan et al., 1994) which has been derived for stratocumulus clouds of intermediate optical thickness. For optically thin clouds, (11.53) leads to smaller corrections while for optically very thick clouds the corrections are somewhat larger (0.6 or even less). For ice clouds, a constant reduction factor f_i is applied in the range of 0.8 to 0.9 (Buschmann, 2001), depending on model resolution.

Using (11.53) and f_i, the optical thicknesses used in the shortwave (SW) radiation code are given by

$$\delta_l^*(SW) = f_l \delta_l \tag{11.54}$$
$$\delta_i^*(SW) = f_i \delta_i \tag{11.55}$$
$$\delta_m^*(SW) = \delta_l^*(SW) + \delta_i^*(SW). \tag{11.56}$$

Note that the corrections are applied only to cloud optical thicknesses. Single scattering albedo and asymmetry factor remain unchanged.

A more consistent correction scheme, the so-called 'beta weighted two stream approximation' (Bäuml, 2002) is currently being tested, which takes advantage of the fact that the cloud scheme provides the subgrid-scale cloud water distribution as a beta distribution (c.f. section 10.2).

11.3.3. Cloud overlap assumption

Total cloudiness in a column A_c^{tot} is computed iteratively, using the maximum-random overlap assumption, from the uppermost clouded layer j_{c1} to the surface. If $A_{c,j}^{tot}$ is the overlapping cloudiness in at the lower boundary of layer j, then $A_{c,j+1}^{tot}$ is computed as follows:

$$A_{c,j+1}^{tot} = \begin{cases} 1 - (1 - A_{c,j+1}) \cdot \frac{1-A_{c,j+1}}{1-A_{c,j}^{tot}}, & A_{c,j+1} > A_{c,j}^{tot} \\ 1 - (1 - A_{c,j+1}) & else \end{cases} \tag{11.57}$$

11.4. Longwave radiation

Terrestrial infrared radiation redistributes energy within the atmosphere depending on the composition of the atmosphere with regard to the active gases, aerosols and cloud particles, and cools the atmosphere to space to balance the solar irradiation. The solution of the transfer differs from that in the shortwave by the presence of emitting sources within the atmosphere and the presence of a diffuse external source, the Earth surface, compared to the solar beam. Scattering may be neglected. Then, for each layer its average outgoing radiance within a frequency range is given by:

$$\overline{R} = \frac{1}{\upsilon_2 - \upsilon_1} \cdot \int_{\upsilon_1}^{\upsilon_2} d\upsilon \left\{ R_0(\upsilon) + \int_{t_\upsilon}^{1} (B(\upsilon, T(t'_\upsilon)) - R_0(\upsilon)) dt' \right\} \tag{11.58}$$

where $R_0(\upsilon)$ is the radiance entering the layer and $B(\upsilon, T(t'_\upsilon))$ is the Planck function for the temperature at a point along the optical path. Transmittance is used as the coordinate along the path.

The longwave (LW) radiative transfer parameterization of ECHAM5 follows the RRTM scheme (Mlawer et al., 1997) as implemented in cycle 23 release 1 (CY23R1) of the IFS model of ECMWF (Morcrette et al., 1998). This scheme makes use of the correlated-k method applied to 16 spectral intervals with a total of 140 intervals in g-space. Absorption coefficients are derived from the LBLRTM line-by-line model (Clough et al., 1989, 1992; Clough and Iacono, 1995) and include the the effects of the CKD2.2 water vapour continuum (Clough et al., 1989). In g-space the radiance may be formulated as:

$$\overline{R} = \int_0^1 dg \left\{ B_{eff}(g, T_g) + [R_0(g) - B_{eff}(g, T_g)] \cdot \exp\left[-k(g, p, T) \frac{\rho \Delta z}{\cos \phi} \right] \right\} \tag{11.59}$$

where $B_{eff}(g, T_g)$ is an effective Planck function that varies with the layer's transmittance in order to maintain continuity of the flux across layer boundaries, and the absorption coefficient $k(g, p, T)$ is dependent on the ambient conditions.

In the implemented RRTM LW-scheme the integral over g is discretized in a number of intervals per band, with a total of 140 intervals. In each of these intervals a characteristic value k_j is chosen, and the integral can be replaced by a weighted sum:

$$\overline{R} = \textstyle\sum_j w_j \cdot (B_{eff,j} + (R_{0,j} - B_{eff,j}) \cdot \exp(-k_j \cdot \frac{\rho dz}{\cos \phi})), \quad \sum_j w_j = 1 \tag{11.60}$$

The k_j values are derived from the LBLRTM. For efficiency reason the integration over the zenith angle ϕ is simplified by the diffusivity approximation, and normal absorber amounts are simply multiplied with the diffusivity factor $r = 1.66$.

11.4.1. Spectral resolution

The RRTM scheme computes fluxes in the spectral range of $10 cm^{-1}$ to $3000 cm^{-1}$. The computation is organized in 16 spectral bands, and includes line absorption by H_2O, CO_2, O_3, CH_4, $CFC11$, $CFC12$, $CFC22$, and aerosols. Aerosols are considered in all spectral bands. The water vapour self continuum is taken into account in the troposphere only, the foreign continuum in the full column, though in bands 1 to 3 only (Table 11.6) .

11.4.2. Cloud optical properties

In the longwave part of the spectrum, the mass absorption coefficient for liquid clouds, K_l [m^2/g], is parameterized as a function of the respective effective radius R_{el} [μm] according to

$$K_l = 1.66 \, [d_0 + d_1 \exp(-d_2 R_{el})] \tag{11.61}$$

with coefficients d_n given in Table 11.7.

For cirrus clouds an inverse dependency of K_i on the ice crystal effective radius R_{ei} has been postulated by Stephens et al. (1990) and also inferred from measurements during the International

interval (cm^{-1})	g-points	trop . abs.	strat. abs.
10-250	8	H_2O,SC,FC	H_2O,FC
250-500	14	H_2O,SC,FC	H_2O,FC
500-630	16	H_2O, CO_2, N_2O,SC,FC	H_2O, CO_2, N_2O,FC
630-700	14	H_2O, CO_2,SC	O_3, CO_2
700-820	16	H_2O, CO_2,SC	O_3, CO_2
820-980	8	$H_2O, CO_2, CFC11, CFC12$,SC	$CFC11, CFC12$
980-1080	12	H_2O, O_3, CO_2,SC	O_3, CO_2
1080-1180	8	$H_2O, CFC12, CFC22, CO_2, N_2O$,SC	$O_3, CFC12, CFC22, CO_2, N_2O$
1180-1390	12	H_2O, CH_4, N_2O,SC	CH_4
1390-1480	6	H_2O	H_2O
1480-1800	8	H_2O,SC	H_2O
1800-2080	8	H_2O, CO_2,SC	-
2080-2250	4	H_2O, N_2O,SC	-
2250-2380	2	CO_2,SC	CO_2
2380-2600	2	N_2O, CO_2,SC	-
2600-3000	2	H_2O, CH_4,SC	-

Table 11.6.: Spectral intervals, number of g points in each interval, gaseous absorbers used in the troposphere and in the stratosphere, SC and FC denote the self and foreign continuum

Coefficient	
d_0	0.015373877
d_1	0.171966914
d_2	-0.088968393

Table 11.7.: Coefficients used in the polynomial fit to Mie calculations of longwave absorption coefficient for liquid droplets, see (11.61).

spectral intervall [cm^{-1}]	a	b
10-250	0.0069	0.718
250-500	0.0060	0.726
500-630	0.0024	1.136
630-700	0.0004	1.320
700-820	-0.0016	1.505
820-980	0.0003	1.290
980-1080	0.0043	0.911
1080-1180	0.0038	0.949
1180-1390	0.0030	1.021
1390-1480	0.0013	1.193
1480-1800	0.0005	1.279
1800-2080	0.0054	0.626
2080-2250	0.0052	0.647
2250-2380	0.0050	0.668
2380-2600	0.0048	0.690
2600-3000	0.0048	0.690

Table 11.8.: Coefficients used in the parameterization of the mass absorption coeeficient for ice crystals, see (11.62).

Cirrus Experiment ICE'89 by Francis et al. (1994). Here the parameterization of Ebert and Curry (1992) is used

$$K_i = 1.66 \left(a + \frac{b}{R_{ei}} \right) \tag{11.62}$$

with R_{ei} in μm. The coefficients a and b vary with wavenumber according to table 11.8

Analogous to (11.54) - (11.56), the corrected infrared optical thicknesses used in the longwave radiation code are defined as

$$\begin{aligned} \delta_l^*(IR) &= f_l K_l LWP & (11.63)\\ \delta_i^*(IR) &= f_i K_i IWP & (11.64)\\ \delta_m^*(IR) &= \delta_l^*(IR) + \delta_i^*(IR). & (11.65) \end{aligned}$$

.

11.4.3. Cloud overlap assumption

Maximum cloud overlap is assumed for contigous cloud layers, random overlap else (c.f., section 11.3.3).

11.4.4. Aerosol optical properties

Currently aerosol emissivities are derived from the Tanre climatology which defines the optical depth at 0.55 micron. This optical depth is rescaled to the spectral intervals of the ECHAM4 LW

scheme, then projected on the bands of the RRTM scheme.[2]

11.4.5. Surface emissivity

The longwave emissivity assumes a constant value of 0.996 for all surfaces and spectral intervals.

[2] A direct estimation for the RRTM intervals is in work.

12. Orbital Variations

12.1. Introduction

In the mid-19th century, Croll (1867b,a) proposed an astronomical theory linking the Pleistocene[1] ice ages with periodic changes in the Earth's orbit around the Sun. Croll's ideas were later refined and elaborated by Milankovitch (1941). Since this theory was put forward, much evidence has been found to support it.

The original Milankovitch theory identifies three types of orbital variations which could act as climate forcing mechanisms, obliquity of the Earth's axis, eccentricity of the Earth orbit around the Sun, and precession of the equinoxes. Each variation has its specific time period.

To allow proper representation of orbital variations for climate simulations in ECHAM5, two orbits are given. The first one is based on very precise orbit determination principles to reflect short term variations for todays climate. It is using the VSOP (Variations Séculaires des Orbites Planétaires) analytical solution by Bretagnon and Francou (1988). This analytical solution is representing the todays orbit for an interval of -4000 and +8000 years with respect to the epoch J2000.0 very accurate. The second orbit given is using the basic Kepler laws only, allowing for simple adjustment for paleoclimate studies using the long term series expansions for obliquity, eccentricity, and precession by Laskar and Boudin (1993).

Before starting to describe the used orbits, the three basic orbital parameters for variations in climate are described as there are the obliquity i, the eccentricity e, and the precession expressed as the longitude of the perihelion ω with respect to the equinox.

12.1.1. Obliquity

Today the Earth is tilted on its rotational axis at an angle of 23.4° relative to a perpendicular to the orbital plane of the Earth. Over a $\tilde{4}1000$ year time period, this angle of inclination fluctuates between 22° and 24.5°, influencing the latitudinal distribution of solar radiation.

Obliquity does not influence the total amount of solar radiation received by the Earth, but affects the distribution of insolation in space and time. As obliquity increases, so does the amount of solar radiation received at high latitudes in summer, whilst insolation decreases in winter. Changes in obliquity have little effect at low latitudes, since the strength of the effect decrease towards the equator. Consequently, variations in the Earth's axial tilt affect the strength of the latitudinal temperature gradient. Increased tilt has the effect of raising the annual receipt of solar energy at high latitudes, with a consequent reduction in the latitudinal temperature gradient.

[1] 2 Million to 10 thousand years ago

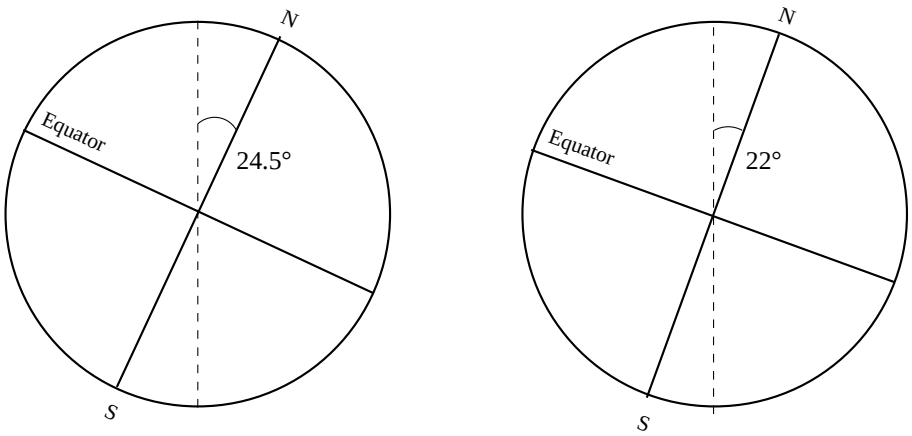

Figure 12.1.: Obliquity

12.1.2. Eccentricity

The Earth's orbit around the Sun is not perfectly circular but follows an elliptical path (see Figure 12.2). A second orbital variation involves the strength of the ellipse, or eccentricity. This parameter, e, is determined by Equation 12.1.

$$e = \frac{1}{2}\frac{(a^2 - b^2)}{a} \tag{12.1}$$

When the orbit is circular, the semimajor axis a and semiminor axis b are equal and $e = 0$. The Earth's orbit has been found to vary from being near circular ($e = 0.005$) to markedly elliptical ($e = 0.06$) with two primary periodicities of approximately 96000 and 413000 years (Berger, 1976). The current value of e is 0.0167 (Meeus, 1998). Variations in eccentricity influence the total amount of solar radiation incident at the top of the Earth's atmosphere. With maximum eccentricity, differences in solar radiation receipt of about 30 % may occur between perihelion and aphelion (Goodess et al., 1992).

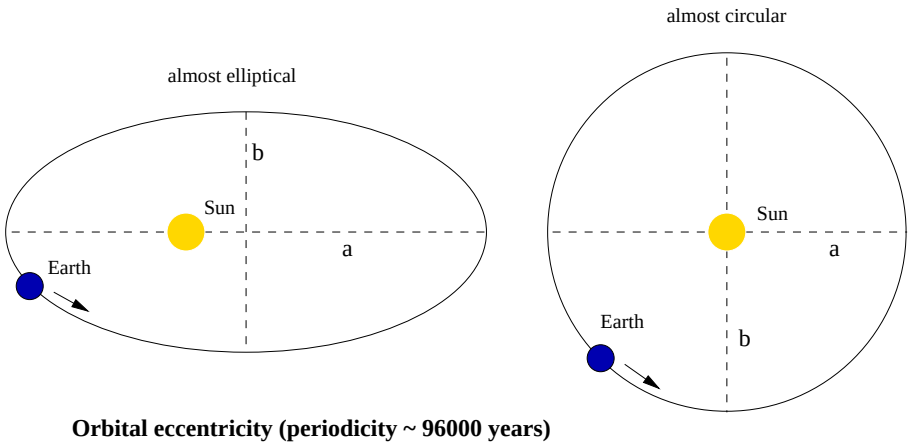

Figure 12.2.: Eccentricity

12.1.3. Precession

The third orbital variation is that of precession. The Sun lies at one of the focal points of the Earth's orbital ellipse. Due to the gravitational interaction of other planetary bodies in the solar system, primarily the Moon and the planet Jupiter, the perihelion (the point at which the Earth passes closest to the Sun) moves in space with a consequent shifting or precessing of the elliptical orbit. This phenomenon is known as the precession of the equinoxes, and effects the intensity of the seasons.

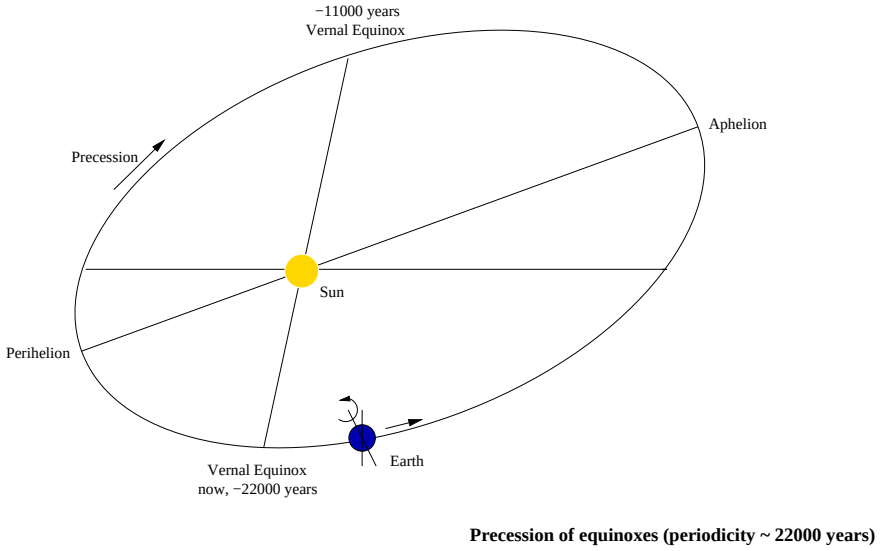

Figure 12.3.: Precession

Precession has two components: an axial precession, in which the torque of the other planets exerted on the Earth's equatorial bulge causes the rotational axis to gyrate like a spinning top, and an elliptical precession, in which the elliptical orbit of the Earth itself rotates about one focus. The net effect describes the precession of the equinoxes with a period of 22000 years. This term is modulated by eccentricity which splits the precession into periods, of 19000 and 23000 years (Crowell and North, 1991).

Like obliquity, precession does not affect the total amount of solar energy received by the Earth, but only its hemispheric distribution over time. If the perihelion occurs in mid-June i.e. when the Northern Hemisphere is tilted toward the Sun, then the receipt of summer solar radiation in Northern Hemisphere will increase. Conversely, if the perihelion occurs in December, the Northern Hemisphere will receive more solar radiation in winter. It should be clear that the direction of changes in solar radiation receipt at the Earth's surface is opposite in each hemisphere.

12.2. Precise orbit determination based on VSOP87

12.2.1. VSOP — Variations Séculaires des Orbites Planétaires

From an analytical solution of the motion of the planets expressed with elliptic elements (Bretagnon, 1982) the position of planets is expressed as a Poisson series expansion. Different sets of coordinate representations have been derived. The solution used in ECHAM5 for the position of Earth is based on heliocentric spherical coordinate variables and the reference frame is the mean equinox and ecliptic of date.

The position of Earth is given by the heliocentric latitude L and longitude B and the distance from the Sun R.

This coordinates are given by the following Poisson series:

$$L = \sum_{n=1}^{6} L_n \sum_{k=1}^{k_N} a_{k_n} \cos(b_{k_n} + c_{k_n} \tau^n) \tag{12.2}$$

$$B = \sum_{n=1}^{2} B_n \sum_{k=1}^{k_N} a_{k_n} \cos(b_{k_n} + c_{k_n} \tau^n) \tag{12.3}$$

$$R = \sum_{n=1}^{5} R_n \sum_{k=1}^{k_N} a_{k_n} \cos(b_{k_n} + c_{k_n} \tau^n) \tag{12.4}$$

where τ is reckoned in thousands of Julian years from epoch J2000.0

$$\tau = \frac{\text{Julian date} - 2451545}{365250} \tag{12.5}$$

The coefficients for the Poisson series expansions are given in tables B.1 till B.13 in appendix B.

To derive the required coordinates of the Sun with respect to Earth the calculated heliocentric spehrical coordinates have to be transformed to geocentric spherical coordinates.

First step is a transformation of the Sun's and Earth's position to heliocentric rectangular coordinates with:

$$\vec{X}_s = f(L_s, B_s, R_s) \quad \text{and} \quad \vec{X}_e = f(L_e, B_e, R_e) \tag{12.6}$$

$\vec{X}$ are the heliocentric rectangular coordinates, (L, B, R) are the heliocentric spherical coordinates. The subscripts s and e are denoting the Sun and Earth respectively. The transformation function f is given by:

$$\begin{aligned} X &= R \cos L \cos B \\ Y &= R \sin L \cos B \\ Z &= R \sin B \end{aligned} \tag{12.7}$$

The geocentric rectangular coordinates are than given by:

$$\vec{x} = \vec{X}_s - \vec{X}_e \tag{12.8}$$

$\vec{x}$ has to be transformed to geocentric spherical coordinates by the inverse f^{-1} of equation 12.7:

$$\begin{aligned} l &= \arctan \frac{y}{x} \quad \text{with} \quad l = l + 2\pi \quad \text{for} \quad l < 0 \\ b &= \arcsin \frac{z}{r} \\ r &= \sqrt{x^2 + y^2 + z^2} \end{aligned} \tag{12.9}$$

The next step is the transformation from the ecliptic geocentric to equatorial geocentric coordinates. This requires the obliquity (or inclination) i of Earth. This is a slowly varying property of the Earth's orbit, see section 12.1.1. For the calculation of the actual obliquity a polynomial series developed by Laskar and Boudin (1993) is used:

$$\begin{aligned} i &= 84381.448 \\ &\quad -4680.93U - 1.55U^2 + 1999.25U^3 - 51.38U^4 - 249.67U^5 \\ &\quad -39.05U^6 + 7.12U^7 + 27.87U^8 + 5.79U^9 + 2.45U^10 \end{aligned} \tag{12.10}$$

U is the time given as $U = 0.01\tau$. The transformation to equatorial geocentric coordinates is given by:

$$\begin{aligned} \alpha &= \arctan\left(\frac{\cos b \sin l \cos i - \sin b \sin i}{\cos b \cos L}\right) \quad \text{with} \quad \alpha = \alpha + 2\pi \quad \text{for} \quad \alpha < 0 \\ \delta &= \arcsin\left(\sin b \cos i + \cos b \sin i \sin l\right) \end{aligned} \tag{12.11}$$

There is another effect which has to be considered in determining the Sun's position in geocentric coordinates and this is the aberration. Aberration is the angular discrepancy between the apparent position of a star and its true position, arising from the motion of an observer relative to the path of the beam of light observed. This motion is the result of velocity components like the speed of the diurnal rotation of the Earth and its orbital speed in revolving around the sun. The change in Earth's position due to aberration regarding the Sun is given by:

$$\Delta\alpha = -9.93639\,10^{-5}\,\frac{(\cos\alpha\cos\lambda\cos i + \sin\alpha\sin\lambda)}{\cos\delta} \tag{12.12}$$

$$\Delta\delta = -9.93639\,10^{-5}\cos\lambda\,(\sin i\cos\delta - \sin\alpha\sin\delta\cos i) + \cos\alpha\sin\delta\sin\lambda \tag{12.13}$$

where λ is the longitude and e the eccentricity of the Sun given by

$$\lambda = L_0 + C \tag{12.14}$$

where L_0 is the Sun's longitude of the ascending node, and C the position of the Sun, these are in terms of mean anomaly M and eccentricity e (in degrees), and time t in hundreds of Julian years:

$$L_0 = 280.46646 + 36000.76983\,t + 0.0003032\,t^2 \tag{12.15}$$

$$M = 357.52910 + 35999.05028\,t - 0.0001561\,t^2 \tag{12.16}$$

$$e = 0.016708617 - 0.000042040\,t + 0.0000001236\,t^2 \tag{12.17}$$

$$C = e\,(2 - 0.25\,e^2)\sin M + 1.25\,e^2\sin 2M + 1.083\,e^3\sin 3M \tag{12.18}$$

with

$$t = \frac{\text{Julian date} - 2451545}{36525}$$

So, the final position is

$$\alpha = \alpha + \Delta\alpha \tag{12.19}$$
$$\delta = \delta + \Delta\delta \tag{12.20}$$

Finaly the mean sidereal time in degrees has to be determined:

$$\theta_0 = \left(280.46061837 + 360.98564736629 \cdot 36525\,t + 0.000387933\,t^2 - \frac{t^3}{38710000}\right) \text{with} \theta_0 = \theta_0 \text{mod} 360 \tag{12.21}$$

12.2.2. Nutation

Nutation is a small wobble of the Earth's rotational axis with an amplitude of about 9 arcsec and period of up to 18.6 years. Traditionally, nutation is represented by variations in ecliptic longitude and obliquity (the angle between the ecliptic and the equator). Current models represent the nutation quantities with well-defined series (Seidelmann, 1982).

The nutation of the Earth is handled by the following equations and added before the transformation from the geocentric ecliptic to the geocentric equatorial coordinate system is performed.

Five auxilliar variables must be calculated which allows the further expansion of a sine/cosine series for the nutation. The five variables are

- longitude of the mean ascending node of the lunar orbit on the ecliptic, measured from the mean equinox of date

$$\Omega = 125.0445222 - 1934.1362608\,t + 0.00207833\,t^2 + 2.220e-6\,t^3 \tag{12.22}$$

- mean longitude of the Sun minus the mean longitude of the Sun's perigee

$$M = 357.5277233 + 35999.0503400\,t - 0.00016030\,t^2 - 3.330e-6\,t^3 \tag{12.23}$$

- mean longitude of the Moon minus the mean longitude of the Moon's perigee

$$M' = 134.9629814 + 477198.8673981\,t + 0.00869720\,t^2 + 1.778e-5\,t^3 \tag{12.24}$$

- mean longitude of the Moon minus the mean longitude of the Moon's node

$$F = 93.2719103 + 483202.0175381\,t - 0.00368250\,t^2 + 3.056e-6\,t^3 \tag{12.25}$$

- mean elongation of the Moon from the Sun

$$D = 297.8503631 + 445267.1114800\,t - 0.00191420\,t^2 + 5.278e-6\,t^3 \tag{12.26}$$

The table B.14 with the require coeeficients is given in appendix B.

12.3. Kepler based orbit for paleoclimate applications

The three components of the orbital variations, obliquity, eccentricity, and precession together effect both the total flux of incoming solar radiation and also the temporal and spatial distribution of terrestrial insolation. These variations have the potential to influence the energy budget of the climate system (Milankovitch, 1941; Berger, 1978), and can therefore be regarded as possible causes of climate change over long time scales.

Milankovitch (1941) considered the changing seasonal (precession) and latitudinal (obliquity) patterns of incoming radiation to be critical factors in the growth of continental ice sheets and in the initiation of ice ages. He hypothesised that when axial tilt was small (large latitudinal temperature gradient), eccentricity was large and perihelion occurred during the Northern Hemisphere winter (warmer winters and colder summers), such a configuration would allow the persistence of accumulated snow throughout the summer months in the Northern Hemisphere. Additionally, the warmer winters and stronger atmospheric general circulation due to the increased temperature gradient would increase the amount of water vapour at the high latitudes available for snowfall.

To allow for paleoclimate studies, ECHAM5 provides an Kepler based orbit which has as basic parameters, to be defined externally, the long term varying orbit parameters obliquity, eccentricity, and, as measure for the precession, the longitude of perihelion from the equinox of date.

Used for the calculation of the position of the Sun is Lacaille's formula which links the true anomaly ν and the eccentric anomaly E:

$$\tan\frac{\nu}{2} = \sqrt{\frac{1+e}{1-e}}\tan\frac{E}{2} \tag{12.27}$$

with $\nu = \omega$, where ω is the longitude of perihelion. This allows the calculation of the eccentric anomaly which is required for the Kepler equation linking the eccentric and the mean anomaly M:

$$M = E - e\sin E \tag{12.28}$$

First, calculate the mean anomaly M of the current longitude λ from the true anomaly ν:

$$M = \lambda - M(\omega) \quad \text{with} \quad M(\omega) = \nu - e\sin\nu \tag{12.29}$$

The true and mean anomaly are identical at the vernal equinox. For solving the Kepler equation 12.28 the Newton method is used:

$$E^{m+1} = E^m - \frac{K(E^m)}{K'(E^m)}$$

with

$$K(E) = M - E + e\sin E = 0 \quad \text{and} \quad K'(E) = 1 + e\cos E$$

so the final iteration expression to solve is:

$$E^{m+1} = E^m - \frac{M - E^m + e\sin E^m}{1 + e\cos E^m} \tag{12.30}$$

This iterative solver does converge for most initial values, but not for all. This has been taken into account. For more details see Meeus (1998).

The final distance between Earth and Sun is given by

$$R = \left(\frac{1}{1 - e \cos E} \right)^2 \tag{12.31}$$

and the true anomaly ν with Lacaille's formula (equation 12.27). The true longitude is $\lambda = \nu + \omega$ and the declination of the Sun (with i the obliquity (or inclination):

$$\delta = \sin i \sin \lambda \tag{12.32}$$

and the right ascension:

$$\alpha = \tan \frac{\cos i \sin \lambda}{\cos \lambda} \tag{12.33}$$

12.4. Differences in the daily insolation due to the two given orbits

The astronomical orbital parameters have to be transformed into the solar constant scaled by the distance Earth — Sun R and the local zenith angle Z.

For comparison of the two given orbits the difference in the orbit parameters against the JPL DE405 are shown. The first set is for the AMIP2 period 1978 to 1996 and the second set for 1870 till 2150.

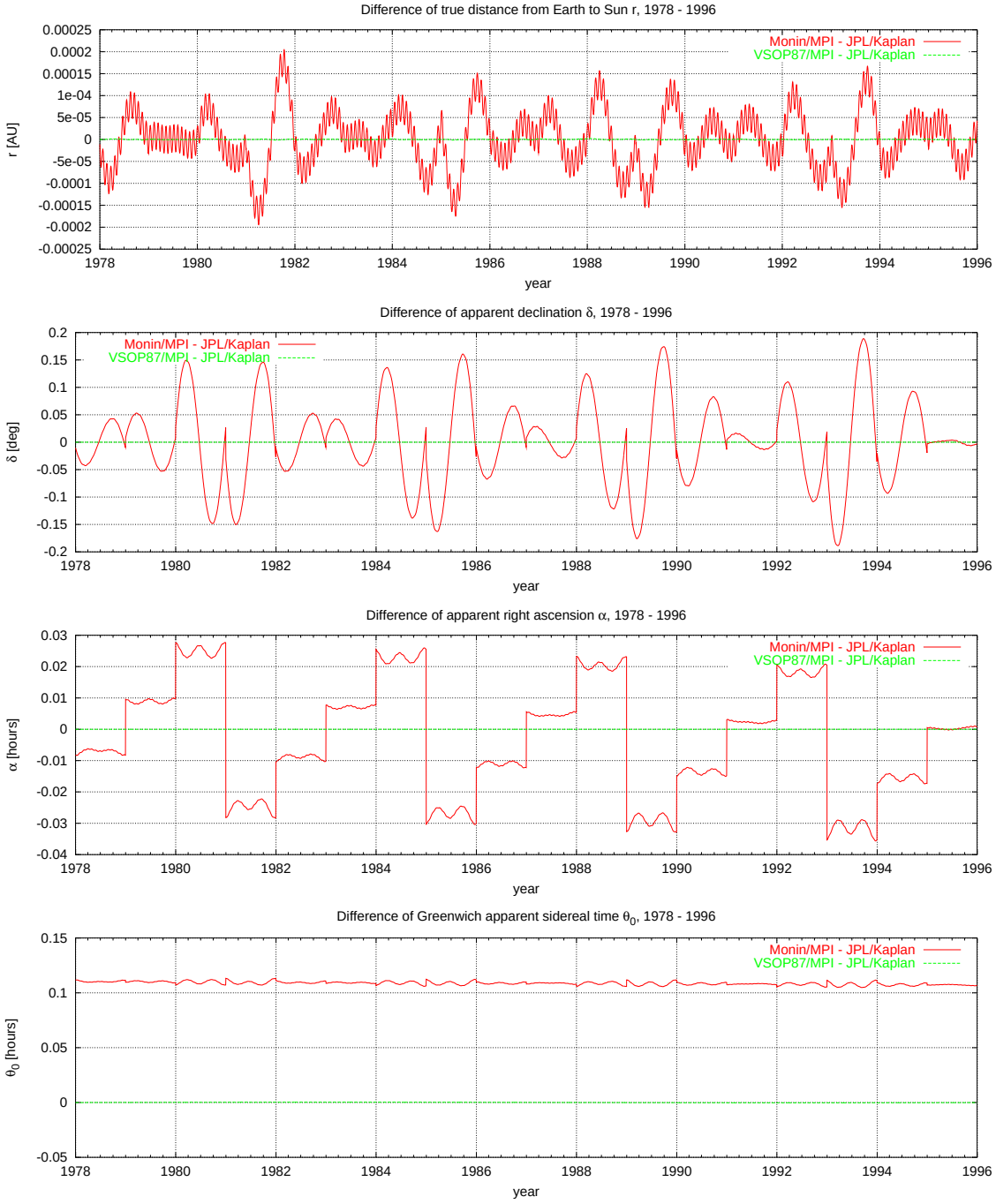

Figure 12.4.: Differences between the VSOP87 and Monin orbit with respect to JPL's DE405 for the peride 1978 till 1996

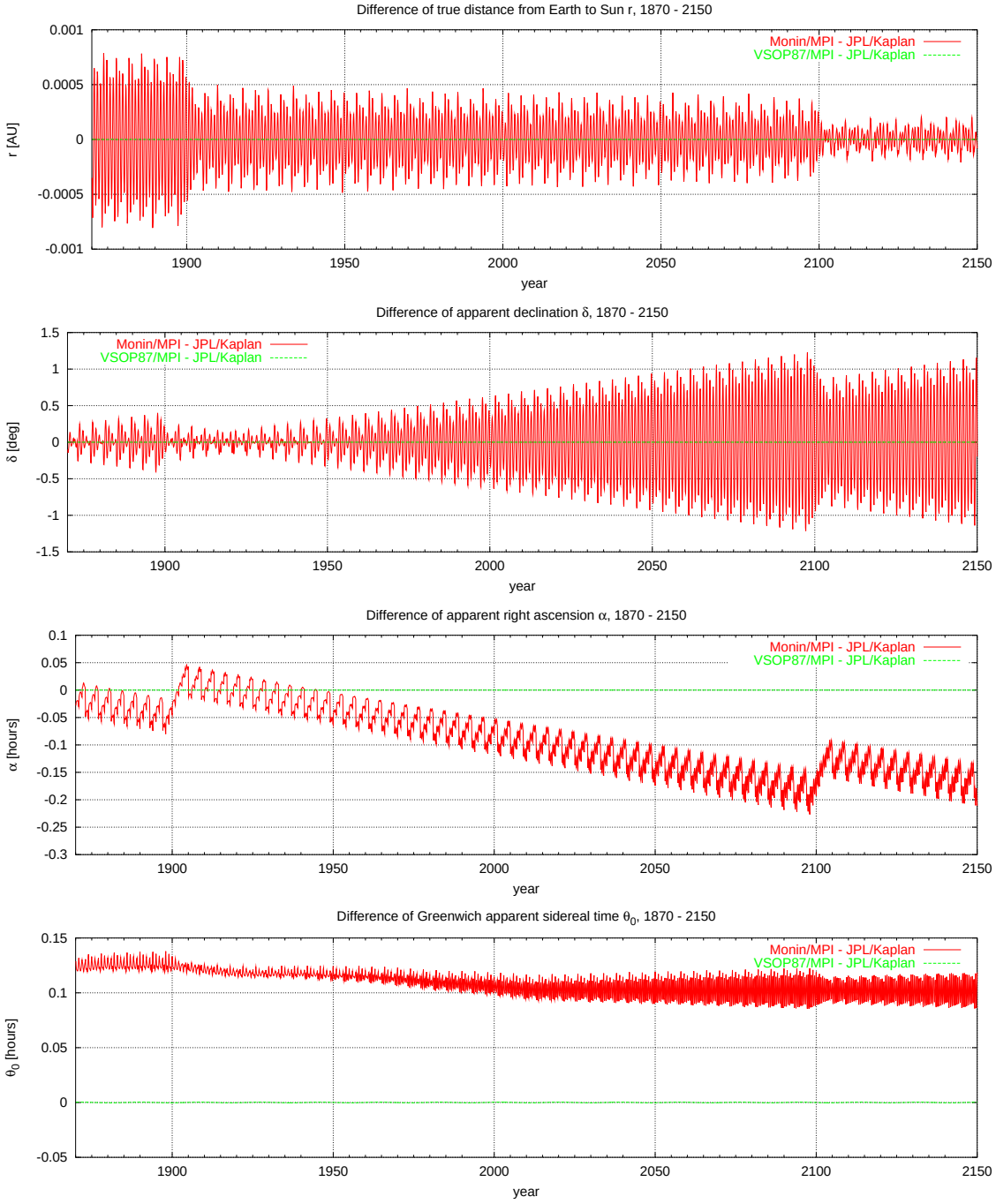

Figure 12.5.: Differences between the VSOP87 and Monin orbit with respect to JPL's DE405 for the peride 1870 till 2150

A. The unparametrized equations

A.1. Introduction

To derive the governing equations given by (2.1)–(2.6) and (2.11)–(2.14), we take start from the unparametrized equations for a mixture of dry air, water vapour, liquid water and ice, and work for convenience in a Cartesian coordinate system. An individual component is denoted by a subscript i, where $i = d, v, l$, or i for dry air, water vapour, liquid water or ice, respectively. The specific mass of component k, denoted by q_k, is defined by

$$q_k = \frac{m_k}{m} = \frac{\rho_k}{\rho} \tag{A.1}$$

where

m_k	is the mass of component of k in a small material volume moving with the local velocity of the atmosphere,
$m = \sum m_k$	is the total mass of the material volume,
ρ_k	is the density of component k, and
$\rho = \sum \rho_k$	is the density of the atmosphere.

The rate of change of m_k is denoted by $\dot{m}_k$. This change occurs because of

a. internal phase changes,

b. rainfall, snowfall, and surface exchanges.

The rate of change due to (a) alone is denoted by $\dot{m}_{ki}$, and that due to (b) by $\dot{m}_{ke}$. Then

$$\dot{m}_k = \dot{m}_{ki} + \dot{m}_{ke} \tag{A.2}$$

$$\dot{m}_{di} = \dot{m}_{de} = 0 \tag{A.3}$$

$$\sum_i \dot{m}_{ki} = 0 \tag{A.4}$$

The rate of change of total mass is given by

$$\dot{m} = \sum_i \dot{m}_k = \sum_i \dot{m}_{ke} \tag{A.5}$$

The rate of change of density of component k satisfies the equation

$$\dot{\rho}_k = \frac{\rho}{m}\dot{m}_k \tag{A.6}$$

provided (as is reasonable) volume changes due to precipitation or phase changes are neglected. The net rate of change of density, $\dot{\rho}$, is then given by

$$\dot{\rho} = \frac{\rho}{m}\sum_k \dot{m}_k = \frac{\rho}{m}\dot{m} \tag{A.7}$$

A.2. The advective form of the unparameterized equations

A.2.1. The material derivative

The material derivative is denoted by $\frac{d}{dt}$. Its definition is

$$\frac{d}{dt} \equiv \frac{\partial}{\partial t} + \vec{v}\cdot\nabla \tag{A.8}$$

where $\vec{v}$ here denotes the three-dimensional velocity vector, and ∇ the ususal three-dimensional vector operator. Horizontal vectors and operators will subsequently be denoted by a subscript h.

A.2.2. The equation of state

We consider a volume V of atmosphere, of which dry air and water vapour occupy a volume V_{d+v}. The equations of state for dry air and water vapour are

$$p_d V_{d+v} = m_d R_d T \tag{A.9}$$

and

$$p_v V_{d+v} = m_v R_v T \tag{A.10}$$

where p_d and p_v are partial pressures. Dalton's Law then shows that the total pressure p is given from A.10 by

$$p = \frac{m_d R_d T + m_v R_v T}{V_{d+v}}. \tag{A.11}$$

Introducing the specific volumes of liquid water v_l, and ice v_i,

$$V_{d+v} = V - m_l v_l - m_i v_i = \frac{m}{\rho}(1 - \rho(q_l v_l + q_i v_i)) \tag{A.12}$$

and A.11 becomes

$$p = \rho T \frac{R_d q_d + R_v q_v}{1 - \rho(q_l v_l + q_i v_i)}. \tag{A.13}$$

or

$$p = \rho T R_d \frac{1 + \left(\frac{1}{\epsilon} - 1\right) q_v - q_l - q_i}{1 - \rho(q_l v_l + q_i v_i)}. \tag{A.14}$$

where

$$\epsilon = R_d / R_v \tag{A.15}$$

A.2.3. Mass conservation

Conservation of mass for element k leads to the equation

$$\frac{d\rho_k}{dt} + \rho_k(\nabla \cdot \vec{v}) = \dot{\rho}_k = \frac{\rho \dot{m}_k}{m} \tag{A.16}$$

Summing over k then gives

$$\frac{d\rho}{dt} + \rho(\nabla \cdot \vec{v}) = \frac{\rho \dot{m}}{m} = \dot{\rho} \tag{A.17}$$

In addition, by definition

$$\frac{dm_k}{dt} = \dot{m}_k \tag{A.18}$$

which gives

$$\frac{dq_k}{dt} = \frac{\dot{m}_k}{m} - \frac{m_k \dot{m}}{m^2} = \frac{1}{m}(\dot{m}_k - q_k \dot{m}) \tag{A.19}$$

A.2.4. The velocity equation

The advective form of the equations for the horizontal components of velocity is unaltered by mass changes. The horizontal velocity components thus satisfy the equation

$$\frac{d\vec{v}_h}{dt} = -\frac{1}{\rho}\nabla_h p - 2(\vec{\Omega} \times \vec{v}_h)_h \tag{A.20}$$

where $\vec{\Omega}$ is the earth's rotation vector. Changes due to molecular stresses are neglected.

A.2.5. The thermodynamic equation

As discussed by Dufour and Van Mieghem (1975, Eq. 5.21), the first law of thermodynamics may be written

$$\delta Q + \alpha dp = d_i H = d_i \left(\sum m_k h_k\right) \tag{A.21}$$

where the h_k are specific enthalpies, $\alpha = 1/\rho$ is the specific volume and the subscript i denotes changes independent of the mass changes due to precipitation. As molecular diffusion is neglected, δQ represents the heat received by the atmospheric element due to radiation and to heat exchange with falling rain or snow.

Under the usual assumptions of perfect gas behaviour for dry air and water vapour, and neglect of variations of the specific enthalpies of water and ice with pressure, we can write

$$h_k = h_k^0 + C_{pk}T \tag{A.22}$$

and (A.21) becomes

$$mC_p dT = \alpha dp + \delta Q - \sum_k h_k d_i m_k \tag{A.23}$$

where

$$C_p = \sum_k C_{pk} q_k \tag{A.24}$$

Thus considering a material volume of the atmosphere, we obtain the thermodynamic equation

$$C_p \frac{dT}{dt} = \frac{1}{\rho}\frac{dp}{dt} + Q_R + Q_M - \sum_k h_k \frac{\dot{m}_{ki}}{m} \tag{A.25}$$

where Q_R and Q_M are the heating rates due to respectively radiation and the heat transferred from falling rain or snow.

A.3. The flux forms of the equations

It is convenient to define the differential operator $\frac{D}{Dt}$ by

$$\frac{DX}{Dt} = \frac{dX}{dt} + X(\nabla \cdot \vec{v}) = \frac{\partial X}{\partial t} + \nabla \cdot (X\vec{v}) \tag{A.26}$$

Note that

$$\rho = \frac{dx}{dt} = \frac{D\rho x}{Dt} \text{ if } \dot{\rho} = 0 \tag{A.27}$$

Equations (A.19), (A.20) and (A.25) may then be written

$$\frac{D\rho}{Dt} = \frac{\rho}{m}\dot{m} = \dot{\rho} \tag{A.28}$$

$$\frac{D\rho q_k}{Dt} = \frac{\rho}{m}\dot{m}_k = \dot{\rho}_k \tag{A.29}$$

$$\frac{D\rho\vec{v}_h}{Dt} = \dot{\rho}\vec{v}_h - \nabla_h p - 2\rho(\vec{\Omega} \times \vec{v}_h)_h \tag{A.30}$$

$$C_p \frac{D\rho T}{Dt} = C_p \dot{\rho} T + \frac{dp}{dt} + \rho(Q_R + Q_M) - \rho \sum_k h_k \frac{\dot{m}_{ki}}{m} \tag{A.31}$$

From the definition (A.24) of C_p we obtain

$$\frac{DC_p\rho T}{DT} = C_p\frac{D\rho T}{DT} + \rho T\frac{d}{dt}\sum_k C_{pk}q_k \tag{A.32}$$

and using (A.24) and (A.31) gives

$$\begin{aligned}\frac{DC_p\rho T}{Dt} = C_p\dot{\rho}T + \frac{dp}{dt} + \rho\left(Q_R + Q_M\right) - \rho\sum_k\left(h_k^0 + C_{pk}T\right)\frac{\dot{m}_{ki}}{m} \\ + \rho T\sum_k C_{pk}\left(\frac{\dot{m}_k}{m} - \frac{q_k\dot{m}}{m}\right)\end{aligned} \tag{A.33}$$

Using (A.2), (A.7) and (A.24), we obtain from (A.33):

$$\frac{DC_p\rho T}{Dt} = \frac{dp}{dt} + \rho\left(Q_R + Q_M\right) - \rho\sum_k h_k^0\frac{\dot{m}_{ki}}{m} + \rho T\sum_k C_{pk}\frac{\dot{m}_{ke}}{m} \tag{A.34}$$

A.4. The introduction of diffusive fluxes

We now introduce a separation of dependent variables into components that will be explicitly resolved in the model and components the effect of which will require parametrization.

If the bar operator represents an average over unresolved scales in space and time, then we write:

$$\begin{aligned} X &= \overline{X} + X' \text{ with } \overline{X}' = 0 \\ \text{and } X &= \overline{\overline{X}} + X'' \text{ with } \overline{\overline{X}}'' = 0 \\ \text{where } \overline{\overline{X}} &= \frac{\overline{\rho X}}{\overline{\rho}} \text{ is a mass weighted average.} \end{aligned}$$

It follows that

$$\begin{aligned} \frac{\overline{\overline{D}\overline{\rho}\overline{\overline{X}}}}{Dt} &= \frac{\overline{D\rho X}}{Dt} - \left(\nabla\cdot\overline{\rho\vec{v}''X''}\right) \\ \frac{\overline{\overline{dX}}}{dt} &= \frac{\overline{dX}}{dt} - \left(\overline{\vec{v}''\cdot\nabla X}\right) \\ \overline{\rho}XY &= \overline{\rho XY} = \overline{\rho}\overline{\overline{X}}\,\overline{\overline{Y}} + \overline{\rho X''Y''} \end{aligned}$$

Using these results, equations (A.27) - (A.29) and (A.33) become

$$\frac{\overline{\overline{D}}\,\overline{\rho}}{Dt} = \overline{\dot{\rho}} = \overline{\rho}\left(\frac{\overline{\overline{\dot{m}}}}{m}\right) \tag{A.35}$$

$$\frac{\overline{\overline{D}}\,\overline{\rho}\,\overline{\overline{q_k}}}{Dt} = \overline{\dot{\rho}_k} - \left(\nabla\cdot\overline{\rho\vec{v}''q_k''}\right) = \overline{\rho}\left(\frac{\overline{\overline{\dot{m}_k}}}{m}\right) - \left(\nabla\cdot\overline{\rho\vec{v}''p_k''}\right) \tag{A.36}$$

$$\begin{aligned}\frac{\overline{\overline{D}}\,\overline{\rho}\,\overline{\overline{\vec{v}_h}}}{Dt} &= \overline{\dot{\rho}\vec{v}_h} - \nabla_h\overline{p} - 2\overline{\rho}\left(\vec{\Omega}\times\overline{\overline{\vec{v}_h}}\right)_h - \left(\nabla\cdot\overline{\rho\vec{v}''\vec{v}_h''}\right) \\ &= \overline{\rho}\left(\frac{\overline{\overline{\dot{m}}}}{m}\right)\overline{\overline{\vec{v}_h}} - \nabla_h\overline{p} - 2\overline{\rho}\left(\vec{\Omega}\times\overline{\overline{\vec{v}_h}}\right)_h - \left(\nabla\cdot\overline{\rho\vec{v}''\vec{v}_h''}\right) - \overline{\rho\left(\frac{\dot{m}}{m}\right)''\vec{v}_h''}\end{aligned} \tag{A.37}$$

and

$$\begin{aligned}\frac{\overline{\overline{D}}}{Dt}\left(\overline{\rho}\,\overline{\overline{C_p}}\,\overline{\overline{T}} + \overline{\rho C_p''T''}\right) &= \frac{\overline{\overline{d}}\overline{p}}{dt} + \overline{\rho}\left(\overline{\overline{Q_R}} + \overline{\overline{Q_M}}\right) - \overline{\rho}\sum_k h_k^0\left(\frac{\overline{\overline{\dot{m}_{ki}}}}{m}\right) \\ &+ \overline{\rho}\,\overline{\overline{T}}\sum_k C_{pk}\left(\frac{\overline{\overline{\dot{m}_{ke}}}}{m}\right) + \overline{\vec{v}''\cdot\nabla p} - \left(\nabla\cdot\overline{\rho\vec{v}''C_pT''}\right) \\ &+ \sum_k C_{pk}\overline{\rho T''\left(\frac{\dot{m}_{ke}}{m}\right)''}\end{aligned} \tag{A.38}$$

The equation of state A.13 gives

$$p = \rho RT \tag{A.39}$$

where $R = (R_d q_d + R_v q_v)/\{1-\rho(q_l v_l + q_i v_i)\}$

whence

$$\overline{\rho} = \overline{\rho RT} = \overline{\rho}\,\overline{\overline{R}}\,\overline{\overline{T}} + \overline{\rho R''T''} \tag{A.40}$$

Using $\overline{\overline{C_p}} = \sum C_{pk}\overline{\overline{q_k}}$, (A.36) and (A.38) may be written

$$\begin{aligned}\overline{\overline{C_p}}\frac{\overline{\overline{D}}\,\overline{\rho}\,\overline{\overline{T}}}{Dt} &= \frac{\overline{\overline{d}}\overline{p}}{dt} + \overline{\rho}\left(\overline{\overline{Q_R}} + \overline{\overline{Q_M}}\right) - \overline{\rho}\sum_k\overline{\overline{h_k}}\left(\frac{\overline{\overline{\dot{m}_{ki}}}}{m}\right) + \overline{\rho}\,\overline{\overline{C_p}}\,\overline{\overline{T}}\left(\frac{\overline{\overline{\dot{m}}}}{m}\right) \\ &+ \overline{\vec{v}''\nabla p} - \nabla\cdot\overline{\rho\vec{v}''(C_pT)''} + \overline{\overline{T}}\sum_k C_{pk}\nabla\cdot\overline{\rho\vec{v}''q_k''} \\ &- \frac{\overline{\overline{D}}}{Dt}(\overline{\rho C_p''T''}) + \sum_k C_{pk}\overline{\rho T''\left(\frac{\dot{m}_{ke}}{m}\right)}\end{aligned} \tag{A.41}$$

A.5. Approximations and definitions

At this stage, we make two approximations. The first is to neglect the higher-order correlations

$$\overline{\rho T''\left(\frac{\dot{m}_{ke}}{m}\right)''}, \quad \frac{\overline{\overline{D}}}{Dt}\overline{(\rho C_p'' T'')}, \quad \overline{\rho T'' R''} \text{ and } \overline{\rho\left(\frac{\dot{m}}{m}\right)''\vec{v}_h}.$$

This is equivalent to assuming higher-order terms are important only when eddy velocities and derivatives are involved. The second is to neglect the term in the equation of state, or equivalently to neglect the volume occupied by liquid water and ice compared with that occupied by dry air and water vapour.

In addition we introduce the following notation:

a. The vertical flux of a variable X, $\overline{\rho w'' X''}$, is denoted by J_X. Here w is the vertical velocity component.

b. The term $\overline{v'' \cdot \nabla p}$ is added to the term $\frac{\partial}{\partial z}\overline{\rho w''(C_p T)''}$ and the resulting sum is expressed as the derivative $\frac{\partial J_S}{\partial z}$ of the vertical flux of dry static energy, plus a term which is written $\overline{\rho}\overline{\overline{Q_D}}$ and regarded as representing unorgnized transfers between enthalpy and sub-grid scale kinetic energy. The latter is parametrized by the heating implied by the dissipation of kinetic energy due to the parametrized vertical momentum fluxes $J_{\vec{v}_h}$.

c. The net effect of horizontal fluxes is represented only by their contribution K_X to the tendency of variable X.

d. The term $-\overline{\rho}\sum_k \overline{\overline{h_k}}\left(\overline{\overline{\frac{\dot{m}_{ki}}{m}}}\right)$ representing the latent heat release associated with internal phase changes is written $\rho\overline{\overline{Q_L}}$

A.6. Return to the advective form

With the above approximations and definitions, we obtain from the equations of Appendix A.4, on dropping the bar operators

$$\frac{d\rho}{dt} + \rho\nabla\cdot\vec{v} = \rho\frac{\dot{m}}{m} \tag{A.42}$$

$$\frac{dq_k}{dt} = S_{q_k} - \frac{1}{\rho}\frac{\partial J_{q_k}}{\partial z} + K_{q_k} \tag{A.43}$$

$$\frac{d\vec{v}_h}{dt} = -\frac{1}{\rho}\nabla_h p - 2\left(\vec{\Omega}\times\vec{v}_h\right)_h - \frac{1}{\rho}\frac{\partial J_{\vec{v}_h}}{\partial z} + K_{\vec{v}_h} \tag{A.44}$$

$$\frac{dT}{dt} = \frac{1}{\rho C_p}\frac{dp}{dt} + \frac{1}{C_p}\left(Q_R + Q_L + Q_M + Q_D - \frac{1}{\rho}\left[\frac{\partial J_S}{\partial z} - T\sum_k C_{pk}\frac{\partial J_{q_k}}{\partial z}\right]\right) + K_T \tag{A.45}$$

where

$$S_{q_k} = \frac{\dot{m}_k}{m} - q_k \frac{\dot{m}}{m}. \tag{A.46}$$

In addition we have the equation of state

$$p = \rho T \left(R_d q_d + R_v q_v \right). \tag{A.47}$$

and the hydrostatic equation

$$\frac{\partial p}{\partial z} = -g\rho. \tag{A.48}$$

A.7. The model equations

The model equations (2.1)–(2.6) and (2.11)–(2.14) are finally obtained by neglecting density changes due to precipitation or evaporation, setting $\dot{m} = 0$ in (A.42). This approximation is traditionally made, although it is open to question.

In addition, Q_M is set to zero, an approximation of the same order as the assumption of no variation of latent heat with temperature that is made in the parametrizations.

The governing equations are

$$\frac{d\vec{v}_h}{dt} = -\frac{1}{\rho}\nabla_h p - 2\left(\vec{\Omega} \times \vec{v_h}\right)_h - \frac{1}{\rho}\frac{\partial J_{\vec{v}_h}}{\partial z} + K_{\vec{v}_h} \tag{A.49}$$

$$\frac{dT}{dt} = \frac{R_d T_v}{p C_p}\frac{dp}{dt} + \frac{1}{C_p}\left(Q_R + Q_L + Q_D - \frac{1}{\rho}\left[\frac{\partial J_s}{\partial z} - C_{pd} T (\delta - 1) \frac{\partial J_{q_v}}{\partial z} \right] \right) + K_T \tag{A.50}$$

$$\frac{dq_i}{dt} = S_{q_i} - \frac{1}{\rho}\frac{\partial J_{q_i}}{\partial z} \tag{A.51}$$

$$p = \rho R_d T_v \tag{A.52}$$

$$\frac{\partial p}{\partial z} = -g\rho \tag{A.53}$$

with

$$T_v = T\left(1 + \left(\frac{1}{\epsilon} - 1\right) q_v\right) \tag{A.54}$$

In this case

$$C_p = C_{pd}\left(1 - q_v\right) + C_{pv} q$$

which is written

$$C_p = C_{pd}\left(1 + (\delta - 1)\, q_v\right) \tag{A.55}$$

where $\delta = \frac{C_{pv}}{C_{pd}}$.

The model equations then follow from a change from z - to η-coordinates, the formalism for which is given by Kasahara (1974), and from rewriting the adiabatic terms in their usual form for a spherical geometry.

B. Orbit tables

The coefficients for the Poisson series expansions required for the VSOP87 orbit calculation.

L1		
a_k	b_k	c_k
1.753470456730000e+00	0.00000000000e+00	0.000000000000000e+00
3.341656456000000e-02	4.66925680417e+00	6.283075849991400e+03
3.489427500000000e-04	4.62610241759e+00	1.256615169998280e+04
3.497056000000000e-05	2.74411800971e+00	5.753384884896800e+03
3.417571000000000e-05	2.82886579606e+00	3.523118349000000e+00
3.135896000000000e-05	3.62767041758e+00	7.771377146812050e+04
2.676218000000000e-05	4.41808351397e+00	7.860419392439200e+03
2.342687000000000e-05	6.13516237631e+00	3.930209696219600e+03
1.324292000000000e-05	7.42463563520e-01	1.150676976979360e+04
1.273166000000000e-05	2.03709655772e+00	5.296909650946000e+02
1.199167000000000e-05	1.10962944315e+00	1.577343542447800e+03
9.902500000000000e-06	5.23268129594e+00	5.884926846583200e+03
9.018550000000000e-06	2.04505443513e+00	2.629831979980000e+01
8.572229999999999e-06	3.50849156957e+00	3.981490034082000e+02
7.797859999999999e-06	1.17882652114e+00	5.223693919802200e+03
7.531410000000000e-06	2.53339053818e+00	5.507553238667400e+03
5.052640000000000e-06	4.58292563052e+00	1.884922754997420e+04
4.923790000000000e-06	4.20506639861e+00	7.755226113240000e+02
3.566550000000000e-06	2.91954116867e+00	6.731030280000000e-02
3.170870000000000e-06	5.84901952218e+00	1.179062908865880e+04
2.841250000000000e-06	1.89869034186e+00	7.962980068163999e+02
2.710390000000000e-06	3.14886076490e-01	1.097707880469900e+04
2.428100000000000e-06	3.44811409060e-01	5.486777843175000e+03
2.061600000000000e-06	4.80646606059e+00	2.544314419883400e+03
2.053850000000000e-06	1.86947813692e+00	5.573142801433100e+03
2.022610000000000e-06	2.45767795458e+00	6.069776754553400e+03
1.555160000000000e-06	8.33060738070e-01	2.132990954380000e+02
1.322120000000000e-06	3.41118275555e+00	2.942463423291600e+03
1.261840000000000e-06	1.08302630210e+00	2.077539549240000e+01
1.151320000000000e-06	6.45449116830e-01	9.803210682000000e-01
1.028510000000000e-06	6.35998467270e-01	4.694002954707600e+03
1.018950000000000e-06	9.75692218240e-01	1.572083878487840e+04
1.017240000000000e-06	4.26679821365e+00	7.113547000800000e+00
9.920600000000000e-07	6.20992940258e+00	2.146165416475200e+03
9.760700000000001e-07	6.81012722700e-01	1.554203994342000e+02
8.580300000000000e-07	5.98322631256e+00	1.610006857376741e+05
8.512800000000000e-07	1.29870743025e+00	6.275962302990600e+03
8.471100000000000e-07	3.67080093025e+00	7.143069561812909e+04
7.963700000000000e-07	1.80791330700e+00	1.726015465469040e+04

table B.1 to be continued ...

L1		
a_k	b_k	c_k
7.875600000000000e-07	3.03698313141e+00	1.203646073488820e+04
7.465100000000000e-07	1.75508916159e+00	5.088628839766800e+03
7.387400000000000e-07	3.50319443167e+00	3.154687084895600e+03
7.354700000000000e-07	4.67926565481e+00	8.018209311238001e+02
6.962700000000000e-07	8.32975969660e-01	9.437762934887000e+03
6.244899999999999e-07	3.97763880587e+00	8.827390269874801e+03
6.114800000000000e-07	1.81839811024e+00	7.084896781115200e+03
5.696300000000000e-07	2.78430398043e+00	6.286598968340400e+03
5.611600000000000e-07	4.38694880779e+00	1.414349524243060e+04
5.557700000000000e-07	3.47006009062e+00	6.279552731642400e+03
5.199200000000000e-07	1.89149458340e-01	1.213955350910680e+04
5.160500000000000e-07	1.33282746983e+00	1.748016413067000e+03
5.114500000000000e-07	2.83068645010e-01	5.856477659115400e+03
4.900000000000000e-07	4.87350650330e-01	1.194447010224600e+03
4.103600000000000e-07	5.36817351402e+00	8.429241266466601e+03
4.093800000000000e-07	2.39850881707e+00	1.965104848109800e+04
3.920000000000000e-07	6.16832995016e+00	1.044738783960440e+04
3.677000000000000e-07	6.04133859347e+00	1.021328554621100e+04
3.659600000000000e-07	2.56955238628e+00	1.059381930189200e+03
3.595400000000000e-07	1.70876111898e+00	2.352866153771800e+03
3.556600000000000e-07	1.77597314691e+00	6.812766815086000e+03
3.329100000000000e-07	5.93094994590e-01	1.778984561978500e+04
3.041200000000000e-07	4.42944641350e-01	8.399684731811189e+04
3.004700000000000e-07	2.73975123935e+00	1.349867409658800e+03
2.535200000000000e-07	3.16470953405e+00	4.690479836358600e+03

Table B.1.: First summand of heliocentric latitude (VSOP87D)

L2		
a_k	b_k	c_k
6.283319667474910e+03	0.00000000000e+00	0.000000000000000e+00
2.060588630000000e-03	2.67823455584e+00	6.283075849991400e+03
4.303430000000000e-05	2.63512650414e+00	1.256615169998280e+04
4.252640000000000e-06	1.59046980729e+00	3.523118349000000e+00
1.192610000000000e-06	5.79557487799e+00	2.629831979980000e+01
1.089770000000000e-06	2.96618001993e+00	1.577343542447800e+03
9.347800000000000e-07	2.59212835365e+00	1.884922754997420e+04
7.212200000000000e-07	1.13846158196e+00	5.296909650946000e+02
6.776800000000000e-07	1.87472304791e+00	3.981490034082000e+02
6.732700000000000e-07	4.40918235168e+00	5.507553238667400e+03
5.902700000000000e-07	2.88797038460e+00	5.223693919802200e+03
5.597600000000000e-07	2.17471680261e+00	1.554203994342000e+02
4.540700000000000e-07	3.98030798050e-01	7.962980068163999e+02
3.636900000000000e-07	4.66247398350e-01	7.755226113240000e+02
2.895800000000000e-07	2.64707383882e+00	7.113547000800000e+00
2.084400000000000e-07	5.34138275149e+00	9.803210682000000e-01
1.909700000000000e-07	1.84628332577e+00	5.486777843175000e+03
1.850800000000000e-07	4.96855124577e+00	2.132990954380000e+02
1.729300000000000e-07	2.99116864949e+00	6.275962302990600e+03
1.623300000000000e-07	3.21648304700e-02	2.544314419883400e+03
1.583200000000000e-07	1.43049285325e+00	2.146165416475200e+03

table B.2 to be continued ...

L2		
a_k	b_k	c_k
1.461500000000000e-07	1.20532366323e+00	1.097707880469900e+04
1.246100000000000e-07	2.83432285512e+00	1.748016413067000e+03
1.187700000000000e-07	3.25804815607e+00	5.088628839766800e+03
1.180800000000000e-07	5.27379790480e+00	1.194447010224600e+03
1.151400000000000e-07	2.07502418155e+00	4.694002954707600e+03
1.064100000000000e-07	7.66141992020e-01	5.535694028424000e+02
9.969000000000000e-08	1.30262991097e+00	6.286598968340400e+03
9.720999999999999e-08	4.23925472239e+00	1.349867409658800e+03
9.452000000000000e-08	2.69957062864e+00	2.427286039740000e+02
8.577000000000001e-08	5.64475868067e+00	9.517184062506000e+02
7.576000000000000e-08	5.30062664886e+00	2.352866153771800e+03
6.385000000000001e-08	2.65033984967e+00	9.437762934887000e+03
6.101000000000000e-08	4.66632584188e+00	4.690479836358600e+03

Table B.2.: Second summand of heliocentric latitude (VSOP87D)

L3		
a_k	b_k	c_k
5.291887000000000e-04	0.00000000000e+00	0.000000000000000e+00
8.719837000000000e-05	1.07209665242e+00	6.283075849991400e+03
3.091250000000000e-06	8.67288188320e-01	1.256615169998280e+04
2.733900000000000e-07	5.29787169100e-02	3.523118349000000e+00
1.633400000000000e-07	5.18826691036e+00	2.629831979980000e+01
1.575200000000000e-07	3.68457889430e+00	1.554203994342000e+02
9.541000000000001e-08	7.57422976750e-01	1.884922754997420e+04
8.937000000000000e-08	2.05705419118e+00	7.771377146812050e+04
6.952000000000000e-08	8.26733054100e-01	7.755226113240000e+02
5.064000000000000e-08	4.66284525271e+00	1.577343542447800e+03
4.061000000000000e-08	1.03057162962e+00	7.113547000800000e+00
3.810000000000000e-08	3.44050803490e+00	5.573142801433100e+03
3.463000000000000e-08	5.14074632811e+00	7.962980068163999e+02
3.169000000000000e-08	6.05291851171e+00	5.507553238667400e+03
3.020000000000000e-08	1.19246506441e+00	2.427286039740000e+02
2.886000000000000e-08	6.11652627155e+00	5.296909650946000e+02
2.714000000000000e-08	3.06378810250e-01	3.981490034082000e+02
2.538000000000000e-08	2.27992810679e+00	5.535694028424000e+02
2.371000000000000e-08	4.38118838167e+00	5.223693919802200e+03
2.079000000000000e-08	3.75435330484e+00	9.803210682000000e-01

Table B.3.: Third summand of heliocentric latitude (VSOP87D)

L4		
a_k	b_k	c_k
2.892260000000000e-06	5.84384198723e+00	6.283075849991400e+03
3.495500000000000e-07	0.00000000000e+00	0.000000000000000e+00
1.681900000000000e-07	5.48766912348e+00	1.256615169998280e+04
2.962000000000000e-08	5.19577265202e+00	1.554203994342000e+02
1.288000000000000e-08	4.72200252235e+00	3.523118349000000e+00
7.140000000000000e-09	5.30045809128e+00	1.884922754997420e+04
6.350000000000000e-09	5.96925937141e+00	2.427286039740000e+02

Table B.4.: Fourth summand of heliocentric latitude (VSOP87D)

L5		
a_k	b_k	c_k
1.140840000000000e-06	3.14159265359e+00	0.000000000000000e+00
7.717000000000000e-08	4.13446589358e+00	6.283075849991400e+03
7.650000000000001e-09	3.83803776214e+00	1.256615169998280e+04

Table B.5.: Fifth summand of heliocentric latitude (VSOP87D)

L6		
a_k	b_k	c_k
8.780000000000000e-09	3.14159265359e+00	0.000000000000000e+00

Table B.6.: Sixth summand of heliocentric latitude (VSOP87D)

B1		
a_k	b_k	c_k
2.796200000000000e-06	3.19870156017e+00	8.433466158130829e+04
1.016430000000000e-06	5.42248619256e+00	5.507553238667400e+03
8.044500000000000e-07	3.88013204458e+00	5.223693919802200e+03
4.380600000000000e-07	3.70444689758e+00	2.352866153771800e+03
3.193300000000000e-07	4.00026369781e+00	1.577343542447800e+03

Table B.7.: First summand of heliocentric longitude (VSOP87D)

B2		
a_k	b_k	c_k
9.029999999999999e-08	3.89729061890e+00	5.507553238667400e+03
6.177000000000000e-08	1.73038850355e+00	5.223693919802200e+03

Table B.8.: Second summand of heliocentric longitude (VSOP87D)

R1		
a_k	b_k	c_k
1.000139887990000e+00	0.00000000000e+00	0.000000000000000e+00
1.670699626000000e-02	3.09846350771e+00	6.283075849991400e+03
1.395602300000000e-04	3.05524609620e+00	1.256615169998280e+04
3.083720000000000e-05	5.19846674381e+00	7.771377146812050e+04
1.628461000000000e-05	1.17387749012e+00	5.753384884896800e+03
1.575568000000000e-05	2.84685245825e+00	7.860419392439200e+03
9.247990000000000e-06	5.45292234084e+00	1.150676976979360e+04
5.424440000000000e-06	4.56409149777e+00	3.930209696219600e+03
4.721100000000000e-06	3.66100022149e+00	5.884926846583200e+03
3.459830000000000e-06	9.63686176870e-01	5.507553238667400e+03
3.287800000000000e-06	5.89983646482e+00	5.223693919802200e+03
3.067840000000000e-06	2.98671395120e-01	5.573142801433100e+03
2.431890000000000e-06	4.27349536153e+00	1.179062908865880e+04
2.118290000000000e-06	5.84714540314e+00	1.577343542447800e+03
1.857520000000000e-06	5.02194447178e+00	1.097707880469900e+04
1.748440000000000e-06	3.01193636534e+00	1.884922754997420e+04
table B.9 to be continued ...		

R1		
a_k	b_k	c_k
1.098350000000000e-06	5.05510636285e+00	5.486777843175000e+03
9.831599999999999e-07	8.86813112770e-01	6.069776754553400e+03
8.649900000000000e-07	5.68959778254e+00	1.572083878487840e+04
8.582500000000000e-07	1.27083733351e+00	1.610006857376741e+05
6.490300000000000e-07	2.72506137870e-01	1.726015465469040e+04
6.291600000000000e-07	9.21771088320e-01	5.296909650946000e+02
5.705600000000000e-07	2.01374292014e+00	8.399684731811189e+04
5.573600000000000e-07	5.24159798933e+00	7.143069561812909e+04
4.938400000000000e-07	3.24501240359e+00	2.544314419883400e+03
4.696300000000000e-07	2.57805070386e+00	7.755226113240000e+02
4.466100000000000e-07	5.53715807302e+00	9.437762934887000e+03
4.251500000000000e-07	6.01110242003e+00	6.275962302990600e+03
3.896800000000000e-07	5.36071738169e+00	4.694002954707600e+03
3.824500000000000e-07	2.39255343974e+00	8.827390269874801e+03
3.749000000000000e-07	8.29529223320e-01	1.965104848109800e+04
3.695700000000000e-07	4.90107591914e+00	1.213955350910680e+04
3.566000000000000e-07	1.67468058995e+00	1.203646073488820e+04
3.453700000000000e-07	1.84270693282e+00	2.942463423291600e+03
3.319300000000000e-07	2.43703000980e-01	7.084896781115200e+03
3.192100000000000e-07	1.83682297810e-01	5.088628839766800e+03
3.184600000000000e-07	1.77775642085e+00	3.981490034082000e+02
2.846400000000000e-07	1.21344868176e+00	6.286598968340400e+03
2.779300000000000e-07	1.89934330904e+00	6.279552731642400e+03
2.627500000000000e-07	4.58896850401e+00	1.044738783960440e+04

Table B.9.: First summand of distance (VSOP87D)

R2		
a_k	b_k	c_k
1.030186080000000e-03	1.10748969588e+00	6.283075849991400e+03
1.721238000000000e-05	1.06442301418e+00	1.256615169998280e+04
7.022150000000000e-06	3.14159265359e+00	0.000000000000000e+00
3.234600000000000e-07	1.02169059149e+00	1.884922754997420e+04
3.079900000000000e-07	2.84353804832e+00	5.507553238667400e+03
2.497100000000000e-07	1.31906709482e+00	5.223693919802200e+03
1.848500000000000e-07	1.42429748614e+00	1.577343542447800e+03
1.007800000000000e-07	5.91378194648e+00	1.097707880469900e+04
8.654000000000001e-08	1.42046854427e+00	6.275962302990600e+03
8.634000000000000e-08	2.71461506020e-01	5.486777843175000e+03

Table B.10.: Second summand of distance (VSOP87D)

R3		
a_k	b_k	c_k
4.359385000000000e-05	5.78455133738e+00	6.283075849991400e+03
1.236330000000000e-06	5.57934722157e+00	1.256615169998280e+04
1.234100000000000e-07	3.14159265359e+00	0.000000000000000e+00
8.792000000000000e-08	3.62777733395e+00	7.771377146812050e+04
5.689000000000000e-08	1.86958905084e+00	5.573142801433100e+03
3.301000000000000e-08	5.47027913302e+00	1.884922754997420e+04

Table B.11.: Third summand of distance (VSOP87D)

R4		
a_k	b_k	c_k
1.445950000000000e-06	4.27319435148e+00	6.283075849991400e+03
6.729000000000000e-08	3.91697608662e+00	1.256615169998280e+04

Table B.12.: Fourth summand of distance (VSOP87D)

R5		
a_k	b_k	c_k
3.858000000000000e-08	2.56384387339e+00	6.283075849991400e+03

Table B.13.: Fifth summand of distance (VSOP87D)

Table for calculating the periodic terms of nutation in longitude (ΔL) and obliquity (Δi).

Argument					ΔL		ΔL	
multiples of					sine arguments		cosine arguments	
D	M	M'	F	Ω	a_k	$b_k t$	c_k	$d_k t$
0	0	0	0	1	-171996.0	-174.2	92025.0	8.9
0	0	2	-2	2	-13187.0	-1.6	5736.0	-3.1
0	0	2	0	2	-2274.0	-0.2	977.0	-0.5
0	0	0	0	2	2062.0	0.2	-895.0	0.5
0	-1	0	0	0	-1426.0	3.4	54.0	-0.1
1	0	0	0	0	712.0	0.1	-7.0	0.0
0	1	2	-2	2	-517.0	1.2	224.0	-0.6
0	0	2	0	1	-386.0	-0.4	200.0	0.0
1	0	2	0	2	-301.0	0.0	129.0	-0.1
0	-1	2	-2	2	217.0	-0.5	-95.0	0.3
-1	0	0	2	0	158.0	0.0	-1.0	0.0
0	0	2	-2	1	129.0	0.1	-70.0	0.0
-1	0	2	0	2	123.0	0.0	-53.0	0.0
1	0	0	0	1	63.0	0.1	-33.0	0.0
0	0	0	2	0	63.0	0.0	-2.0	0.0
-1	0	2	2	2	-59.0	0.0	26.0	0.0
-1	0	0	0	1	-58.0	-0.1	32.0	0.0
1	0	2	0	1	-51.0	0.0	27.0	0.0
-2	0	0	2	0	-48.0	0.0	1.0	0.0
-2	0	2	0	1	46.0	0.0	-24.0	0.0
0	0	2	2	2	-38.0	0.0	16.0	0.0
2	0	2	0	2	-31.0	0.0	13.0	0.0
2	0	0	0	0	29.0	0.0	-1.0	0.0
1	0	2	-2	2	29.0	0.0	-12.0	0.0
0	0	2	0	0	26.0	0.0	-1.0	0.0
0	0	2	-2	0	-22.0	0.0	0.0	0.0
-1	0	2	0	1	21.0	0.0	-10.0	0.0
0	2	0	0	0	17.0	-0.1	0.0	0.0
0	2	2	-2	2	-16.0	0.1	7.0	0.0
-1	0	0	2	1	16.0	0.0	-8.0	0.0
0	1	0	0	1	-15.0	0.0	9.0	0.0
1	0	0	-2	1	-13.0	0.0	7.0	0.0
0	-1	0	0	1	-12.0	0.0	6.0	0.0
2	0	-2	0	0	11.0	0.0	0.0	0.0
-1	0	2	2	1	-10.0	0.0	5.0	0.0
1	0	2	2	2	-8.0	0.0	3.0	0.0
0	-1	2	0	2	-7.0	0.0	3.0	0.0
0	0	2	2	1	-7.0	0.0	3.0	0.0
1	1	0	-2	0	-7.0	0.0	0.0	0.0
0	1	2	0	2	7.0	0.0	-3.0	0.0
-2	0	0	2	1	-6.0	0.0	3.0	0.0
0	0	0	2	1	-6.0	0.0	3.0	0.0
2	0	2	-2	2	6.0	0.0	-3.0	0.0
1	0	0	2	0	6.0	0.0	0.0	0.0
1	0	2	-2	1	6.0	0.0	-3.0	0.0
0	0	0	-2	1	-5.0	0.0	3.0	0.0
0	-1	2	-2	1	-5.0	0.0	3.0	0.0
2	0	2	0	1	-5.0	0.0	3.0	0.0
to be continued ...								

Argument					ΔL		ΔL	
multiples of					sine arguments		cosine arguments	
D	M	M'	F	Ω	a_k	$b_k t$	c_k	$d_k t$
1	-1	0	0	0	5.0	0.0	0.0	0.0
1	0	0	-1	0	-4.0	0.0	0.0	0.0
0	0	0	1	0	-4.0	0.0	0.0	0.0
0	1	0	-2	0	-4.0	0.0	0.0	0.0
1	0	-2	0	0	4.0	0.0	0.0	0.0
2	0	0	-2	1	4.0	0.0	-2.0	0.0
0	1	2	-2	1	4.0	0.0	-2.0	0.0
1	1	0	0	0	-3.0	0.0	0.0	0.0
1	-1	0	-1	0	-3.0	0.0	0.0	0.0
-1	-1	2	2	2	-3.0	0.0	1.0	0.0
0	-1	2	2	2	-3.0	0.0	1.0	0.0
1	-1	2	0	2	-3.0	0.0	1.0	0.0
3	0	2	0	2	-3.0	0.0	1.0	0.0
-2	0	2	0	2	-3.0	0.0	1.0	0.0
1	0	2	0	0	3.0	0.0	0.0	0.0
-1	0	2	4	2	-2.0	0.0	1.0	0.0
1	0	0	0	2	-2.0	0.0	1.0	0.0
-1	0	2	-2	1	-2.0	0.0	1.0	0.0
0	-2	2	-2	1	-2.0	0.0	1.0	0.0
-2	0	0	0	1	-2.0	0.0	1.0	0.0
2	0	0	0	1	2.0	0.0	-1.0	0.0
3	0	0	0	0	2.0	0.0	0.0	0.0
1	1	2	0	2	2.0	0.0	-1.0	0.0
0	0	2	1	2	2.0	0.0	-1.0	0.0
1	0	0	2	1	-1.0	0.0	0.0	0.0
1	0	2	2	1	-1.0	0.0	1.0	0.0
1	1	0	-2	1	-1.0	0.0	0.0	0.0
0	1	0	2	0	-1.0	0.0	0.0	0.0
0	1	2	-2	0	-1.0	0.0	0.0	0.0
0	1	-2	2	0	-1.0	0.0	0.0	0.0
1	0	-2	2	0	-1.0	0.0	0.0	0.0
1	0	-2	-2	0	-1.0	0.0	0.0	0.0
1	0	2	-2	0	-1.0	0.0	0.0	0.0
1	0	0	-4	0	-1.0	0.0	0.0	0.0
2	0	0	-4	0	-1.0	0.0	0.0	0.0
0	0	2	4	2	-1.0	0.0	0.0	0.0
0	0	2	-1	2	-1.0	0.0	0.0	0.0
-2	0	2	4	2	-1.0	0.0	1.0	0.0
2	0	2	2	2	-1.0	0.0	0.0	0.0
0	-1	2	0	1	-1.0	0.0	0.0	0.0
0	0	-2	0	1	-1.0	0.0	0.0	0.0
0	0	4	-2	2	1.0	0.0	0.0	0.0
0	1	0	0	2	1.0	0.0	0.0	0.0
1	1	2	-2	2	1.0	0.0	-1.0	0.0
3	0	2	-2	2	1.0	0.0	0.0	0.0
-2	0	2	2	2	1.0	0.0	-1.0	0.0
-1	0	0	0	2	1.0	0.0	-1.0	0.0

to be continued ...

Argument					ΔL		ΔL	
multiples of					sine arguments		cosine arguments	
D	M	M'	F	Ω	a_k	$b_k t$	c_k	$d_k t$
0	0	-2	2	1	1.0	0.0	0.0	0.0
0	1	2	0	1	1.0	0.0	0.0	0.0
-1	0	4	0	2	1.0	0.0	0.0	0.0
2	1	0	-2	0	1.0	0.0	0.0	0.0
2	0	0	2	0	1.0	0.0	0.0	0.0
2	0	2	-2	1	1.0	0.0	-1.0	0.0
2	0	-2	0	1	1.0	0.0	0.0	0.0
1	-1	0	-2	0	1.0	0.0	0.0	0.0
-1	0	0	1	1	1.0	0.0	0.0	0.0
-1	-1	0	2	1	1.0	0.0	0.0	0.0
0	1	0	1	0	1.0	0.0	0.0	0.0

Table B.14.: periodic terms of nutation in longitude (ΔL) and obliquity (Δi)

Bibliography

Allen, S. J. and Vincent, R. A. (1995): *Gravity wave activity in the lower atmosphere: Seasonal and latitudinal variations*. J. Geophys. Res., **100**, 1327–1350.

Andrews, D. G., Holton, J. R. and Leovy, C. B. (1987): *Middle atmospheric dynamics*. Academic Press.

Asselin, R. (1972): *Frequency filter for time integrations*. Mon. Wea. Rev., **100**, 487–490.

Baines, P. G. and Palmer, T. N. (1990): *Rationale for a new physically-based parameterization of subgridscale orographic effects*. Technical Memorandum 169, ECMWF, Reading, UK.

Barker, H. W., Wielicki, B. A. and Parker, L. (1996): *A parameterization for computing grid-averaged solar fluxes for inhomogeneous marine boundary layer clouds. Part II: Validation using satellite data*. J. Atmos. Sci., **53**, 2304–2316.

Bäuml, G. (2002): *Influence of sub-grid scale variability of clouds on the solar radiative transfer computations in the ECHAM5 climate model*. PhD thesis 89, Max Planck-Institut für Meteorologie, Hamburg.

Beheng, K. D. (1994): *A parameterization of warm cloud microphysical conversion processes*. Atmos. Res., **33**, 193 – 206.

Berger, A. (1976): *Obliquity and precession for the last 5,000,000 years*. Astronomy and Astrophysics, **51**, 127–135.

Berger, A. (1978): *Long-term variations of daily insolation and quaternary climatic changes*. J. Atmos. Sci., **35**, 2362–2367.

Bigg, E. K. (1953): *The supercooling of water*. Proc. Roy. Soc., **66**, 688–694.

Blackadar, A. K. (1962): *The vertical distribution of wind and turbulent exchange in a neutral atmosphere*. J. Geophys. Res., **67**, 3095–3102.

Bourke, W. (1972): *An efficient one level primitive-equation spectral model*. Mon. Wea. Rev., **100**, 683–689.

Bourke, W. (1974): *A multi-level spectral model: Formulation and hemispheric integrations*. Mon. Wea. Rev., **102**, 688–701.

Bretagnon, P. (1982): *Theory for the motion of all the planets - the VSOP 82 solution*. Astronomy and Astrophysics, **114**, 278–288.

Bretagnon, P. and Francou, G. (1988): *Planetary theories in rectangular and spherical variables - VSOP 87 solutions*. Astronomy and Astrophysics, **202**, 309–315.

Brinkop, S. and Roeckner, E. (1995): *Sensitivity of a general circulation model to parameterizations of cloud-turbulence interactions in the atmospheric boundary layer*. Tellus, **47A**, 197–220.

Burridge, D. M. and Haseler, J. (1977): *A model for medium range weather forecasting - Adiabatic formulation*. Technical Report 4, ECMWF, Reading, UK.

Buschmann, N. (2001): *Inhomogenitäten in Cirren und ihre Auswirkungen auf den solaren Strahlungstransport*. Phd thesis, GKSS Geesthacht, Geesthacht.

Cahalan, R. F. et al. (1994): *The albedo of fractal stratocumulus clouds*. J. Atmos. Sci., **51**, 2434–2455.

Charnock, M. (1955): *Wind stress on a water surface*. Quart. J. Roy. Meteor. Soc., **81**, 639–640.

Claussen, M. (1991): *Estimation of areally-averaged surface fluxes*. Bound.-Layer Meteor., **54**, 387–410.

Clough, S. A. and Iacono, M. I. (1995): *Line-by-line calculation of atmospheric fluxes and cooling rates. II. application to carbon dioxide, ozone, methane, nitrous oxide and the halocarbons*. J. Geophys. Res., **100**, 16519–16536.

Clough, S. A., Iacono, M. J. and Moncet, J.-L. (1992): *Line-by-line calculations of atmospheric fluxes and cooling rates: Application to water vapor*. J. Geophys. Res., **97**, 15761–15786.

Clough, S. A., Kneizys, F. X. and Davies, R. W. (1989): *Line shape and the water vapor continuum*. Atmos. Res., **23**, 229–241.

Croll, J. (1867a): *On the change in the obliquity of the eliptic, its influence on the climate of the polar regions and on the level of the sea*. Philosophical Magazine, **33**, 426–445.

Croll, J. (1867b): *On the excentricity of the earth's orbit, and its physical relations to the glacial epoch*. Philosophical Magazine, **33**, 119–131.

Crowell, J. C. and North, G. R. (1991): *Palaeoclimatology*. No. 18 in Oxford Monographs on Geology and Geophysics. Oxford University Press, New York.

Deardorff, J. W. (1974): *Three-dimensional numerical study of the height and mean structure of a heated boundary layer*. Bound.-Layer Meteor., **7**, 81–106.

Dewan, E. M. and Good, R. E. (1986): *Saturation and the universal spectrum for vertical profiles of horizontal scalar winds in the atmosphere*. J. Geophys. Res., **91**, 2742–2748.

Dümenil, L. and Todini, E. (1992): *A rainfall-runoff scheme for use in the Hamburg climate model*. In: *Advances in Theoretical Hydrology, A Tribute to James Dooge*, edited by Kane, J. O., European Geophysical Society Series on Hydrological Sciences, pp. 129–157. Elsevier, Amsterdam.

Ebert, E. E. and Curry, J. A. (1992): *A parameterization of cirrus cloud optical properties for climate models*. J. Geophys. Res., **97**, 3831–3836.

Eckermann, S. D., Hirota, I. and Hocking, W. K. (1994): *Gravity wave and equatorial morphology of the stratosphere derived from long-term rocket sounding*. Quart. J. Roy. Meteor. Soc., **112**, 149–186.

Eliasen, E., Machenhauer, B. and Rasmussen, E. (1970): *On a numerical method for integration of the hydrodynamical equations with a spectral representation of the horizontal fields*. Tech. Rep. 2, Institute of Theoretical Meteorology, University of Copenhagen.

Fortuin, J. P. F. and Kelder, H. (1998): *An ozone climatology based on ozonesonde and satellite measurements*. J. Geophys. Res., **103**, 31709–31734.

Fouquart, Y. and Bonnel, B. (1980): *Computations of solar heating of the earth's atmosphere: A new parameterization*. Beitr. Phys. Atmos., **53**, 35–62.

Francis, P. N. et al. (1994): *An observational study of the radiative properties of cirrus: Some results from ICE'89*. Quart. J. Roy. Meteor. Soc., **120**, 809–848.

Fritsch, J. M. and Chapell, C. G. (1980): *Numerical prediction of convectively driven mesoscale pressure systems, Part I: Convective parameterization*. J. Atmos. Sci., **37**, 1722–1733.

Fritts, D. C. (1984): *Gravity wave saturation in the middle atmosphere: A review of theory and observations*. Rev. Geophys. Space Sci., **22**, 275–308.

Fritts, D. C. (1989): *A review of gravity wave saturation processes, effects, and variability in the middle atmosphere*. Pure Appl. Geophys., **130**, 343–371.

Fritts, D. C. and Nastrom, G. D. (1992): *Sources of mesoscale variability of gravity waves. Part II: Frontal, convective and jet stream excitation*. J. Atmos. Sci., **49**, 111–127.

Garratt, J. R. (1992): *The atmospheric boundary layer*. Cambridge Atmospheric and Space Science Series. Cambridge University Press, Cambridge.

Girard, C. and Jarraud, M. (1982): *Short and medium range forecast differences between a spectral and a grid-point model: An extensive quasi-operational comparison*. Technical Report 32, ECMWF, Reading, UK.

Goodess, C. M., Palutikof, J. P. and Davies, T. D. (1992): *The nature and causes of climate change*. Belhaven Press, London.

Gunn, K. L. S. and Marshall, J. S. (1958): *The distribution with size of aggregate snowflakes*. Journal of Meteorology, **15**, 452–461.

Hagemann, S. (2002): *An improved land surface parameter dataset for global and regional climate models*. Report 336, Max-Planck-Institut für Meteorologie, Hamburg.

Hamilton, K. (1991): *Climatological statistics of stratospheric inertia-gravity waves deduced from historical rocketsonde wind and temperature data*. J. Geophys. Res., **96**, 20831–20839.

Heymsfield, A. J. and Donner, L. J. (1990): *A scheme for parameterizing ice-cloud water content in general cirulation models*. J. Atmos. Sci., **47**, 1865–1877.

Hines, C. O. (1991a): *The saturation of gravity waves in the middle atmosphere. Part I: Critique of linear-instability theory*. J. Atmos. Sci., **48**, 1348–1359.

Hines, C. O. (1991b): *The saturation of gravity waves in the middle atmosphere. Part II: Development of Doppler-spread theory*. J. Atmos. Sci., **48**, 1360–1379.

Hines, C. O. (1991c): *The saturation of gravity waves in the middle atmosphere. Part III: Formation of the turbopause and of turbulent layers beneath it*. J. Atmos. Sci., **48**, 1380–1385.

Hines, C. O. (1993): *The saturation of gravity waves in the middle atmosphere. Part IV: Cutoff of the incident wave spectrum.*. J. Atmos. Sci., **50**, 3045–3060.

Hines, C. O. (1997a): *Doppler spread parameterization of gravity wave momentum deposition in the middle atmosphere. Part I: Basic formulation*. J. Atmos. Solar Terr. Phys., **59**, 371–386.

Hines, C. O. (1997b): *Doppler spread parameterization of gravity wave momentum deposition in the middle atmosphere. Part II: Broad and quasi monochromatic spectra and implementation*. J. Atmos. Solar Terr. Phys., **59**, 387–400.

Hirota, I. (1984): *Climatology of gravity waves in the middle atmosphere*. J. Atm. Terr. Phys., **46**, 767–773.

Hoskins, B. J. and Simmons, A. J. (1975): *A multi-layer spectral model and the semi-implicit method*. Quart. J. Roy. Meteor. Soc., **101**, 637–655.

ICAO (1964): *Manual of the ICAO Standard Atmosphere*. U.S. Government Printing Office, Washington, D.C.

Jakob, C. and Klein, S. A. (1999): *A scheme for parameterizing ice-cloud water content in general cirulation models*. J. Atmos. Sci., **47**, 1865–1877.

Jarraud, M., Girard, C. and Cubasch, U. (1981): *Comparison of medium-range forecasts made with the models using spectral or finite-difference techniques in the horizontal*. Technical Report 23, ECMWF, Reading, UK.

Jarraud, M., Girard, C. and Geleyn, J.-F. (1982): *Note on a possible linearization of the vorticity equation in a primitive equations spectral model*. In: *Research Activities in Atmospheric and Oceanic Modelling*, no. 3 in Working Group on Numerical Experimentation, pp. 4.2–4.4, Geneva. WMO.

Johnson, D. W. (1993): *Parameterisation of the cloud topped boundary layer: Aircraft measurements*. In: *ECMWF Workshop on 'Parameterization of the cloud topped boundary layer'*, pp. 77–117, Reading.

Kasahara, A. (1974): *Various vertical coordinate systems used for numerical weather prediction*. Mon. Wea. Rev., **102**, 509–522.

Kessler, E. (1969): *On the distribution and continuity of water substance in atmospheric circulation*. Met. Mon. American Meteorological Society, **32**. Boston, Mass.

Krylov, V. I. (1962): *Approximate calculation of integrals*. Macmillan, York.

Large, W. G. and Pond, S. (1982): *Sensible and latent heat flux measurements over the ocean*. J. Phys. Oceanogr., **12**, 464–482.

Laskar, J., F. J. and Boudin, F. (1993): *Orbital, precessional, and insolation quantities for the earth from -20 myr to +10 myr*. Astronomy and Astrophysics, **270**, 522–533.

Levkov, L., Rockel, B., Kapitza, H. and Raschke, E. (1992): *3d mesoscale numerical studies of cirrus and stratus clouds by their time and space evolution*. Beitr. Phys. Atmos., **65**, 35–58.

Liao, X. and Rind, D. (1997): *Local upper tropospheric/lower stratospheric clear-sky water vapor and tropospheric deep convection*. J. Geophys. Res., **102**, 19543–19557.

Lin, S. J. and Rood, R. B. (1996): *Multidimensional flux form semi-Lagrangian transport*. Mon. Wea. Rev., **124**, 2046–2068.

Lin, Y.-L., Farley, R. D. and Orville, H. D. (1983): *Bulk parameterization of the snow field in a cloud model*. Journal of Climate and Applied Meteorology, **22**, 1065–1092.

Lindzen, R. S. (1981): *Turbulence and stress due to gravity wave and tidal breakdown*. J. Geophys. Res., **86**, 9707–9714.

Lohmann, U. and Roeckner, E. (1996): *Design and performance of a new cloud microphysics scheme developed for the ECHAM4 general circulation model*. Clim. Dyn., **12**, 557–572.

Lott, F. (1999): *Alleviation of stationary biases in a GCM through a mountain drag parameterization scheme and a simple representation of mountain lift forces*. Mon. Wea. Rev., **127**, 788–801.

Lott, F. and Miller, M. J. (1997): *A new-subgrid-scale orographic drag parameterization: Its formulation and testing*. Quart. J. Roy. Meteor. Soc., **123**, 101–127.

Louis, J. F. (1979): *A parametric model of vertical eddy fluxes in the atmosphere*. Bound.-Layer Meteor., **17**, 187–202.

Machenhauer, B. and Rasmussen, E. (1972): *On the integration of the spectral hydrodynamical equations by a transform method*. Tech. Rep. 4, Institute of Theoretical Meteorology, University of Copenhagen.

Mailhot, J. and Benoit, R. (1982): *A finite-element model of the atmospheric boundary layer suitable for use with numerical weather prediction models*. J. Atmos. Sci., **39**, 2249–2266.

Manzini, E. and McFarlane, N. A. (1998): *The effect of varying the source spectrum of a gravity wave parameterization in a middle atmosphere general circulation model*. J. Geophys. Res., **103**, 31523–31539.

Manzini, E., McFarlane, N. A. and McLandress, C. (1997): *Impact of the Doppler spread parameterization on the simulation of the middle atmosphere circulation using the MA/ECHAM4 general circulation model*. J. Geophys. Res., **102**, 25751–25762.

Marshall, J. S. and Palmer, W. M. (1948): *The distribution of raindrops with size*. Journal of Meteorology, **5**, 165–166.

Meeus, J. (1998): *Astronomical Algorithms*. Willmann-Bell, Richmond, 2nd edn..

Mellor, G. L. and Yamada, T. (1982): *Development of a turbulence closure model for geophysical fluid problems*. Rev. Geophys. Space Phys., **20**, 851–875.

Milankovitch, M. M. (1941): *Canon of Insolation and the Ice Age Problem*. Königlich Serbische Academie, Belgrade. English translation by the Israel Program for Scientific Translations, United States Department of Commerce and the National Science Foundation, Washington D.C.

Miller, M. J., Beljaars, A. and Palmer, T. N. (1992): *The sensitivity of the ECMWF model to the parameterization of evaporation from the tropical oceans*. J. Climate, **5**, 418–434.

Miller, M. J., Palmer, T. N. and Swinbank, R. (1989): *Parameterization and influence of subgrid scale orography in general circulation and numerical weather prediction models*. Meteor. Atmos. Phys., **40**, 84–109.

Mlawer, E. J. et al. (1997): *Radiative transfer for inhomogeneous atmospheres: RRTM, a validated correlated-k model for the longwave*. J. Geophys. Res., **102**, 16663–16682.

Morcrette, J.-J., Clough, S. A., Mlawer, E. J. and Iacono, M. J. (1998): *Impact of a validated radiative transfer scheme, RRTM, on the ECMWF model climate and 10-day forecasts*. Technical Memorandum 252, ECMWF, Reading, UK.

Murakami, M. (1990): *Numerical modeling of dynamical and microphysical evolution of an isolated convective cloud - the 19 July 1981 CCOPE cloud*. Journal of the Meteorological Society of Japan, **68**, 107–128.

Nordeng, T. E. (1994): *Extended versions of the convective parameterization scheme at ECMWF and their impact on the mean and transient activity of the model in the tropics*. Technical Memorandum 206, ECMWF, Reading, UK.

Orszag, S. A. (1970): *Transform method for calculation of vector coupled sums*. J. Atmos. Sci., **27**, 890–895.

Palmer, T. N., Shutts, G. J. and Swinbank, R. (1986): *Alleviation of systematic weasterly bias in general circulation and numerical weather prediction models through an orographic gravity wave drag parameterization*. Quart. J. Roy. Meteor. Soc., **112**, 2056–2066.

Paltridge, G. W. and Platt, C. M. R. (1976): *Radiative Processes in Meteorology and Climatology*. No. 5 in Developments in Atmospheric Science. Elsevier, Amsterdam.

Phillips, N. A. (1957): *A coordinate system having some special advantages for numerical forecasting*. Journal of Meteorology, **14**, 184–185.

Potter, B. E. (1991): *Improvements to a commonly used cloud microphysical bulk parameterization*. J. Appl. Meteorol., **30**, 1040–1042.

Pruppacher, H. R. and Klett, J. D. (1978): *Microphysics of Clouds and Precipitation*. D. Reidel Publishing Company, Amsterdam.

Robert, A. J. (1981): *A stable numerical integration scheme for the primitive meteorological equations*. Atmos. Ocean, **19**, 35–46.

Robert, A. J. (1982): *A semi-Lagrangian and semi-implicit numerical integration scheme for the primitive meteorological equations*. J. Met. Soc. Japan, **60**, 319–325.

Robert, A. J., Henderson, J. and Turnbull, C. (1972): *An implicit time integration scheme for baroclinic models in the atmosphere*. Mon. Wea. Rev., **100**, 329–335.

Rockel, B., Raschke, E. and Weyres, B. (1991): *A parameterization of broad band radiative transfer properties of water, ice, and mixel clouds*. Beitr. Phys. Atmos., **64**, 1–12.

Roeckner, E. et al. (1996): *The atmospheric general circulation model ECHAM-4: Model description and simulation of present-day climate*. Report 218, Max-Planck-Institut für Meteorologie, Hamburg.

Roeckner, E. et al. (2003): *The atmospheric general circulation model ECHAM5. Part II: Simulated climatology and comparison with observations*. Report in preparation, Max-Planck-Institut für Meteorologie, Hamburg.

Roesch, A., Wild, M., Gilgen, H. and Ohmura, A. (2001): *A new snow cover fraction parameterization for the ECHAM4 GCM*. Clim. Dyn., **17**, 933–946.

Rotstayn, L. D. (1997): *A physically based scheme for the treatment of stratiform precipitation in large-scale models. I: Description and evaluation of the microphysical processes*. Quart. J. Roy. Meteor. Soc., **123**, 1227–1282.

Schulz, J.-P., Dümenil, L. and Polcher, J. (2001): *On the land surface-atmosphere coupling and its impact in a single-column atmospheric model*. J. Appl. Meteorol., **40**, 642–663.

Seidelmann, P. K. (1982): *1980 IAU theory of nutation: The final report of the IAU working group on nutation*. Celestial Mechanics, **27**, 79–106.

Simmons, A. J. et al. (1989): *The ECMWF medium-range prediction model: Development of the numerical formulations and the impact of increased resolution*. Meteorol. Atmos. Phys., **40**, 28–60.

Simmons, A. J. and Burridge, D. M. (1981): *An energy and angular-momentum conserving vertical finite difference scheme and hybrid vertical coordinates*. Mon. Wea. Rev., **109**, 758–766.

Simmons, A. J. and Chen, J. (1991): *The calculation of geopotential and pressure-gradient in the ecmwf atmospheric model: Influence on the simulation of the polar atmosphere and on temperature analyses*. Quart. J. Roy. Meteor. Soc., **117**, 29–58.

Simmons, A. J., Hoskins, B. J. and Burridge, D. M. (1978): *Stability of the semi-implicit time scheme*. Mon. Wea. Rev., **106**, 405–412.

Simmons, A. J. and Strüfing, R. (1981): *An energy and angular-momentum conserving finite difference scheme, hybrid coordinates and medium-range weather prediction*. Technical Report 28, ECMWF, Reading, UK.

Simpson, J. and Wiggert, V. (1969): *Models of precipitating cumulus towers*. Mon. Wea. Rev., **97**, 471–489.

Smith, S. A., Fritts, D. C. and VanZandt, T. E. (1987): *Evidence for a saturated spectrum of atmospheric gravity waves*. J. Atmos. Sci., **44**, 1404–1410.

Stephens, G. L., Tsay, S.-C., Stackhouse, P. W. and Flateau, P. J. (1990): *The relevance of the microphysical and radiative properties of cirrus clouds to climate and climate feedback*. J. Atmos. Sci., **47**, 1742–1753.

Tanre, D., Geleyn, J.-F. and Slingo, J. M. (1984): *First results of the introduction of an advanced aerosol-radiation interaction in the ecmwf low resolution global model*. In: *Aerosols and Their Climatic Effects*, edited by Gerber, H. and Deepak, A., pp. 133–177. A. Deepak, Hampton, Va.

Tiedtke, M. (1989): *A comprehensive mass flux scheme for cumulus parameterization in large-scale models*. Mon. Wea. Rev., **117**, 1779–1800.

Tiedtke, M. (1993): *Representation of clouds in large-scale models*. Mon. Wea. Rev., **121**, 3040–3061.

Tiedtke, M. (1996): *An extension of cloud-radiation parameterization in the ECMWF model: The respresentation of of subgrid-scale variations of optical depth*. Mon. Wea. Rev., **124**, 745–750.

Tompkins, A. (2002): *A prognostic parameterization for the subgrid-scale variability of water vapor and clouds in large-scale models and its use to diagnose cloud cover*. J. Atmos. Sci., **59**, 1917–1942.

Turner, J. S. (1963): *The motion of buoyant elements in turbulent surroundings*. J. Fluid Mech., **16**, 1–16.

Verseghy, D. L. (1991): *CLASS-A Canadian land surface scheme for GCMs. I. Soil model*. Int. J. Climatol., **13**, 347–370.

Vincent, R. A., Allen, S. J. and Eckermann, S. D. (1997): *Gravity wave processes and their parameterization in global climate models*. In: *Gravity wave parameters in the lower stratosphere*, edited by Hamilton, K., NATO ASI Series I, pp. 7–25. Springer.

MPI-Report-Reference: *Reprinted in

Report 1 - 302 Please order the reference list from MPI for Meteorology, Hamburg

Report No. 303
December 1999
The leading variability mode of the coupled troposphere-stratosphere winter circulation in different climate regimes
Judith Perlwitz, Hans-F. Graf, Reinhard Voss
* Journal of Geophysical Research, 105, 6915-6926, 2000

Report No. 304
January 2000
Generation of SST anomalies in the midlatitudes
Dietmar Dommenget, Mojib Latif
* Journal of Climate, 1999 (submitted)

Report No. 305
June 2000
Tropical Pacific/Atlantic Ocean Interactions at Multi-Decadal Time Scales
Mojib Latif
* Geophysical Research Letters, 28,3,539-542,2001

Report No. 306
June 2000
On the Interpretation of Climate Change in the Tropical Pacific
Mojib Latif
* Journal of Climate, 2000 (submitted)

Report No. 307
June 2000
Observed historical discharge data from major rivers for climate model validation
Lydia Dümenil Gates, Stefan Hagemann, Claudia Golz

Report No. 308
July 2000
Atmospheric Correction of Colour Images of Case I Waters - a Review of Case II Waters - a Review
D. Pozdnyakov, S. Bakan, H. Grassl
* Remote Sensing of Environment, 2000 (submitted)

Report No. 309
August 2000
A Cautionary Note on the Interpretation of EOFs
Dietmar Dommenget, Mojib Latif
* Journal of Climate, 2000 (submitted)

Report No. 310
September 2000
Midlatitude Forcing Mechanisms for Glacier Mass Balance Investigated Using General Circulation Models
Bernhard K. Reichert, Lennart Bengtsson, Johannes Oerlemans
* Journal of Climate, 2000 (accepted)

Report No. 311
October 2000
The impact of a downslope water-transport parameterization in a global ocean general circulation model
Stephanie Legutke, Ernst Maier-Reimer

Report No. 312
November 2000
The Hamburg Ocean-Atmosphere Parameters and Fluxes from Satellite Data (HOAPS): A Climatological Atlas of Satellite-Derived Air-Sea-Interaction Parameters over the Oceans
Hartmut Graßl, Volker Jost, Ramesh Kumar, Jörg Schulz, Peter Bauer, Peter Schlüssel

Report No. 313
December 2000
Secular trends in daily precipitation characteristics: greenhouse gas simulation with a coupled AOGCM
Vladimir Semenov, Lennart Bengtsson

Report No. 314
December 2000
Estimation of the error due to operator splitting for micro-physical-multiphase chemical systems in meso-scale air quality models
Frank Müller
* Atmospheric Environment, 2000 (submitted)

Report No. 315
January 2001
Sensitivity of global climate to the detrimental impact of smoke on rain clouds (only available as pdf-file on the web)
Hans-F. Graf, Daniel Rosenfeld, Frank J. Nober

Report No. 316
March 2001
Lake Parameterization for Climate Models
Ben-Jei Tsuang, Chia-Ying Tu, Klaus Arpe

Report No. 318
March 2001
On North Pacific Climate Variability
Mojib Latif
* Journal of Climate, 2001 (submitted)

MPI-Report-Reference: *Reprinted in

Report 1 - 302 Please order the reference list from MPI for Meteorology, Hamburg

Report No. 319
March 2001
The Madden-Julian Oscillation in the ECHAM4 / OPYC3 CGCM
Stefan Liess, Lennart Bengtsson, Klaus Arpe
* Climate Dynamics, 2001 (submitted)

Report No. 320
May 2001
Simulated Warm Polar Currents during the Middle Permian
A. M. E. Winguth, C. Heinze, J. E. Kutzbach, E. Maier-Reimer,
U. Mikolajewicz, D. Rowley, A. Rees, A. M. Ziegler
* Paleoceanography, 2001 (submitted)

Report No. 321
June 2001
Impact of the Vertical Resolution on the Transport of Passive Tracers in the ECHAM4 Model
Christine Land, Johann Feichter, Robert Sausen
* Tellus, 2001 (submitted)

Report No. 322
August 2001
Summer Session 2000
Beyond Kyoto: Achieving Sustainable Development
Edited by Hartmut Graßl and Jacques Léonardi

Report No. 323
July 2001
An atlas of surface fluxes based on the ECMWF Re-Analysis- a climatological dataset to force global ocean general circulation models
Frank Röske

Report No. 324
August 2001
Long-range transport and multimedia partitioning of semivolatile organic compounds:
A case study on two modern agrochemicals
Gerhard Lammel, Johann Feichter, Adrian Leip
* Journal of Geophysical Research-Atmospheres, 2001 (submitted)

Report No. 325
August 2001
A High Resolution AGCM Study of the El Niño Impact on the North Atlantic / European Sector
Ute Merkel, Mojib Latif
* Geophysical Research Letters, 2001 (submitted)

Report No. 326
August 2001
On dipole-like varibility in the tropical Indian Ocean
Astrid Baquero-Bernal, Mojib Latif
* Journal of Climate, 2001 (submitted)

Report No. 327
August 2001
Global ocean warming tied to anthropogenic forcing
Berhard K. Reichert, Reiner Schnur, Lennart Bengtsson
* Geophysical Research Letters, 2001 (submitted)

Report No. 328
August 2001
Natural Climate Variability as Indicated by Glaciers and Implications for Climate Change: A Modeling Study
Bernhard K. Reichert, Lennart Bengtsson, Johannes Oerlemans
* Journal of Climate, 2001 (submitted)

Report No. 329
August 2001
Vegetation Feedback on Sahelian Rainfall Variability in a Coupled Climate Land-Vegetation Model
K.-G. Schnitzler, W. Knorr, M. Latif, J.Bader, N.Zeng
Geophysical Research Letters, 2001 (submitted)

Report No. 330
August 2001
Structural Changes of Climate Variability **(only available as pdf-file on the web)**
H.-F.Graf, J. M. Castanheira
Journal of Geophysical Research -Atmospheres, 2001 (submitted)

Report No. 331
August 2001
North Pacific - North Atlantic relationships under stratospheric control? (only available as pdf-file on the web)
H.-F.Graf, J. M. Castanheira
Journal of Geophysical Research -Atmospheres, 2001 (submitted)

Report No. 332
September 2001
Using a Physical Reference Frame to study Global Circulation Variability (only available as pdf-file on the web)
H.-F.Graf, J. M. Castanheira, C.C. DaCamara, A.Rocha

MPI-Report-Reference: *Reprinted in

Report 1 - 302 Please order the reference list from MPI for Meteorology, Hamburg

Journal of Atmospheric Sciences, 2001 (in press)

Report No. 333
November 2001
Stratospheric Response to Global Warming in the Northern Hemisphere Winter
Zeng-Zhen Hu

Report No. 334
October 2001
On the Role of European and Non-European Emission Sources for the Budgets of Trace Compounds over Europe
Martin G. Schultz, Johann Feichter, Stefan Bauer, Andreas Volz-Thomas

Report No. 335
November 2001
Slowly Degradable Organics in the Atmospheric Environment and Air-Sea Exchange
Gerhard Lammel

Report No. 336
January 2002
An Improved Land Surface Parameter Dataset for Global and Regional Climate Models
Stefan Hagemann

Report No. 337
May 2002
Lidar intercomparisons on algorithm and system level in the frame of EARLINET
Volker Matthias, J. Bösenberg, H. Linné, V. Matthias, C. Böckmann, M. Wiegner, G. Pappalardo, A. Amodeo, V. Amiridis, D. Balis, C. Zerefos, A. Ansmann, I. Mattis, U. Wandinger, A. Boselli, X. Wang, A. Chaykovski, V. Shcherbakov, G. Chourdakis, A. Papayannis, A. Comeron, F. Rocadenbosch, A. Delaval, J. Pelon, L. Sauvage, F. DeTomasi, R. M. Perrone, R. Eixmann, J. Schneider, M. Frioud, R. Matthey, A. Hagard, R. Persson, M. Iarlori, V. Rizi, L. Konguem, S. Kreipl, G. Larchevêque, V. Simeonov, J. A. Rodriguez, D. P. Resendes, R. Schumacher

Report No. 338
June 2002
Intercomparison of water and energy budgets simulated by regional climate models applied over Europe
Stefan Hagemann, Bennert Machenhauer, Ole Bøssing Christensen, Michel Déqué, Daniela Jacob, Richard Jones, Pier Luigi Vidale

Report No. 339
September 2002
Modelling the wintertime response to upper tropospheric and lower stratospheric ozone anomalies over the North Atlantic and Europe
Ingo Kirchner, Dieter Peters

Report No. 340
November 2002
On the determination of atmospheric water vapour from GPS measurements
Stefan Hagemann, Lennart Bengtsson, Gerd Gendt

Report No. 341
November 2002
The impact of international climate policy on Indonesia
Armi Susandi, Richard S.J. Tol

Report No. 342
December 2002
Indonesian smoke aerosols from peat fires and the contribution from volcanic sulfur emissions (only available as pdf-file on the web)
Bärbel Langmann, Hans F. Graf

Report No. 343
January 2003
Modes of the wintertime Arctic temperature variability
Vladimir A. Semenov, Lennart Bengtsson

Report No. 344
February 2003
Indicators for persistence and long-range transport potential as derived from multicompartment chemistry-transport modelling
Adrian Leip, Gerhard Lammel

Report No. 345
February 2003
The early century warming in the Arctic – A possible mechanism
Lennart Bengtsson, Vladimir A. Semenov, Ola Johannessen

Report No. 346
May 2003
Variability of Indonesian Rainfall and the Influence of ENSO and Resolution in ECHAM4 Simulations and in the Reanalyses
Edvin Aldrian, Lydia Dümenil Gates, F. Heru Widodo

MPI-Report-Reference: *Reprinted in

Report 1 - 302 Please order the reference list from MPI for Meteorology, Hamburg

Report No. 347
June 2003
Sensitivity of Large Scale Atmospheric Analyses to Humidity Observations and its Impact on the Global Water Cycle and Tropical and Extra-Tropical Weather Systems
L. Bengtsson, K. I. Hodges, S. Hagemann

Report No. 348
September 2003
EARLINET: A European Aerosol Research Lidar Network to Establish an Aerosol Climatology
J. Bösenberg, V. Matthias, et al.

ISSN 0937 - 1060